Film Blowing:
from Polymer to Product

Proefschrift

ter verkrijging van de graad van doctor
aan de Technische Universiteit Eindhoven
op gezag van de Rector Magnificus, prof.dr. J.H. van Lint,
voor een commissie aangewezen door het College van Dekanen
in het openbaar te verdedigen op
vrijdag 28 oktober 1994 om 14.00 uur

door

Paul Prudent Tas

geboren te Aardenburg

Dit proefschrift is goedgekeurd door de promotoren:

prof.dr.ir. H.E.H. Meijer
prof.dr.ir. F.P.T. Baaijens

en de copromotor:

dr. H.C. Booij

This work was financially supported by DSM Research, Geleen, The Netherlands.

Film Blowing:
from Polymer to Product

CIP-GEGEVENS KONINKLIJKE BIBLIOTHEEK, DEN HAAG

Tas, Paul Prudent

Film blowing: from polymer to product / Paul Prudent Tas.
-[S.l. : s.n.]
Proefschrift Eindhoven. - Met lit. opg.
ISBN 90-386-0204-9
Trefw.: reologie / folieblazen

Druk: Febodruk, Enschede

Imagination is more important than knowledge

Contents

Summary

Amongst all plastic materials, polyethylene is one of the oldest and most important in quantity. Three groups of polyethylene can be distinguished: high density polyethylene (HDPE), low density polyethylene (LDPE) and linear low density polyethylene (LLDPE). From these, LDPE, which in itself can be divided into a large number of distinct grades, is by far the most widely produced. Applications of this material are commonly found in the film business: shrink films, food packaging, heavy duty bags etc.. The most frequently used production method to make films is the film blowing process, which is almost as old as polyethylene itself. Despite of its long history, up till now no thorough understanding of the influence of machine design, processing parameters and material on the ultimate mechanical and optical properties of the films produced is available.

A literature survey (Chapter 1) shows that past research has been focused on the description of the exact kinematics of the process, especially of the flow between the exit of the die and the freeze line. In all studies, however, processing parameters or material constants had to be altered to obtain agreement between theoretical predictions and experiments. The experimental research mainly focused on the influences of the material characteristics (especially the rheological properties) on the bubble stability during processing and only sometimes the influence of stresses at the freeze line on the ultimate film morphologies is mentioned. It was concluded that a unique correlation exists between these stresses and the resulting film morphologies. Given these seemingly relevant results it is striking that no one reported the influence of these stresses on the ultimate film properties. The goal of this thesis is, therefore, to investigate this influence and to search for a representative rheological constitutive relation which enables us to calculate these stresses in advance, depending on both raw material characteristics and processing conditions.

Three LDPE's were selected with different rheological behaviour (two

melt index 1 materials and one melt index 8 material) and film performance (mainly the optics).

In Chapter 2 the experimentally determined rheological behaviour of all three LDPE's in shear and uniaxial elongation is discussed. Pronounced differences are present between the MI 8 material on one side and the two MI 1 materials on the other side. Four types of constitutive equations were used to describe their rheological behaviour: Wagner's integral equation, and Leonov's, Giesekus' and Phan Thien and Tanner's equations, which are all of differential form. No clear distinctions are observed in describing the basic simple flows, and, consequently, good agreement between experiments and theory is obtained. For one of the MI 1 materials, also flow induced birefringence was measured in a tapered duct. In this geometry, the flow is a combination of shear and planar elongation. Using the stress optical law, the stresses in the flowing polymer were deduced from these data. Calculations at the centerline using the Wagner model showed that this model is inadequate to describe the experimentally determined stresses: the non-linearity function obtained from shear and uniaxial elongational flow proves to yield a too pronounced strain thinning behaviour. Using the three equations of differential form, finite element calculations were performed and in the comparison with the experiments it was found that, qualitatively, all three constitutive equations predicted the stresses reasonably. Quantitatively, however, the Leonov equation exhibits a somewhat too distinct strain thinning behaviour, while the Giesekus and the Phan Thien and Tanner equations gave correct predictions of the stresses. So, in order to check the validity of constitutive equations in describing different types of flow, it seems that standard experiments (in shear and uniaxial elongation) are not sufficiently discriminating. In contrast, the measurements of flow induced birefringence in combined complex flows seem to contain enough information for this discrimination, at the cost of more elaborate (finite element) calculations.

To check whether any of these constitutive equations is appropriate to calculate the stresses in the film during processing, film blowing experiments were performed on all three LDPE's (Chapter 3). Processing parameters were varied systematically. Using the kinematics and film temperatures measured as input data, stresses were calculated. Using specially designed pressure- and force transducers, stresses were also determined experimentally. Comparison of both stresses showed that the most appropriate constitutive equation is the Phan Thien and Tanner equation. Wagner's equation and Leonov's equation exhibit a too strain thinning behaviour and, conse-

quently, the experimentally observed stresses are underpredicted by these models. On the other hand, Giesekus' equation showed a too strain hardening behaviour and the stresses were overpredicted.

It is shown that in modelling the film blowing process, the flow inside the die may not be neglected. Since then, apparently, films were obtained with equal principal stresses. This was shown experimentally to be not true. For all films produced, the stresses in the extrusion direction exceeded the stresses in the transverse direction significantly. Calculations including the flow in the die were in agreement with the experimental findings.

In Chapter 4 the influence of the stresses on the final film morphologies is discussed. First, the basic concepts of orientation induced crystallization are highlighted. Secondly, the resulting film morphologies, consisting of stacked lamellae originating from row nucleation, are presented. The orientation of the lamellae proved to depend on the stresses at the freeze line. Because of the fact that the stresses in the extrusion direction exceed those in the transverse direction to a great extent, the main orientation of the lamellae is in the extrusion direction. Some TEM results are shown and confirm these findings.

Finally, in Chapter 5 the mechanical and optical properties, as well as the shrinkage of the finished films, are discussed. A number of mechanical properties (longitudinal and transverse moduli, tensile strength and elongation at break in the extrusion direction, yield stress and tear resistance in the extrusion direction) do correlate well with the stress in the extrusion direction at the freeze line, independent of the die geometries, processing parameters and type of LDPE. Shrink properties seem to be mainly determined by the frozen-in orientation induced in the flowing melt and calculations of the recoverable strain using the Phan Thien and Tanner model show good agreement with experimentally determined shrink values. The optical properties, finally, seem to be mostly dependent on extrusion defects induced by the flow inside the die, and relate to the (elasticity) ratio of the normal stress difference to the shear stress. Extrusion of highly elastic melts resulted in rougher film surfaces and, consequently, in only moderate optical performance.

Chapter 1

Introduction

1.1 Film blowing: the process

Amongst all plastic materials, PolyEthylene is one of the oldest and most important in quantity. In 1993, the production of PE in Western Europe was estimated to be approximately 8.8 10^6 tonnes. This was split in 4.4 10^6 tonnes Low Density PolyEthylene (LDPE), 1.2 10^6 tonnes Linear Low Density PolyEthylene (LLDPE) and 3.2 10^6 tonnes High Density PolyEthylene (HDPE). In 1993 in Western Europe, 74 % of the LDPE and LLDPE was used for making films (Oonk [1994]). Although a small proportion of PE film is made by film casting , the most widely and frequently used process to make PE films is the tubular film blowing process.

The tubular film blowing process is one of the oldest polymer processing techniques. In the late thirties, the first commercial film blowing line was built in the USA. Applications of PE films can be found in *e.g.* carrier bags, shrink films, food wrapping, refuse bags and films for agricultural purposes. Films of infinite length can be made with a width varying between a few centimeters to several meters. Thicknesses range from about 15 μm up to 500 μm.

The principles of the film blowing process are shown in figure 1.1. Polymer feedstock is transported, pressurized and melted in an extruder. At the end of the extruder the melt is forced into an annular die. Leaving the annular die, a tube is formed while the flowing melt is cooled by blowing air along the film. During the time the polymer is in the molten state the film will be stretched in two directions. First, by blowing air through the orifice in the annular die the tube is inflated, where no air can escape because

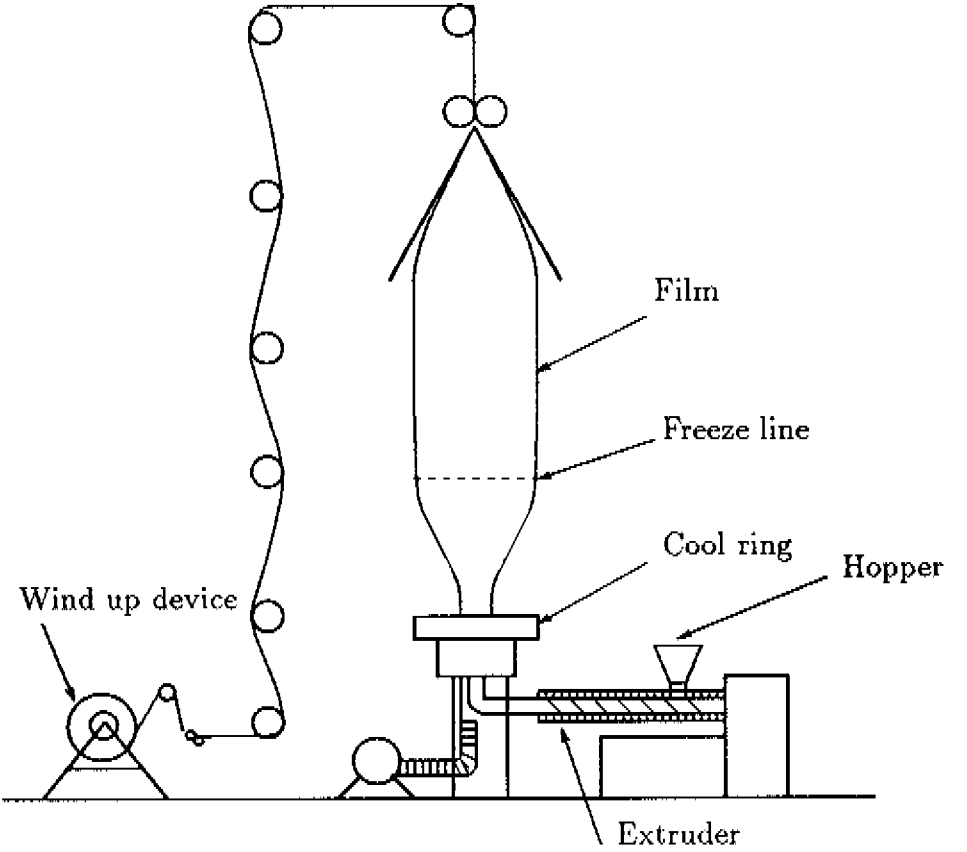

Figure 1.1: The film blowing process.

the nip rolls are pushed together. Due to this inflation the film is being stretched in the so-called circumferential (or transverse) direction. At the end of the extrusion line, the extruded film is wound up, causing elongation in the machine direction and yielding the so-called draw down. The height at which solidification of the melts starts is referred to as the freeze line height. The ratio of bubble diameter at the freeze line height to the die diameter is known as the blow up ratio (BUR), the ratio of the haul off rate to the natural extrusion rate as the draw ratio (DR). Processing plastic materials this way results in biaxially oriented films.

The ultimate film properties will depend on the polymer used and the processing conditions. A schematic diagram of this dependence is shown in figure 1.2. It is generally known that product properties are influenced to a

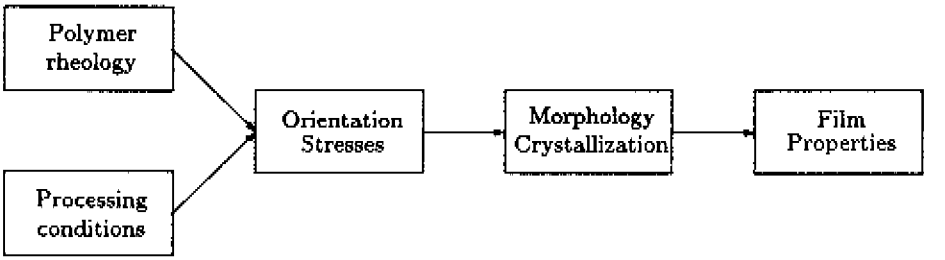

Figure 1.2: From polymer to product: a rather extremely simplified view.

great extent by its morphology (Ward [1985]). The morphology on its part will be affected by orientation induced crystallization (Eder, [1990]), where the orientation is build up in the bubble forming region. Since polymeric melts exhibit nonlinear viscoelastic behaviour this orientation build-up is a complex function of the processing parameters and the material used (Douven [1991]).

1.2 Film blowing: the materials used

PolyEthylene is a relatively old plastic. Because of the developments in the last decades many grades of PE are available. The properties of all these grades differ one way or another and can be controlled by:

- Variation in the degree of short chain branching
- Variation in the degree of long chain branching
- Variation in the average molecular weight
- Variation in the molecular weight distribution
- The presence of a small amount of comonomer residues
- The presence of additives or polymerisation residues.

Low Density PolyEthylene (LDPE) is the oldest of the three PE's. Because of the long chain branching in LDPE the crystallinity of LDPE is limited to approximately 40 %. Consequently, the density of LDPE is in between 910 kg/m^3 and 935 kg/m^3. The absence of chain branching in High Density PolyEthylene is responsible for a higher crystallinity which can reach to about 70 %. Densities of HDPE are in between 940 kg/m^3 and 970 kg/m^3. The third type of PE is Linear Low Density PolyEthylene. Due to the use of a small amount of C_4 or C_8 comonomers, LLDPE is a linear polymer with regular short branches and with a limited crystallinity. Densities of LLDPE reach from 915 kg/m^3 to 940 kg/m^3.

This thesis focuses on the manufacturing of LDPE films. Three materials with different rheological behaviour (two melt index 1 materials and one melt index 8 material) and film performance (mainly the optics) have been investigated. These LDPE's are commercial grades supplied by DSM. Some characteristics of the materials are given in table 1.1.

code	grade (Stamylan LD)	Melt Index dg/min	M_n	M_w	M_z	Density kg/m^3 °C	T_c
L1o	2201TH17	0.85	17000	175000	780000	922	101.7
L1	2101TN47	0.85	18000	187000	840000	921	100.8
L8	2008XC43	8	13000	155000	780000	920	98.6

Table 1.1: Characteristics of the LDPE's investigated in this thesis

The number in the codes denotes the melt index and the difference between the two melt index 1 materials, given by L1o and L1, is such that the former exhibits the better optical performance. The molecular weight averages M_n, M_w and M_z have been measured by GPC. The crystallization temperature T_c has been measured by Perkin Elmer DSC7 at a cooling rate of 1 $°C/min$.

1.3 Modelling the film blowing process: a literature review

Despite numerous papers on experimental and theoretical research towards the film blowing process, it is still not quite well understood how film properties relate to the polymer feedstock and the processing parameters. In this literature survey, it was chosen to make a division according to the various

literature survey, it was chosen to make a division according to the various research groups all over the world who worked on understanding and modelling of the film blowing process. The choice for this geographical division proved to roughly coincide with distinct periods of time. In the early seventies, in England Pearson and Petrie created the foundation of the modelling of film blowing, followed by the group of Schenkel at the IKT in Stuttgart, Germany. In the eighties, it was mainly the group of White (at the time still in Knoxville, Tenessee, nowadays in Akron, Ohio) who was active on understanding the film blowing process, while in the nineties, Campbell and coworkers are the most publishing group.

The seventies: pioneering work in England

Pearson and Petrie [1970a,1970b,1970c] derived and solved the equations for isothermal film blowing for a Newtonian fluid. Attention was paid to describing the bubble shape and film velocity. Petrie [1973] extended the model to isothermal viscoelastic film blowing using a constitutive model of the Oldroyd type. Due to numerical problems he was not able to solve the resulting set of equations. In a later paper, Petrie [1975] solved the non-isothermal problem for a Newtonian fluid and the isothermal problem for a purely elastic fluid. The main outcomes of this research suggested that accurate modelling of the heat transfer and the use of a suitable viscoelastic constitutive equation was required.

In the same period, Han and Park [1975a] reported an experimental study on the film blowing process. They tried to use a film blowing line as a rheometer to determine extensional viscosities. In a subsequent paper, Han and Park [1975b] simulated the non-isothermal film blowing process for a generalised Newtonian model. The dimensional take-up force and bubble pressure were used as fitting parameters to achieve reasonable agreement with experimentally observed bubble radii and film thickness profiles.

Schenkel's group at IKT Stuttgart, Germany

Two subsequent Ph.D. theses on film blowing were prepared in the Institut für Kunstofftechnologie in Stuttgart, under supervision of professor Schenkel, later followed by a Ph.D. thesis on film blowing under supervision of professor Fritz. An experimental and theoretical investigation on cooling of the film was performed by Ast [1976]. Solving the energy equation, he was able to calculate the temperature profiles in the film during processing. The heat

transfer coefficient was used as a parameter to determine the freeze line height.

Wagner [1976b] reported a study on non-isothermal modelling with a Newtonian, a purely elastic and a Maxwell fluid. Interesting in his work was the accurate measurement of the take-up force with a specially constructed device. For the Newtonian and the purely elastic model, it was not possible to describe the kinematics of the film with the correct bubble pressure and take-up force. This was possible with the one mode Maxwell model. However, to describe different experiments the relaxation time and the accompanying viscosity had to be altered. Apparently, the one mode Maxwell model is not suitable to model the film blowing process.

Fisher [1983] used measured temperature- and deformation profiles to calculate the stresses in the machine- and transverse direction, which were compared with experimentally determined stresses. The constitutive equation he investigated was Wagner's nonlinear integral equation. By using parameters as determined in shear and uniaxial elongation, the experimentally observed stresses were highly underpredicted. To meet with this problem, the nonlinearity had to be left intact in the die, while a linear integral equation had to be used for the melt that has left the die. It should be mentioned that such a modification of Wagner's model results in an inconsistent constitutive model.

The eighties: other groups with related approaches

A similar approach to calculate stresses in the film was adapted by Gupta [1980]. He introduced a modified Maxwell model in such a way that temperature rate effects were taken into account. Stresses calculated in a polymer melt under non-isothermal deformation proved to be higher than calculated with a temperature rate independent model. In trying to describe the stresses in the film for a polystyrene, the axial stresses served as data to fit the proper relaxation time. Clearly, the axial stresses were predicted well. The calculated circumferential stresses, however, underpredicted the experimentally observed stresses. No decisive proof was given that a temperature rate dependent model should be used to model the film blowing process, as was pointed out later by Luo and Tanner [1985].

Other efforts to incorporate the viscoelastic nature of polymer melts in modelling the film blowing process were reported by Luo and Tanner [1985] and Cain and Denn [1988]. Luo and Tanner performed a study on the non-isothermal flow of an Upper Convected Maxwell and a Leonov fluid. The

Leonov model did not seem to be stiff enough and good agreement between predictions of the kinematics measured (by Gupta [1980]) and calculated with this model was not obtained. The UCM model predicted the experimental bubble shapes and velocities reasonably. The relaxation time chosen for the UCM model, however, had to be set to 0.4 times the relaxation time Gupta reported. Note that Wagner [1976b] also had to alter the relaxation time for a Maxwell model to obtain agreement between experiments and simulations. Furthermore, it was found that the temperature dependency (activation energy) of rheological properties had a great influence on the kinematics calculated.

Cain and Denn [1988] calculated deformation and temperature profiles for a Newtonian, an Upper Convected Maxwell and a Marrucci fluid. The set of equations was solved using a Newman's banded matrix technique, in which the bubble pressure and the take-up force were unknowns. Solving the problem this way, less troubles with numerical instabilities were encountered. The most striking result of their calculations was that multiple solutions seemed to exist for one pair of bubble pressure and take-up force, which is rather unrealistic.

The Tenessee - and later the Akron - group of White: an experimental approach

Choi, White and Spruiell [1980] investigated the orientation development in tubular film extrusion of a polystyrene. The take-up force was measured with a tensiometer and birefringence of the finished films was experimentally determined. It should be mentioned that due to the low tension in the film during tubular film blowing, the measurement of the take-up force with the tensiometer is not accurate. Yet, they found a correlation between the stresses at the freeze line height and the optical birefringence of the finished films. In a later paper, Choi, White and Spruiell [1982] showed that, for a HDPE, the crystalline biaxial orientation factors were unique functions of the stresses at the freeze line, as was later once more pointed out by White and Cakmak [1988] for HDPE, LLDPE, LDPE and PP. Similar results were reported by Kwack, Han and Vickers [1988] for a LDPE. They found the stress at the freeze line height in the machine direction to be an important factor in influencing the crystalline axis orientation, while the stress ratio (machine direction stress/ transverse direction stress) appeared to be a determining factor in the distribution of fibrillous nuclei and crystalline texture, as well as in the film anisotropy. Choi, White and Spruiell [1982], White and

Cakmak [1988] and later Simpson [1993] also proposed a model for the crystalline morphology of the films. They concluded that crystallization under the influence of stresses resulted in the formation of row-nucleated lamellae, as was long ago described by Keller and Machin [1967]. Simpson also showed that the molecular orientation of the amorphous phase was mainly in the machine direction. Despite of the fact that the above mentioned authors concluded that the stresses have a great impact on the morphology of the films, none of them investigated the impact of stresses on the ultimate film properties, which seemed to be the next logical step.

Though the results of Choi *et al.* [1980,1982], White and Cakmak [1988] and Kwack *et al.* [1988] were encouraging, the concept certainly was not new. In an earlier study by Nagasawa *et al.* [1973], who measured the on line birefringence in a HDPE film during blowing, it was found that a slight orientation of molecular chains in the molten state could increase the nucleation rate substantially. Moreover, these authors concluded that the crystalline orientation is independent of the temperature gradient across the film, but did depend mainly on the molecular orientation caused by the elongational flow in the melt.

Kanai and White [1984,1985] published a series of papers on film blowing. In the first, they reported on an experimental study on film blowing of LDPE, HDPE and LLDPE. The most notable result was that increasing the cooling rates did not affect the crystallization temperatures, but only the crystallization rates. The second paper dealt with a theoretical model of the dynamics, heat transfer and crystallization process in tubular film blowing. A Newtonian model, with a temperature dependence according to the Arrhenius equation and an exponential dependence on the crystallization degree was used. Using this model it appeared that the bubble shapes are most influenced by the activation energy, while the crystallinity retards the continued growth of the velocity and the thinning of the film. Yamane and White [1988] replaced the Newtonian model by a generalized Newtonian model. The obtained results were similar to those of Kanai and White [1985]. It should be mentioned that, due to the choice of the constitutive model, they were not able to incorporate the viscoelastic behaviour of polymer melts.

An identical model as Yamane and White [1988] was used by Kanai [1987]. In this paper, Kanai focused on stresses in the film and suggested that these stresses might be related to the film physical properties. Unfortunately, no results were shown of the impact of stresses on the film properties. Furthermore, it remained questionable whether the calculated stresses coincided with the true stresses in the film.

The same idea that the stresses relate to the physical film properties was used by Kanai *et al.* [1986] to set up a scale-up theory. For a HDPE, it was concluded that orientation factors of films and film properties were independent of film width and thickness, under the correct scale-up conditions, i.e. the same stresses at the freeze line. So, according to this scale-up rule, one is able to predict the film properties in a large scale film blowing line, once the tubular film extrusion is carried out using a lab-scale machine.

Simpson and Harrison [1992] used strains and strain rates to set up the scale-up rules. Films produced under the same strains and strain rates had similar molecular orientations and mechanical properties, regardless of the size of the equipment used to produce them. These results are not surprising, since the films on the lab-scale and the commercial film blowing line have experienced the same thermo-mechanically history.

Minoshima and White [1986a,1986b] investigated a series of LLDPE's, HDPE's and LDPE's in shear and uniaxial elongation, as well as in film blowing performance. Attention was focused on instability phenomena. Increasing long chain branching, and to a less degree, broadening the molecular weight distribution, seemed to enhance the stability during tubular film blowing. Similar results were found by White and Yamane [1987], Fleissner [1988] and Ghijssels and Ente [1990].

Fleissner also stated that too much orientation in the die is harmful since a great deal of the required strain hardening is anticipated. Although strain hardening might work as a stabilizing factor, only rather unbalanced films result (machine direction stress $\gg$ transverse direction stress).

In a collaborative study on the relation between film blowing performance and rheological properties of two LDPE's and two HDPE's, Winter [1983] found that crystallization and extensional rheology seemed to be the most important areas in laboratory testing to be used to discriminate between PE film blowing grades.

The nineties: Campbell's group in Potsdam, New York

Cao and Campbell [1990] introduced a viscoelastic plastic model, for which the traditionally kinematic boundary conditions were replaced by a rheological boundary condition, the so-called plastic elastic transition (PET). The main reason for introducing the new constitutive equation was the fact that existing viscoelastic constitutive equations (e.g. Phan Thien and Tanner, White-Metzner, UCM, Giesekus and Larson's model) predicted a continued increase of film velocity and a decrease of bubble radius once the freeze line

was exceeded (Campbell and Cao [1990]). Obviously, this is not a surprising result, since viscoelastic constitutive equations hold for polymer melts and not so much for solidifying materials, at least not with the same set of parameters. Simulations with the viscoelastic plastic model showed good agreement with experimentally observed bubble shapes by Gupta [1980]. The material parameters had to be altered, however, to reach this achievement (compare e.g. Luo and Tanner [1985]). Furthermore, their PET does not have to coincide with the freeze line, meaning that the material can exhibit plastic behaviour even when it is still in the molten phase.

Ashok and Campbell [1992] performed a two phase simulation of tubular film blowing using the viscoelastic plastic model. In this two phase modelling, the film is divided into a liquid part, a solid-liquid part and finally a solid part. Although, the polymer can be partly in the liquid phase and partly in the solid phase across the film thickness, the temperature gradients in the radial direction were ignored. One of the major drawbacks of the model is that in simple shear flow the model reduces to the Upper Convected Maxwell model. Therefore, in simulating the film blowing process the flow in the annular die can not be taken into account, since the normal stresses at the die would become too high to obtain reasonable results. In the simulations performed with the two phase model, the pressure at the die, the initial angle and the initial hoop stress were therefore taken as parameters to be able to fit the correct bubble shapes. Moreover, in order to avoid the so-called die-swell problem, the calculations started at approximately 6 cm. above the die. The temperature at this height was experimentally determined. Although the model has its limitations, the predicted deformations in the film blowing process were in good agreement with experimentally observed deformations. This holds especially also for the region above the freeze line.

Babel and Campbell [1993] related mechanical properties to the plastic strain, which they defined as the strain in the film after the onset of crystallization. However, a limited set of experimental data was available and no clear correlation between plastic strain and properties could be distinguished. Nevertheless, they claimed that this plastic strain is the key factor to predicting the ultimate film properties. This idea was already stated by Farber and Dealy [1974].

In an experimental investigation on the temperature profiles, Cao, Sweeney and Campbell [1990] made a set-up to measure the bulk temperature of the film and the surface temperature simultaneously. Using an Infrared Radiation technique with a wavelength of 3.43 μm, the surface temperature was

detected, while with a wavelength of 1.8-3 μm the bulk temperature was found. They reported temperature variations across the film thickness of 15 $^{\circ}C$ for a HDPE, immediately after the die exit. This temperature variations fade away as the distance from the die increases. At the freeze line height all temperature variations have disappeared. This work suggests that simulations of the film blowing process need an incorporation of 2-D heat transfer.

Discussion

Although some authors (Farber and Dealy [1974], Babel and Campbell [1993]) claim that the key to predicting film properties is the plastic strain in the immediate neighbourhood of the freeze line, it seems more likely that the stresses at the freeze line height play a crucial role. Kanai [1987] indicated the importance of these stresses to the film properties for HDPE, while Kanai *et. al.* [1986] showed that film properties and film morphologies of films made on different film blowing lines were approximately identical if stresses at the freeze line height were kept constant. Nagasawa *et. al.* [1973], White and Cakmak [1988], Kwack *et. al.* [1988] and Choi *et. al.* [1980,1982] showed that the morphologies of blown films are correlated to the stresses at the freeze line height. Unfortunately, none of these authors did investigate the impact of stresses at the freeze line on the physical properties of the films.

With respect to the speculated importance of stresses in discriminating between the impact of the polymer feedstock and the processing conditions on film properties, it is a pity that only a few of the theorists focused on stresses in modelling the film blowing process. Many attempts have been made to describe the kinematics of the film in the bubble forming region, either with (generalised) Newtonian models (Pearson and Petrie [1970a,1970b,1970c], Han and Park [1975b], Petrie [1975], Wagner [1976b], Kanai and White [1985] and Yamane and White [1987]), viscoelastic models (Petrie [1973], Wagner [1976b], Luo and Tanner [1985], Cain and Denn [1988] and Campbell and Cao [1990]) or viscoelastic plastic models (Cao and Campbell [1990] and Ashok and Campbell [1992]). In all simulations, either the material parameters or the processing parameters had to be adapted to achieve agreement between calculations and experiments.

The only two authors who focused on predicting stresses in the film were Fisher [1983] and Gupta [1980]. Despite of the fact that Gupta used measured axial stresses to determine the material parameters, he was not

able to predict the transverse stresses satisfactory using a modified Upper Convected Maxwell model including temperature rate dependency of the relaxation times. Fisher was able to predict stresses in both directions, but had to modify the Wagner integral equation in such a way that the resulting constitutive relation was inconsistent with respect to the non linear behaviour of polymer melts in various types of flow.

1.4 Outline of the thesis

The objective of the research, reported in this thesis, is to understand the dependence of film properties on the type of polymer **and** on the processing conditions. The procedure followed to obtain this objective can be divided in two main sections:

1. Modelling aspects: attention is focused on viscoelastic constitutive models and their capability to predict experimentally observed stresses in the film during processing.

2. The impact of these stresses at the freeze line height on the ultimate properties of the films.

In Chapter 2 the rheological behaviour of the three grades of LDPE, especially selected for this study, is discussed. Experiments in the linear and the nonlinear viscoelastic region have been performed and are reported. Stresses have been measured in simple shear, uniaxial elongation, biaxial elongation and, finally, in a tapered duct. Four types of constitutive equations are used to describe these experiments: Wagner's integral equation, Phan Thien and Tanner's, Giesekus' and Leonov's differential equations. Comparison is made between the different LDPE's and between the constitutive relations.

In Chapter 3, experimental and theoretical investigations of the film blowing process are presented. On a lab-scale extruder, D=30 mm, films with various BUR's and DR's have been produced. Deformation and temperature profiles in the bubble forming region have been measured, along with the forces acting on the bubble. Using the balance equations as stated by Pearson and Petrie [1970a,1970b,1970c], the stresses in the film are determined. Taking the deformation and temperature history as an input for the constitutive equations, the stresses are calculated and compared with the experimental data for the three LDPE's selected.

Chapter 4 deals with orientation induced crystallization and the film morphologies. The basic concept of orientation induced crystallization is

treated and the impact of orientation on the ultimate blown film morphology is discussed.

In Chapter 5, the dependence of the film properties on the stresses at the freeze line height is eludicated. Optical properties and mechanical properties are separately discussed. The shrinkage of the films is calculated using the constitutive equations and the complete deformation history of the films.

Finally, in Chapter 6 the main results of the present research are summarized and suggestions for further research are given.

Chapter 2

Rheology

2.1 Introduction

In polymer processing, the rheological behaviour of polymer melts plays an important role. The thermal and deformation history that a polymer has experienced during processing may affect the microstructure in the films and therefore also the ultimate properties. For instance, in injection moulded products the flow induced residual stresses, caused by viscoelastic flow during processing, determine the anisotropy of mechanical, thermal and optical properties and influence the long term dimensional stability (Douven [1991]). The processability of a polymer is mainly determined by its rheological behaviour. For example, Minoshima and White [1986b] found that long chain branching elevated the normal stresses in shear and introduced a substantial uniaxial elongation rate hardening. This behaviour yields a stable bubble during film blowing. In contrast, however, polymers with a lower elongational viscosity can be drawn into thinner films (Winter [1983]).

Usually, material behaviour can be described by constitutive equations. Well known and limiting constitutive relations are those for a Newtonian fluid and a Hookean spring. Polymer melts exhibit nonlinear viscoelastic behaviour and consequently, the constitutive relations are complex. For an introduction of nonlinear viscoelasticity the reader is referred to the textbook by Ferry [1980]. A survey of constitutive models used for polymer melts can be found in e.g. Larson [1988]. In the research presented in this thesis four models have been selected. From the K-BKZ type of equations, the Wagner integral equation is chosen, while from the possible set of differential equations three distinct models are selected, namely Phan Thien and

Tanner's, Giesekus' and Leonov's models. In section 2.2 these constitutive relations are briefly summarized.

The experimental part will be described in section 2.3, emphasizing the differences found between the grades L1o, L1 and L8. Section 2.4 deals with the differences between the constitutive equations and their capacity to predict the rheological behaviour of the LDPE's in various types of flow, followed by a brief discussion of the results obtained (section 2.5).

2.2 Constitutive equations

In the textbooks of Larson [1988] and of Tanner [1988] the merits and demerits of various constitutive equations are discussed. Taking their approach as a guideline, four constitutive equations have been selected. They will be discussed briefly in the following section.

2.2.1 Integral models

The equation proposed by Wagner [1976a, 1977] is a modification of the K-BKZ model (Kaye [1962], Bernstein *et al.* [1963]). In the latter model, the extra stress tensor at time t is expressed as an integral over the complete deformation history. The integrand is a combination of a time dependent part and a deformation dependent part. The deformation dependent part is a sum of the Finger strain tensor and the Cauchy strain tensor, both multiplied by an energy potential. The first simplification of Wagner is the neglect of the Cauchy strain tensor. As a result, there is no second normal stress difference in simple shear flow. The second modification is the replacement of the energy potential by a nonlinearity function. The final equation is written as

$$\tau(t) = \int_{-\infty}^{t} m(t-t')h(I_1(t,t'),I_2(t,t'))C_t^{-1}(t')dt' \tag{2.1}$$

with $\tau(t)$ the extra stress tensor, t the present time at which the stress is evaluated, t' some time in the past, $m(t-t')$ the memory function, $h(I_1(t,t'),I_2(t,t'))$ the nonlinearity function, I_1 and I_2 the first and second invariant of the relative Finger strain tensor $C_t^{-1}(t')$. The memory function is completely determined if the relaxation time spectrum is known (see e.g.

Leblans [1986]). In the case a continuous spectrum is used, the memory function is given by

$$m(t-t') = \int_{-\infty}^{\infty} \frac{H(\lambda)}{\lambda} e^{-\frac{t-t'}{\lambda}} dln\lambda \tag{2.2}$$

The spectrum is given by the continuous function $H(\lambda)$, of which λ is the relaxation time and H the relaxation intensity. This spectrum can be obtained by fitting the dynamic modulus G_d and the phase angle δ measured via dynamical mechanical spectrometry. An iterative procedure to attain this spectrum is given by Booij and Palmen [1982].

If a discrete relaxation time spectrum is used, the following expression for the memory function is obtained

$$m(t-t') = \sum_{i=1}^{N} \frac{G_i}{\lambda_i} e^{-\frac{t-t'}{\lambda_i}} \tag{2.3}$$

Now the set (λ_i, G_i) is the discrete relaxation time spectrum. The best method to obtain this discrete spectrum is by fitting the storage modulus G' and the loss modulus G'' measured by dynamical mechanical spectrometry. As pointed out by Honerkamp [1989], the problem to be solved in the fitting procedure is an ill posed problem. Various authors (Honerkamp and Weese [1990], Baumgaertel and Winter [1989], Orbey and Dealy [1991]) have dealt with this problem. Zoetelief [1992] investigated four different mathematical techniques to solve this problem: linear least squares, linear least squares with regularization, Levenberg-Marquardt and the Bayesian estimation method. From a mathematical point of view, it was concluded that the Bayesian estimation method, which is used in the present research, gives the best results.

Many propositions for the nonlinearity function h have been proposed by various authors, *e.g.* Papanastasiou *et al.* [1983], Soskey and Winter [1984] and Wagner *et al.* [1979]. In the sequel, the form for h as reported by Wagner *et al.* is used

$$\begin{aligned} h(I_1, I_2) &= a\, e^{-n_1\sqrt{J-3}} + (1-a)e^{-n_2\sqrt{J-3}} \\ J &= \beta I_1 + (1-\beta) I_2 \end{aligned} \tag{2.4}$$

The parameters a, n_1 and n_2 are fitted on the nonlinear behaviour in shear. Since in shear $I_1 = I_2$, the parameter β has to be obtained from elongational experiments. To satisfy the irreversibility condition (Wagner [1979]), h should meet

$$h(t,t') = \text{minimum } h(t'',t'), \quad t' \leq t'' \leq t \tag{2.5}$$

It should be mentioned that in later work, Wagner *et al.* [1990, 1992] showed that the nonlinearity of the various components of the stress tensor are not equal. Apparently, the function h is not a scalar but a tensor.

2.2.2 Differential models

In recent years, the interest in constitutive equations in differential form has grown, partly due to the development of viscoelastic numerical simulations. Many simulations have been performed using the most simple case of the upper convected Maxwell model. The major shortcoming of this model is the impossibility to model nonlinear behaviour. From the many possible extensions of the UCM model that can include nonlinearity, here three types of differential equations have been chosen.

All of these contain more than one relaxation time, since in order to be able to describe the rheological behaviour of polymer melts reasonably, multi modes are required. In this research, for each model, 8 distinct modes have been chosen. The procedure to fit the set (λ_i, G_i) was discussed in the preceding subsection.

Giesekus equation

The Giesekus constitutive equation (Giesekus [1966,1982]) reads

$$\lambda_i \overset{\nabla}{\tau_i} + \frac{\alpha}{G_i}\tau_i^2 + \tau_i = 2\eta_i D \tag{2.6}$$

where τ_i is the extra tensor belonging to the i^{th} mode, η_i is the viscosity given by $G_i\lambda_i$ and D is the strain rate tensor. The upper convected derivative $\overset{\nabla}{\tau_i}$ is defined as

$$\overset{\nabla}{\tau_i} = \frac{D\tau_i}{Dt} - \nabla v^T.\tau_i - \tau_i.\nabla v \tag{2.7}$$

where the term $\frac{D\tau_i}{Dt}$ is the material derivative, ∇v^T the velocity gradient and ∇v the transpose of the velocity gradient. Since a multimode model is used, the total extra stress tensor is given by

$$\tau = \sum_{i=1}^{N} \tau_i \tag{2.8}$$

where N is the number of modes. It is well known that stresses calculated with the Giesekus model describe experiments in shear flows quite well. For elongational flow, the steady state viscosities reach asymptotical values at high elongation rates. Independent on the type of elongational flow (planar, uniaxial or equibiaxial) the asymptotical value reached equals $4\frac{\eta_0}{\alpha}$, where η_0 is the zero shear rate viscosity. If $\alpha = 0$, the Giesekus model reduces to the upper convected Maxwell model.

Phan Thien and Tanner equation

Phan Thien and Tanner [1977] derived a constitutive equation based on non-affine motion. It should be mentioned, however, that for all models based on non-affine motion, like the PTT and the Johnson and Segalman model (Johnson and Segalman [1977]), the Lodge-Meissner relation (Lodge and Meissner [1972], Lodge [1975]), which states that in a step strain experiment the first normal stress relaxation function $N_1(t,\gamma)$ equals γ times the shear stress relaxation function $\sigma(t,\gamma)$, is not satisfied. The equation proposed by Phan Thien and Tanner reads

$$\lambda_i \overset{\nabla}{\tau_i} + \xi(D.\tau_i + \tau_i.D) + Y(\tau_i)\tau_i = 2\eta_i D \tag{2.9}$$

In this equation a slip factor is added to the upper convected time derivative. This factor originates from the assumption of non-affine motion. The slip parameter ξ mainly determines the nonlinear behaviour in shear flow. If $\xi = 0$ the upper convected derivative is obtained, while $\xi = 1$ yields the corotational derivative and $\xi = 2$ the lower convected derivative. In shear flow the ratio of the first normal stress difference to the second normal stress difference equals $-\xi/2$, independent of the shear rate. Meissner *et al* [1989] experimentally found for a branched LDPE that this ratio equals to -0.25. Two propositions have been made for the function $Y(\tau_i)$. These are

$$Y(\tau_i) = \begin{cases} 1 + \frac{\epsilon}{G_i}\mathrm{tr}(\tau_i) & (a) \\ \\ e^{\frac{\epsilon}{G_i}\mathrm{tr}(\tau_i)} & (b) \end{cases} \tag{2.10}$$

The parameter ϵ mainly determines the rheological behaviour in elongational flows.

Clearly, these two possibilities are identical if $\frac{\epsilon}{G_i}\mathrm{tr}(\tau_i)$ remains small ($\ll 1$). At high elongation rates, however, this factor may become large and differences are observed. For example, in uniaxial elongational flow, equation (2.10 a) predicts a constant steady state viscosity for high elongation rates, while equation (2.10 b) predicts strain thinning behaviour in this range. As Laun [1984] and Dajan and Mackay [1994] reported, data in uniaxial elongation on a LDPE showed strain rate thinning behaviour at high elongation rates. Consequently, here equation (2.10 b) was chosen.

Leonov equation

Leonov [1976,1987] relates the stress tensor σ to the elastic strain tensor ${C_e}^{-1}$. In its simplest form the model reduces to

$$\begin{aligned} &\overset{\nabla}{{C_e}^{-1}} + \tfrac{1}{2\lambda_i}({C_e}^{-1}.{C_e}^{-1} - I - \tfrac{1}{3}(\mathrm{tr}({C_e}^{-1}) - \mathrm{tr}(C_e)){C_e}^{-1}) = 0 \\ &\sigma_i = G_i {C_e}^{-1} \end{aligned} \tag{2.11}$$

where $\overset{\nabla}{{C_e}^{-1}}$ denotes the upper convected time derivative of ${C_e}^{-1}$ and C_e is the inverse of ${C_e}^{-1}$. The stress tensor σ_i is related to the extra stress tensor τ_i according to

$$\tau_i = \sigma_i - G_i I \tag{2.12}$$

Apart from a relaxation time spectrum no fit parameters are present in this model. So, to determine the rheological behaviour for the Leonov model experiments in the linear viscoelastic region are sufficient.

In planar flows, including simple shear and planar elongation, the Leonov model reduces to the Giesekus model with $\alpha = 0.5$. For uniaxial elongation an asymptotical value for the viscosity is reached at high elongation rates, given by $6\eta_0$. For biaxial elongation the viscosity at high elongation rates reaches the asymptote $\eta_0\sqrt{\frac{12}{\epsilon\lambda_i}}$.

2.2.3 General remarks

For all models the relaxation time spectrum should be fitted on dynamical mechanical experiments (DMS) in the linear viscoelastic region. Since in that region all models predict identical behaviour, this spectrum is independent of the model used.

Obviously, the parameters taking care for nonlinear behaviour should be fitted on experiments in the nonlinear viscoelastic region. An overview of the experiments needed to fit the various parameters is given in table 2.1.

model	DMS	Shear	elongation
Wagner	λ_i, G_i	a, n_1, n_2	β
Giesekus	λ_i, G_i	α	
PTT	λ_i, G_i	ξ	ϵ
Leonov	λ_i, G_i		

Table 2.1: Experiments needed to fit the nonlinearity parameters of the constitutive models discussed.

The rheological behaviour of polymer melts is temperature dependent. For thermo-rheologically simple materials like PolyEthylene this dependence can be obtained from the time-temperature superposition principle (see e.g. the textbook of Ferry [1980]). The change in relaxation time and modulus, with varying temperature is assumed to behave according to

$$\begin{aligned} \lambda(T) &= a(T, T_{ref})\lambda(T_{ref}) = a_T\lambda(T_{ref}) \\ G(T) &= \frac{\rho(T)T}{\rho(T_{ref})T_{ref}} G(T_{ref}) = c_T G(T_{ref}) \end{aligned} \tag{2.13}$$

where T is temperature, T_{ref} is the reference temperature corresponding to the temperature of the so called mastercurve, a_T the horizontal shift factor and c_T the vertical shift factor. The vertical shift is due to thermal expansion and for many polymers close to unity and therefore often omitted. However, for LPDE it is known that the vertical shift factor is of considerable magni-

tude and can not be neglected. The horizontal shift factor a_T is assumed to behave according to the Arrhenius equation (Ferry [1980])

$$a_T = a(T, T_{ref}) = e^{\frac{E_A}{R_G}(\frac{1}{T} - \frac{1}{T_{ref}})} \tag{2.14}$$

with R_G the universal gas constant and E_A the material dependent flow activation energy.

2.3 Experimental

A review of the type of experiments performed in the linear and the nonlinear regime, the obtained quantities and the equipment employed, is given in table 2.2. Additionally, for LDPE L1o, flow birefringence experiments have been performed in a tapered duct. In the following sections the experimental results are discussed.

Experiment	Measured quantity	Apparatus
	Linear viscoelastic	
Dynamical mechanical spectrometry	Dynamic modulus G_d Loss angle δ Loss modulus G'' Storage modulus G'	Rheometrics RDA II
Step strain	Relaxation modulus $G(t)$	Rheometrics RMS 800
	Shear	
Start-up flow	Shear stress growth coefficient $\eta^+(t)$ First normal stress growth coefficient $\psi^+(t)$	Rheometrics RMS 800
Cessation of steady shear flow	Shear stress decay coefficient $\eta^-(t)$ First normal stress decay coefficient $\psi^-(t)$	Rheometrics RMS 800
Steady shear flow in capillary	Steady state viscosity $\eta(\dot{\gamma})$	Göttfert Rheograph
	Uniaxial elongation	
Tensile start-up flow	Tensile stress growth coefficient $\eta_E{}^+(t)$	Göttfert Rheostrain
	Biaxial elongation	
Tensile start-up flow	Tensile stress growth coefficient $\eta_B{}^+(t)$	Squeeze flow apparatus

Table 2.2: Rheological experiments performed on LDPE L1o, L1 and L8.

2.3.1 Sample preparation

Samples for the experiments with the RDA II and RMS 800 were compression moulded at 170 ^{o}C applying 8.3 $10^4 Pa$ for 5 minutes, followed by 8.3 $10^5 Pa$ for 5 minutes. The samples were cooled to room temperature at a pressure of 3.1 $10^6 Pa$ in a time span of 20 minutes. Samples for uniaxial and biaxial elongation were compression moulded at 160 ^{o}C applying 6.7 $10^4 Pa$ for 7 minutes, followed by 6.7 10^5 for 5 minutes and 3.4 $10^6 Pa$ for 5 minutes. The samples were cooled to room temperature at 3.4 $10^6 Pa$.

2.3.2 The rheological behaviour in shear

Dynamical mechanical spectrometry. On all three samples dynamical mechanical spectrometry has been performed on a Rheometrics RDA II. In a parallel plate geometry (diameter 25 mm, thickness $\pm$ 2 mm) dynamic modulus and loss angle have been measured at temperatures varying from 110 ^{o}C to 230 ^{o}C with temperature steps of 20 ^{o}C. A gas connected oven was used, heated via nitrogen gas. Time temperature shifting (Ferry [1980]) yielded master curves at a reference temperature 190 ^{o}C and horizontal and vertical shift factors were deduced. In figure 2.1 the master curves are depicted. The moduli of LDPE L1o and L1 are almost equal. The phase angle of L1 seems to be a little lower than the phase angle of L1o. Clearly, LDPE L8 has a lower modulus and a higher phase angle, which indicates that this grade exhibits a more viscous behaviour than L1o and L1.

Following the procedure proposed by Booij and Palmen [1982], the continuous relaxation time spectra, shown in figure 2.2, have been determined. Clearly, grade L8 exhibits the least amount of long relaxation times. Small differences are observed in the spectra of L1o and L1. Because of the slightly lower phase angle of L1, this grade shows somewhat more long relaxation times than L1o. The differences are, however, small.

Table 2.3 contains the discrete relaxation time spectra. They have been calculated using the Bayesian estimation method reported by Zoetelief [1992]. The fit on the loss and storage moduli G'' and G' of L1o with the discrete spectrum is shown in figure 2.3. The irregular curve of the fitted line is due to the limited number of modes. Furthermore it is observed that for high frequencies, G' is overpredicted while G'' is underpredicted (see also Laun [1978]).

The flow activation energies E_A were 66 $kJ/mole$ for grades L1 and L1o and 59 $kJ/mole$ for grade L8.

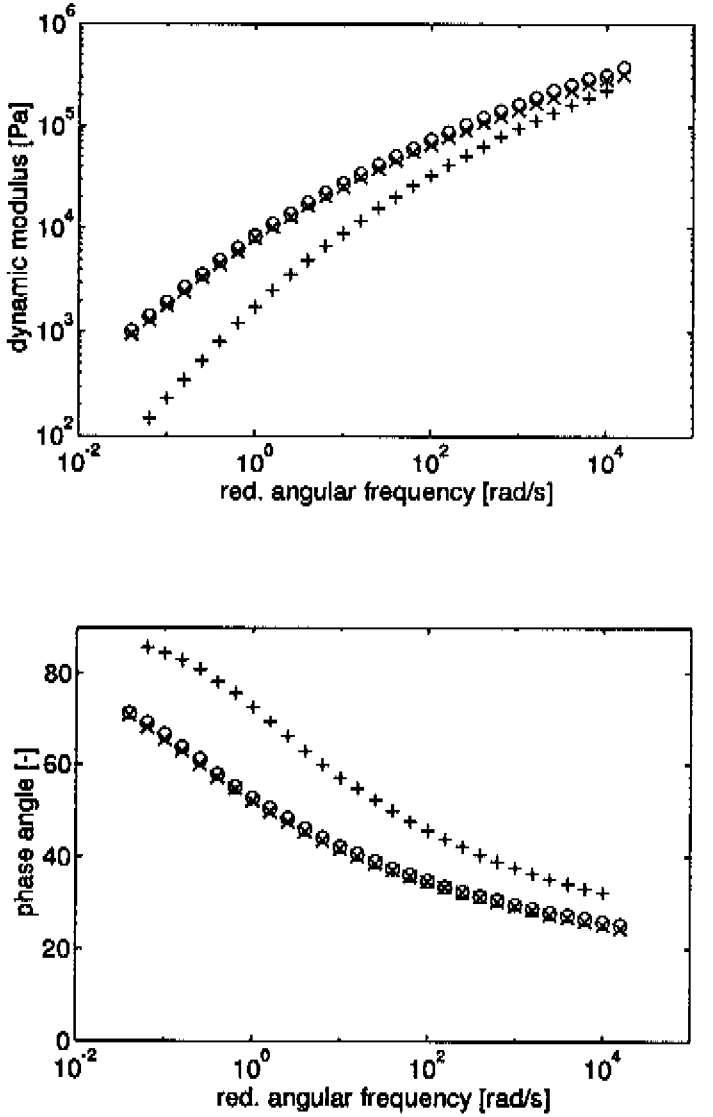

Figure 2.1: Master curves at 190 ^oC for dynamic modulus G_d and phase angle δ for L1o (o), L1 (x) and L8 (+).

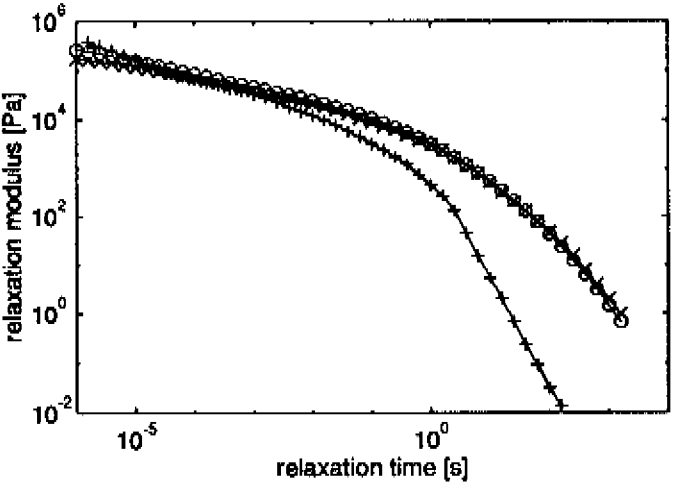

Figure 2.2: Continuous relaxation time spectra at 190 °C for L1o (o), L1 (x) and L8 (+).

L1o		L1		L8	
λ_i	G_i	λ_i	G_i	λ_i	G_i
7.70e-5	2.72e5	6.07e-5	2.29e5	4.28e-5	2.17e5
7.05e-4	1.05e5	4.29e-4	9.51e4	2.07e-4	9.18e4
5.13e-3	6.02e4	2.41e-3	5.65e4	1.34e-3	5.75e4
3.59e-2	3.16e4	1.35e-2	3.33e4	9.02e-3	2.43e4
2.42e-1	1.37e4	7.29e-2	1.78e4	5.69e-2	8.91e3
1.58e0	4.52e3	3.94e-1	8.41e3	3.53e-1	2.34e3
1.01e1	1.01e3	2.04e0	3.28e3	1.82e0	3.21e2
7.20e1	1.46e2	1.24e1	9.57e2	9.94e0	1.24e1

Table 2.3: Discrete relaxation time spectra at 190 °C.

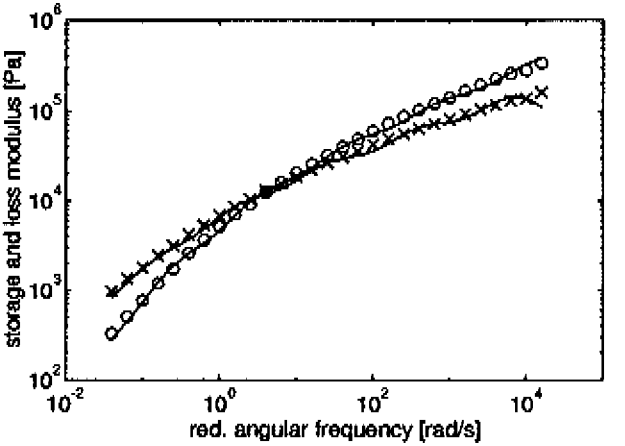

Figure 2.3: Fits on storage modulus G' and loss modulus G'' at 190 ^oC with discrete spectrum for L1o. G' experimental (o), G'' experimental (x), fit with spectrum (–).

Step strain. At 190 ^oC, again in a nitrogen environment, step strain experiments have been performed in a parallel plate geometry (diameter=25 mm, thickness $\pm$ 2 mm) on a Rheometrics RMS 800. At time $t = 0$ a sudden strain is imposed on the sample and the stress relaxation curve is measured. Experiments have been performed in the linear viscoelastic range. In figure 2.4 the relaxation moduli $G(t)$ are presented. Symbols are measured points, the full lines are fitted curves using the continuous relaxation time spectrum

$$G(t) = \int_{-\infty}^{\infty} H(\lambda) e^{-\frac{t}{\lambda}} dln\lambda \tag{2.15}$$

Obviously, grade L8 exhibits the most rapid decay, which is in accordance with the absence of long relaxation times. At short times it is seen that L1 has a lower modulus than L1o. This is in agreement with the lower dynamic modulus G_d of L1 at high frequencies (compare figure 2.1). At long times, the curves of both L1o and L1 coincide. The expectation is that for even longer times, the curves will cross due to the presence of longer relaxation times of grade L1. Unfortunately, measurements in this range could not be performed because of the limited sensitivity of the transducer.

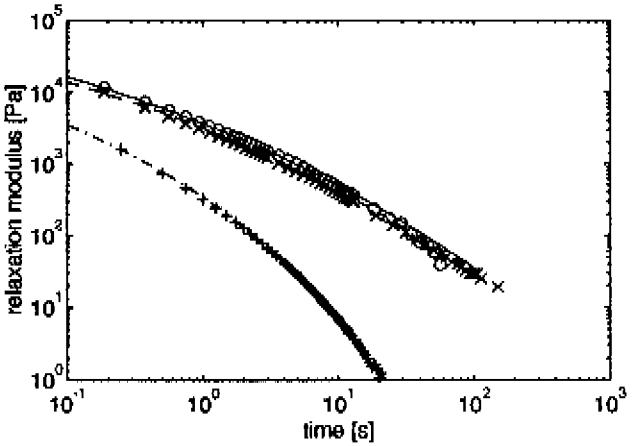

Figure 2.4: Shear stress relaxation modulus $G(t)$ at 190 ^oC for L1o (o: experimental, —: fit), L1 (x: experimental, - -: fit) and L8 (+: experimental, - .: fit).

Start-up flow and cessation of steady shear flow. Constant shear rate experiments have been performed on a RMS 800. Samples were sheared in a cone plate geometry, diameter 25 mm, cone angle 0.1958 radians, at 190 ^oC under nitrogen. At time $t = 0$ the samples were sheared at a constant shear rate. For grades L1o and L1 shear rates were 0.04, 0.1, 0.16, 0.25, 0.4, 0.63, 1, 1.6 and 2.5 s^{-1}. Because of the lower viscosity of grade L8, shear rates for this grade were 1.6, 2.5, 4, 6.3, 10, 16 and 25 s^{-1}. At time $t = 80/\dot{\gamma}$ the deformation was stopped and the relaxation of the viscosity and the normal stress coefficient was measured.

Results of the stress growth experiments are shown in figure 2.5. For convenience, not all shear rates are plotted. The solid lines are the predictions of linear viscoelastic theory

$$\begin{aligned} \eta^+(t) &= \int_{-\infty}^{\infty} H(\lambda)\lambda(1-\epsilon^{-\frac{t}{\lambda}})dln\lambda \\ \psi^+(t) &= 2\int_{-\infty}^{\infty} H(\lambda)\lambda^2(1-\epsilon^{-\frac{t}{\lambda}}-\tfrac{t}{\lambda}\epsilon^{-\frac{t}{\lambda}})dln\lambda \end{aligned} \tag{2.16}$$

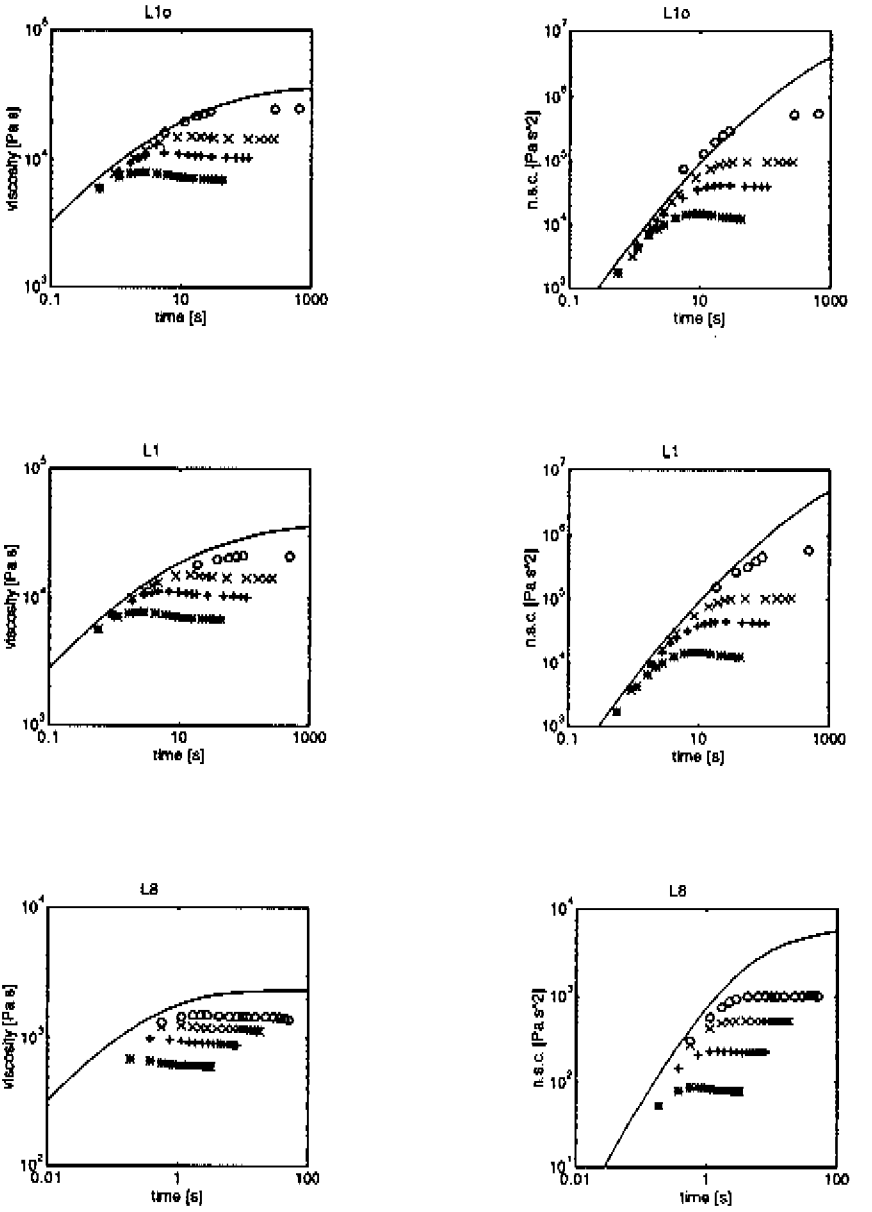

Figure 2.5: Shear stress growth coefficient $\eta^+(t)$ and first normal stress growth coefficient $\psi^+(t)$ at 190 ^oC for: L1o and L1, $\dot{\gamma}$=0.04 (o), 0.25 (x), 0.63 (+) and 1.6 s^{-1} (*); L8, $\dot{\gamma}$=1.6 (o), 4 (x), 10 (+) and 25 s^{-1} (*). Full lines are predictions for linear viscoelastic behaviour.

No significant difference is seen between grades L1o and L1. For all three grades, a distinct deviation from linear viscoelastic behaviour is observed. Even at the lowest shear rates applied to the different samples the materials show nonlinear behaviour.

Because the samples behave linear viscoelastic at short times, it is expected that at these times theory and experiments should coincide. At these times, however, a moderate difference between theory and experiments is observed. As for the normal stress coefficient, this effect might be explained by the possible presence of radial flow in the cone-plate (Laun [1986]). For the discrepancy in the viscosity $\eta^+(t)$, no explanation is present. Support is, however, found in Laun's results (Laun [1984]), which showed the same phenomenon. A possible explanation could be the discrepancy between the desired and the actual deformation. A second possible explanation is given by Attané *et al.* [1988], who claimed that a minimum time t_s is required before the measurements of the torque are reliable. This time t_s depends on plate-radius, cone angle, zero shear rate viscosity and compliances of the transducers. For the experiments reported here, this time t_s was, however, calculated to be less than 10^{-2} seconds.

The relaxation of the viscosity and the normal stress coefficient, is given in figure 2.6. The solid lines denote the linear viscoelastic predictions

$$\begin{aligned} \eta^-(t) &= \int_{-\infty}^{\infty} H(\lambda)\lambda e^{-\frac{t}{\lambda}} d\ln\lambda \\ \psi^-(t) &= 2\int_{-\infty}^{\infty} H(\lambda)\lambda^2 e^{-\frac{t}{\lambda}} d\ln\lambda \end{aligned} \tag{2.17}$$

Again, not much difference is obtained between the grades L1o and L1. The relaxation of grade L8 is much faster because of the lack of long relaxation times. As expected, because from figure 2.5 it is seen that even at time $t = 0$ the shear stress and the normal stress are overpredicted by the linear viscoelastic theory, the theoretical lines exceed the experiments to a great extent.

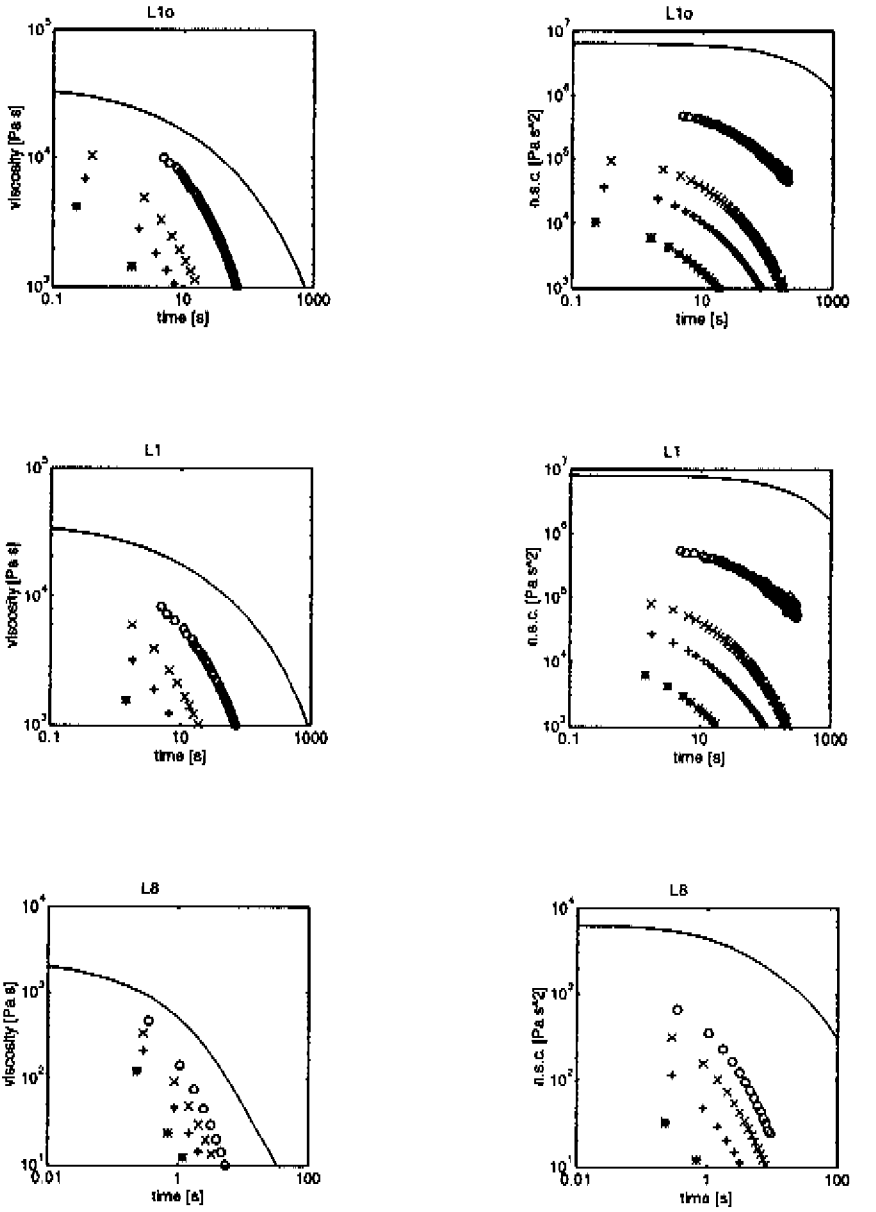

Figure 2.6: Shear stress decay coefficient $\eta^-(t)$ and first normal stress decay coefficient $\psi^-(t)$ at 190 ^oC for: L1o and L1, $\dot{\gamma}$=0.04 (o), 0.25 (x), 0.63 (+) and 1.6 s^{-1} (*); L8, $\dot{\gamma}$=1.6 (o), 4 (x), 10 (+) and 25 s^{-1} (*). Full lines are predictions for linear viscoelastic behaviour.

Capillary Rheometry. On a Göttfert Rheograph, viscosity curves have been measured at 190 ^oC. Bagley and Rabinowitsch corrections have been applied (see for instance the textbook by Collyer and Clegg [1988]). Results are shown in figure 2.7. To be able to compare the results to dynamic measurements, the shear stress is plotted as a function of the shear rate.

In contrast with dynamic moduli (see figure 2.1), the shear stress of grade L1 is slightly higher than the stress of grade L1o. If the Cox-Merz rule [1958], which reads

$$G_d(\omega) = \sigma(\dot{\gamma}) \quad \text{at} \quad \omega = \dot{\gamma} \tag{2.18}$$

is checked, it is observed that the shear stresses from capillary measurements are exceeding the dynamic moduli. This can be described to the moderate nonlinearity of PolyEthylenes (Booij *et al.* [1983]).

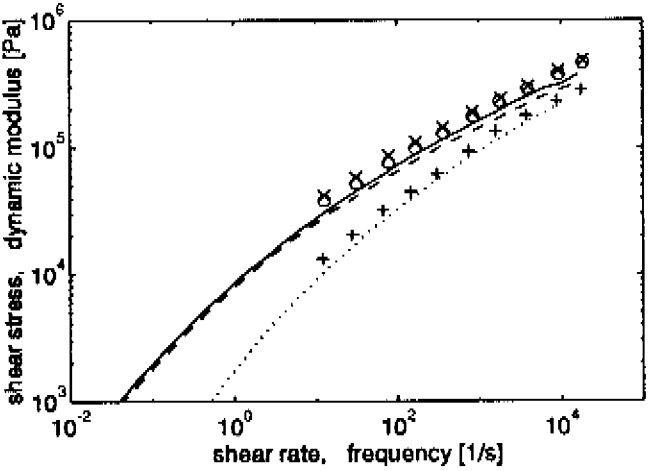

Figure 2.7: Flow curves at 190 ^oC for L1o (o), L1 (x) and L8 (+), as obtained from capillary experiments. Dynamic moduli L1o (—), L1 (- -), L8 (..).

2.3.3 The rheological behaviour in elongation

Tensile start-up flow in uniaxial elongation. Uniaxial elongation experiments have been performed on a uniaxial stretching apparatus of the conventional clamp type (Petrie [1979]), the Göttfert Rheostrain. Constant strain rate experiments have been performed at various Hencky strain rates. Cylindrical samples of diameter 5 mm and length ± 25 mm were stretched in a silicon oil bath. The oil had approximately the same density as the samples. Before starting a test, the samples were held in the heated oil bath for about 5 minutes, in order to allow complete stress relaxation. Testing temperature for the grades L1o and L1 was 150 $^{\circ}C$, for grade L8 130 $^{\circ}C$. Because of the low viscosity of L8, gravitational effects are likely to occur at higher temperatures.

Results of the experiments are shown in figure 2.8. Drawn lines are the zero elongation rate viscosities as predicted by the continuous relaxation time spectrum. These equal three times the zero shear rate viscosities as given by equation (2.16). Clearly, no steady state is achieved in any experiment. This does not mean that no steady viscosity value exists, as they have been measured by Laun [1984]. In our experiments no steady plateau is reached due to geometrical limitations of the Rheostrain.

Although the temperature for grade L8 was low, viscosity levels are beneath the levels of the two other grades. Note that for grades L1o and L1 only strain rates 0.05 s^{-1} and 0.1 s^{-1} can be compared. The viscosity level of grade L1 seems to be higher than the viscosity of grade L1o for both rates. So in elongation these two grades seem to differ slightly, whereas in shear no differences were observed. The higher elongational viscosity of L1 might be important in film blowing, as, for example, Ghijsels and Ente [1990] showed that a high uniaxial elongational viscosity goes along with better stability in film blowing.

Tensile start-up flow in biaxial elongation. Constant biaxial elongation rate experiments were performed using the lubricated squeezing flow technique (see e.g. Soskey and Winter [1985]). A compression moulded disk of diameter 25 mm, thickness 2mm is placed between two parallel plates, placed in a silicon oil bath in order to enhance lubrication between sample and plates. If perfect lubrication is achieved, no contribution of shear stresses is measured. Although Hsu and Harrison have reported successful biaxial measurements, using this technique, on a PolyStyrene melt (Hsu and Harrison [1991]), in our experiments repeatedly the lubricant was squeezed

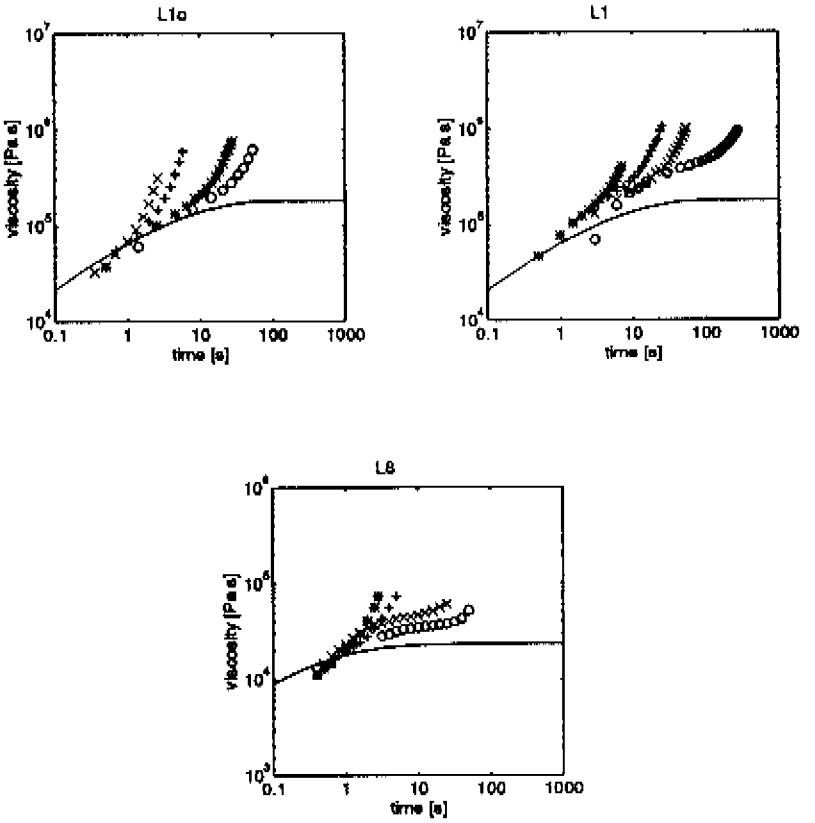

Figure 2.8: Tensile stress growth coefficient $\eta_E^+(t)$ for: L1o, $\dot{\epsilon}$=0.05 (o), 0.1 (x), 0.5 (+) and 1 s^{-1} (*), T=150 °C; L1, $\dot{\epsilon}$=0.01 (o), 0.05 (x), 0.1 (+) and 0.25 s^{-1} (*), T=150 °C; L8, $\dot{\epsilon}$=0.05 (o), 0.1 (x), 0.5 (+) and 1 s^{-1} (*), T=130 °C. Full lines are predictions for linear viscoelastic behaviour.

out the plane between sample and plates at total strains of about 0.5. Therefore, only reliable results could be obtained at small deformations where the materials exhibit linear viscoelastic behaviour. Since this behaviour does not give any significant information, the results are not discussed in fuller detail.

2.3.4 Flow birefringence in a tapered duct

For grade L1o flow induced birefringence has been recorded in the flow through a tapered duct with contraction ratio 3:1 (see figure 2.9). where the flow is in the x direction. The temperature was set to 190 ^{o}C. Flow rates were 6.4 $10^{-9}m^3/s$ and 17.2 $10^{-9}m^3/s$, yielding average deformation rates of approximately 0.13 s^{-1} and 0.35 s^{-1}.

The flow in the duct is a combination of shear and planar extension. So, measurements of the stresses in the flowing melt will give an idea of the capability of the constitutive equations to describe such a complex flow. Therefore, finite element simulations were performed.

An extensive description of the experimental work is found in the master's thesis of de Bie [1994]. Velocities have been measured using laser Doppler anemometry. For the evaluation of the Wagner model, the velocities at the centerline were used to calculate the elongational stresses, using the trapezium rule to compute the resulting integral.

To determine the stresses, the flow birefringence has been recorded. According to the stress optical rule the birefringence is linearly related to the stresses (see e.g. Janeschitz-Kriegl [1983]). Since for PolyEthylene more than one value for the stress optical coefficient C is reported (Wales [1976], for

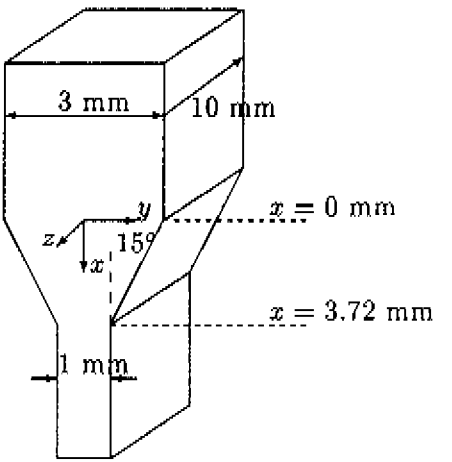

Figure 2.9: Geometry of the tapered duct.

instance, concluded that C depends on the amount of long chain branching), it is a priori not clear what value should be taken. Therefore, experiments have been performed to determine the stress optical coefficient of grade L1o (Gurp *et al.* [1993]).

At two flow rates, birefringence of the flowing melt in a rectangular slit, with cross sectional area 10 x $1mm^2$, has been recorded. Using a Carreau-Yasuda model

$$\eta(\dot{\gamma}) = \eta_0(1 + (\lambda\ \dot{\gamma})^a)^{\frac{n-1}{a}} \tag{2.19}$$

stresses have been calculated for a fully developed shear flow. Parameters for the Carreau-Yasuda model at 190 ^oC are η_0 =3.9 $10^4 Pas$, λ = 2.58s, a = 0.41 and n = 0.31. Using the calculated shear stresses and the measured birefringence, the stress optical coefficient has been determined determined. With increasing flow rate (Q=6.5 $10^{-9}m^3/s$ and Q=15 $10^{-9}m^3/s$), values obtained for C decreased from 1.66 $10^{-9}Pa^{-1}$ to 1.50 $10^{-9}Pa^{-1}$. For the flow in the tapered duct the mean value 1.58 $10^{-9}Pa^{-1}$ was taken. In figure 2.10 the results of the calculations in the rectangular slit are shown, along with the experimentally determined shear stresses.

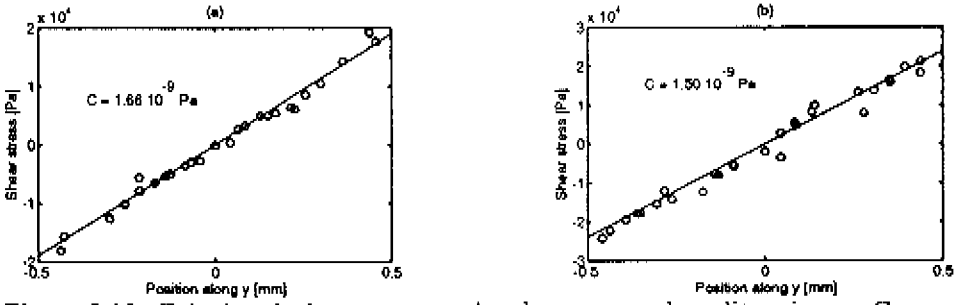

Figure 2.10: Calculated shear stresses in the rectangular slit using a Carreau-Yasuda equation (—) and measured shear stresses (o) for LDPE L1 at 190 ^oC. Output rates 6.5 $10^{-9}m^3/s$ (a) and 15 $10^{-9}m^3/s$ (b).

With the viscoelastic module of the finite element package SEPRAN (Zanden [1990]), calculations were performed using the different constitutive equations of the differential type. Pressure, stresses and velocities were calculated. An extensive description of the numerical methods used can be

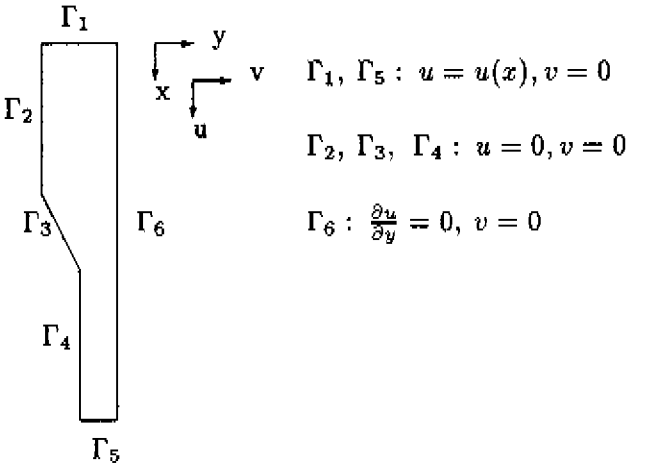

Figure 2.11: Boundary conditions for finite element calculations of flow through a tapered duct.

found in the Ph.D. thesis of Hulsen [1988] and in a paper by Hulsen and van der Zanden [1991]. The discretization methods used are

- the finite element method ($P_2{}^+ - P_1$ Crouzeix-Raviart elements) for the equations of motion
- numerical integration of the constitutive equations along the streamlines

In the simulations, a 2-D flow is assumed with the z axis the neutral direction. Because of symmetry only one half of the die is modelled. The boundary conditions are depicted in figure 2.11. The inflow length (Γ_2) and the outflow length (Γ_4) were $2L$ and $5L$ respectively , where L is the length of the converging part (3.72 mm). Taking the inflow length $4L$ and outflow length $7L$ did not affect the numerical results. At the inflow boundary (Γ_1) and the outflow boundary (Γ_5) a fully developed shear flow was prescribed. The mesh was optimized such that no mesh dependency was detected. Results of the measurements and calculations are discussed in section 2.4.4.

2.3.5 Conclusions

To summarize this experimental part (minus the birefringence measurements) the main conclusions are listed below:

- Given its low molecular weight, it is not surprising that grade L8 shows the least elastic features in all types of flow. This is clearly seen in the absence of long relaxation times and the stress levels in shear and elongation are far below the levels reached by grades L1o and L1.
- In shear flow no significant differences are observed between grade L1o and grade L1. In uniaxial elongation, grade L1 exhibits a slightly stronger strain hardening behaviour than grade L1o.
- In accordance with the elongational data, a slightly lower phase angle in the DMS measurements indicates that grade L1 exhibits somewhat more long relaxation times than grade L1o.
- Biaxial elongational viscosities in the nonlinear region could not be measured using the lubricated squeezing flow technique since the lubricant was squeezed out between the samples and the plates before nonlinearity started to play any role.

2.4 Model predictions in various types of flow

In this section the different constitutive models are subjected to some further research. The various fit parameters are presented, differences between the models are investigated and the capacity of the models to describe various types of flow is discussed.

2.4.1 Model parameters

The relaxation time spectra used were already presented in table 2.3. Consequently, the linear viscoelastic behaviour is completely captured. The parameters which enable the various constitutive equations to describe nonlinear behaviour are given in table 2.4.

Model	parameter	L1o	L1	L8
Wagner	a	0.96	0.92	0.92
	$n1$	0.25	0.25	0.21
	$n2$	0.04	0.04	0.07
	β	0.06	0.08	0.06
PTT	ξ	0.15	0.13	0.13
	ϵ	0.05	0.05	0.05
Giesekus	α	0.35	0.28	0.31
Leonov				

Table 2.4: Nonlinearity parameters for LDPE L1o, L1 and L8 for various constitutive models.

In shear, they have been determined such that visually the best fit was obtained in stress growth experiments at various shear rates. In uniaxial elongation the procedure is rather dubious, since the parameters mainly determine the steady state viscosity levels. As seen before, no steady state has been measured and in the fitting procedure adapted it had to be assumed that steady state is reached at a level just above the measured curves.

Remarkable is the difference in the parameter α of the Giesekus model for grades L1o and L1. This parameter is fitted on stress growth experiments in shear. Since no differences between these two grades were observed in their nonlinear behaviour in shear, it is expected that the parameter α should have the same value for both grades. However, in the determination of parameter α for grade L1 a problem arised which was not encountered for

grade L1o. The viscosity growth was overpredicted, while the normal stress growth coefficient was underpredicted. The parameter α was chosen such that both viscosity and normal stress coefficient were predicted satisfactory, leading to a value which differs from α for grade L1o. The differences in the parameters a of the Wagner model and ξ of the PTT model can be explained in a similar way.

If the parameter α of the Giesekus model equals 0.5, Giesekus and Leonov give the same predictions in shear flow. Since for none of the LDPE's this is the case, the Leonov predictions in shear slightly differ and proved to be not as good as the Giesekus predictions.

2.4.2 The rheological behaviour in shear

Here the model predictions in shear flow are presented. Since the purpose of this section is to compare the different models, only results for grade L1 are shown. Figure 2.12 demonstrates the shear stress growth coefficient $\eta^+(t,\dot{\gamma})$, figure 2.13 the first normal stress growth coefficient $\psi^+(t,\dot{\gamma})$, figure 2.14 the shear stress decay coefficient $\eta^-(t,\dot{\gamma})$ and, finally, figure 2.15 demonstrates the first normal stress decay coefficient $\psi^-(t,\dot{\gamma})$.

It is well known that the Wagner integral equation describes the rheological behaviour of polymer melts in shear well (Leblans [1986], Tanner [1988]). Indeed, this can be seen in figures 2.12-2.15. This especially holds for the relaxation of the viscosity and the first normal stress coefficient after cessation of shear flow: compare with the description of the differential models in figures 2.14 and 2.15.

Because of the introduction of the slip parameter ξ in the PTT model, oscillations in $\eta^+(\dot{\gamma})$ and $\psi^+(\dot{\gamma})$ occur, as can be seen in figures 2.12 and 2.13. These oscillations grow in magnitude with increasing shear rate and fade away with increasing time. For numerical simulations of stationary problems this does not give any problem, but for instationary problems the oscillations might be deceptive. Compared to Giesekus' and Leonov's models, the PTT model predicts the stress relaxation after shear quite well. However, Wagner's model is still superior.

Although all four models predict the experimental results in shear satisfactory in the investigated range of shear rates, major differences between the various models can be seen in the prediction of the first normal stress difference at high shear rates (see figure 2.16). Unfortunately, no experimental data were available in this shear rate range.

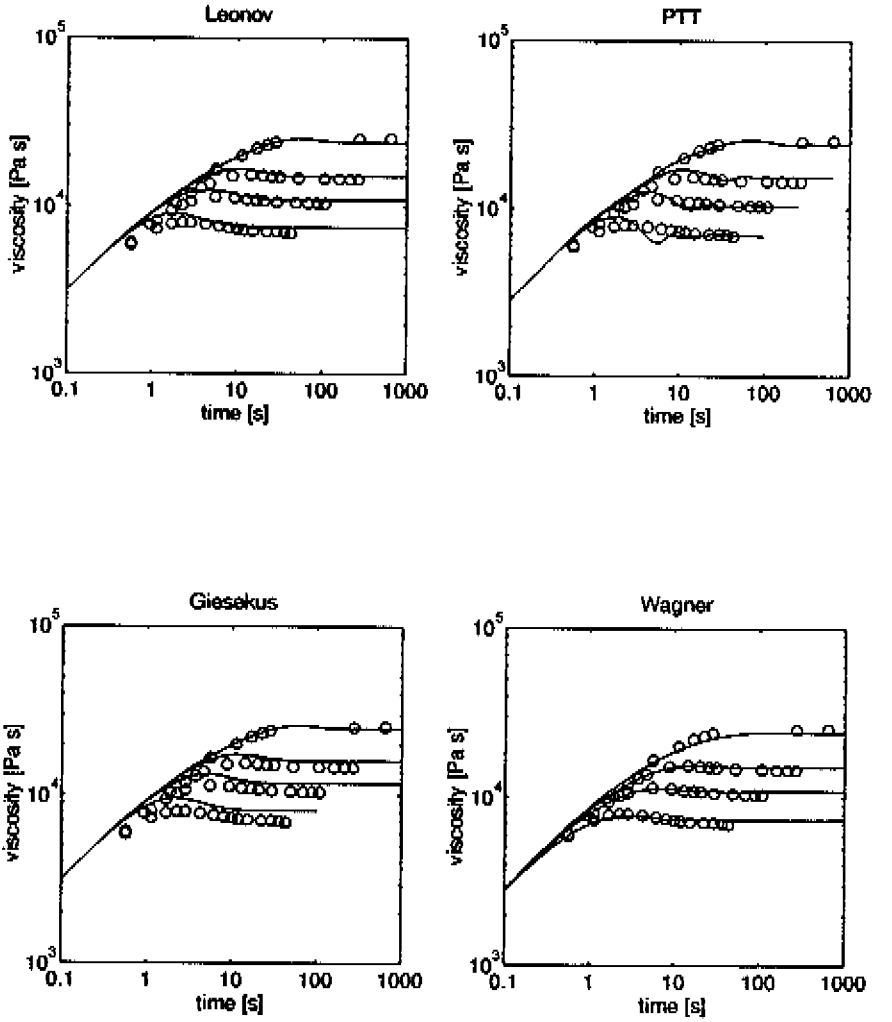

Figure 2.12: Shear stress growth coefficient $\eta^+(t)$ at 190 ^oC for L1o as predicted with the various kinds of models. $\dot{\gamma}$= $0.04s^{-1}$ (o), $0.25s^{-1}$ (x), $0.63s^{-1}$ (+), $1.6s^{-1}$ (*) and fits (--).

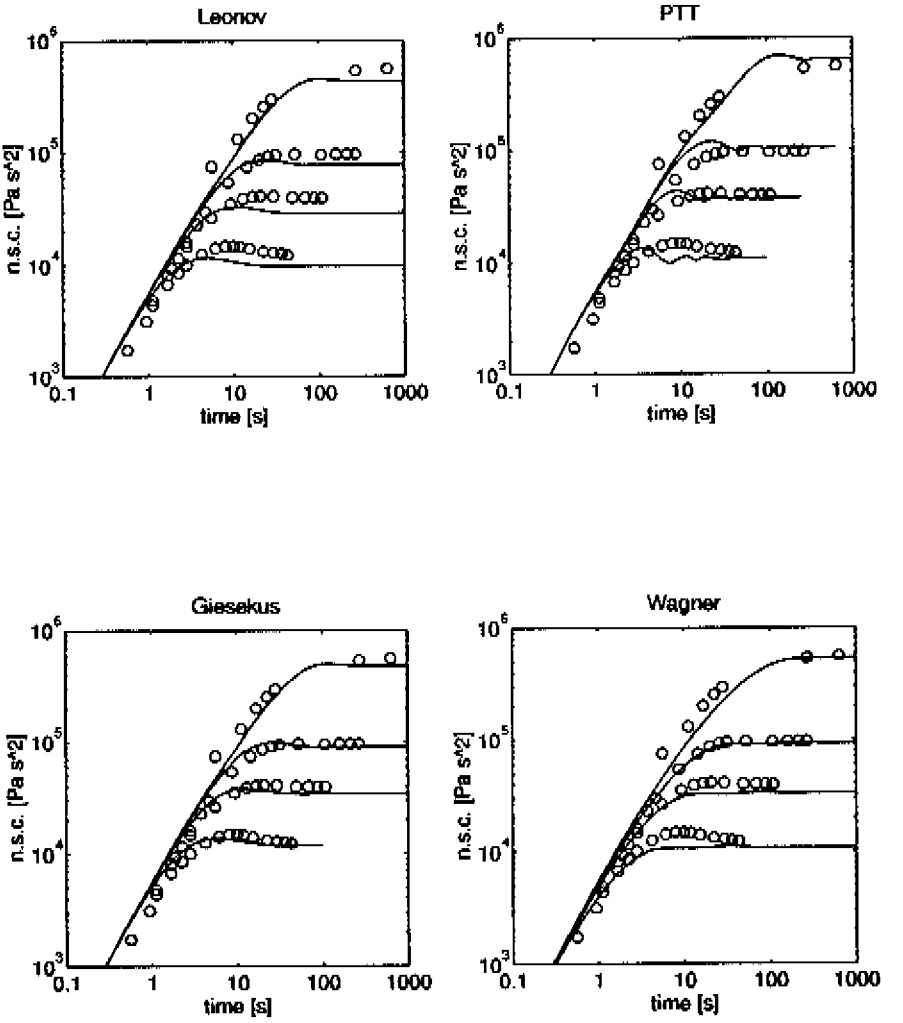

Figure 2.13: First normal stress growth coefficient $\psi^+(t)$ at 190 ^oC for L1o as predicted with the various kinds of models. $\gamma = 0.04s^{-1}$ (o), $0.25s^{-1}$ (x), $0.63s^{-1}$ (+), $1.6s^{-1}$ (*) and fits (—).

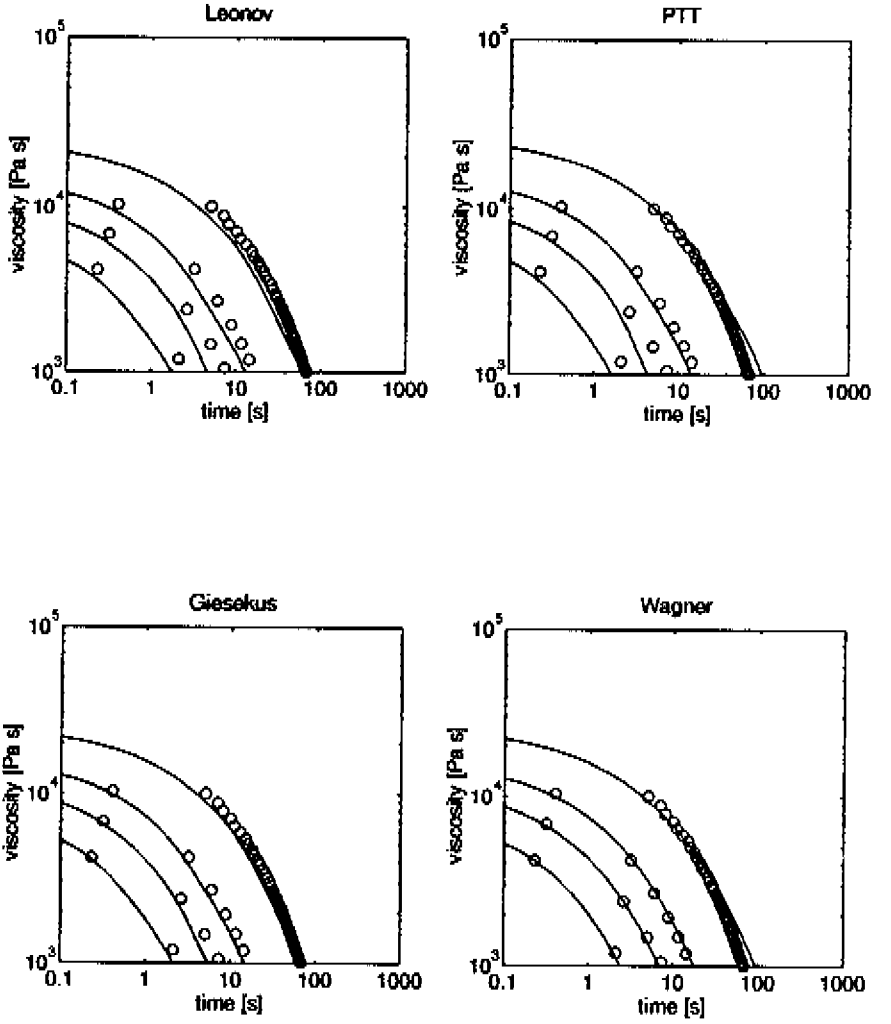

Figure 2.14: Shear stress decay coefficient $\eta^-(t)$ at 190 °C for L1o as predicted with the various kinds of models. $\dot{\gamma}$= $0.04s^{-1}$ (o), $0.25s^{-1}$ (x), $0.63s^{-1}$ (+), $1.6s^{-1}$ (*) and fits (—).

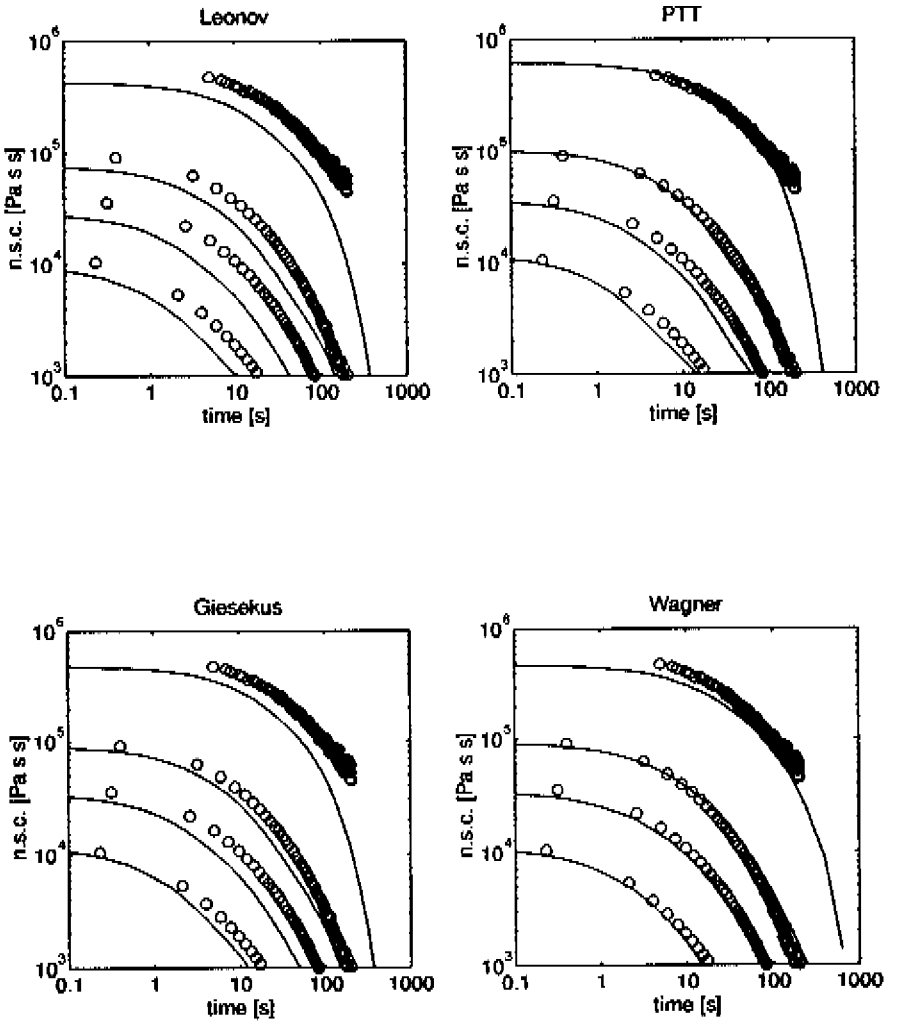

Figure 2.15: First normal stress decay coefficient $\psi^*(t)$ at 190 ^oC for L1o as predicted with the various kinds of models. $\dot{\gamma} = 0.04s^{-1}$ (o), $0.25s^{-1}$ (x), $0.63s^{-1}$ (+), $1.6s^{-1}$ (*) and fits (—).

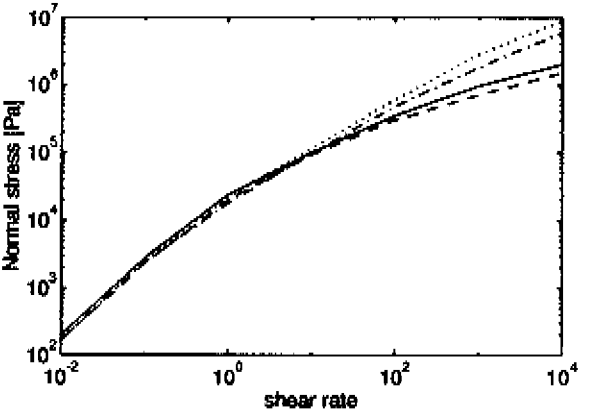

Figure 2.16: Prediction of normal stress N1 at high shear rates at T=190 $^\circ C$ for LDPE L1o. PTT (—), Wagner (- -), Leonov (- .), Giesekus (..).

2.4.3 The rheological behaviour in elongation

In figure 2.17, the model predictions in uniaxial elongational flow are depicted. Since both the Wagner model and the PTT model dispose a parameter to determine the elongational behaviour, it is not surprising that the predictions for these models show good agreement with experimental data. Although Giesekus' model and Leonov's model do not possess such a parameter, the predictions of these models also match the experiments fairly well, at least in the range investigated.

Two major differences are observed in the model predictions. First, the Wagner model predicts an overshoot before reaching a steady state level, which becomes more distinct with increasing elongation rate. It should be mentioned that it is not clear whether such an overshoot exists in experimental reality. Secondly, at high elongation rates, Wagner's model and the PTT model predict strain thinning behaviour, while Leonov's and Giesekus' models fail to describe this experimentally observed behaviour (Laun [1984]), see figure 2.18. Larson [1983] proposed a modified Leonov model which is also capable to predict strain thinning behaviour at high elongation rates. Unfortunately, in this modification an extra fit parameter is introduced, which has to be fit on elongational experiments. Consequently, the major advantage of the Leonov model that only DMS measurements are required to obtain all model parameters is then lost.

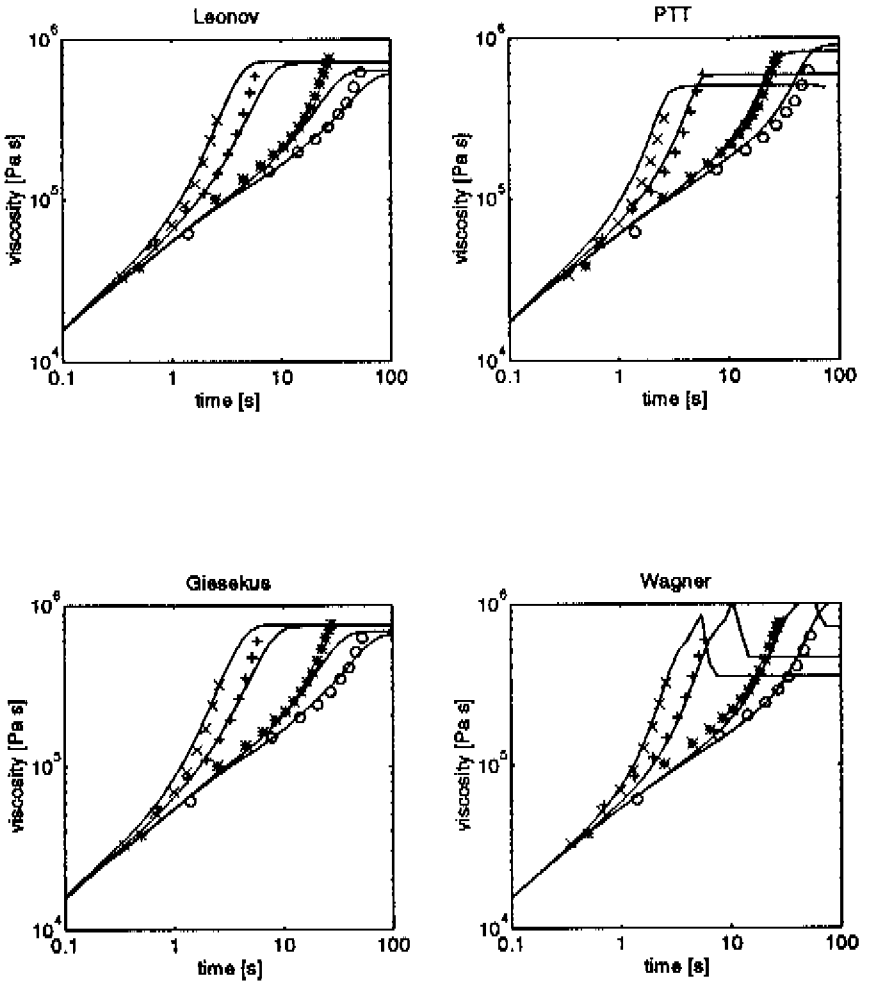

Figure 2.17: Tensile stress growth coefficient $\eta_E^+(t)$ at 190 ^oC for L1o as predicted with the various kinds of models. $\dot{\epsilon} = 0.05s^{-1}$ (o), $0.1s^{-1}$ (x), $0.5s^{-1}$ (+), $1s^{-1}$ (*) and fits (—)

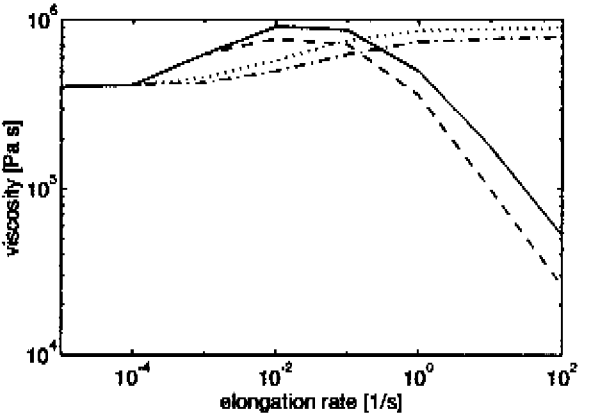

Figure 2.18: Prediction of uniaxial elongation viscosity in a broad range of elongation rates at T=190 ^oC for LDPE L1o. PTT (—), Wagner (- -), Leonov (- .), Giesekus (..).

2.4.4 Flow birefringence in a tapered duct

Integral model. For the Wagner model, a decoupled method was employed to evaluate the stresses at the centerline. The velocity was calculated with a power law model, where the power law constant was fitted on the measured velocity field. The obtained centerline velocity was used as input for the calculations of the stresses. From figure 2.19, where the stresses calculated are depicted along with the measured data, it can be concluded that the model underpredicts the experimentally determined stresses. This is in accordance with the findings of Demarmels and Meissner [1986] and Samurkas *et al.* [1989], who found that the model with nonlinearity parameters obtained from shear predicts a too much strain thinning behaviour in planar elongation.

Soskey and Winter [1985] showed that either shear and uniaxial elongation or shear and biaxial elongation could be described. The combination of shear, uniaxial elongation and biaxial elongation could not be described adequately with one set parameters. They found that the parameter β for LDPE was close to 0 in uniaxial elongation and close to 1 in biaxial elongation.

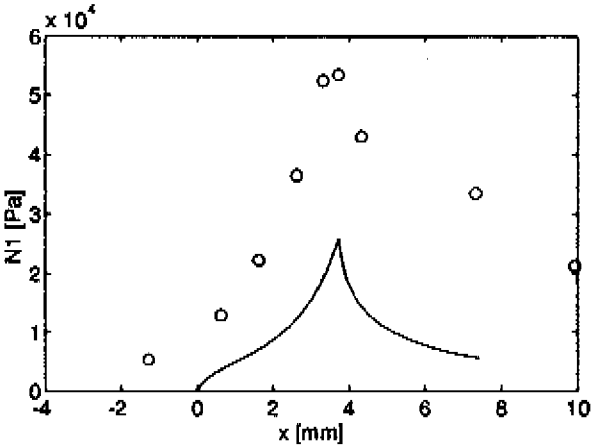

Figure 2.19: Normal stress N1 at centerline in tapered duct for LDPE L1o: measurements (o) and fits with Wagner model (—).

In recent papers, Wagner *et al.* [1990, 1992] modified the original equation according to

$$\tau(t) = \int_{-\infty}^{t} m(t-t')[H_1(t,t')C_t^{-1}(t,t') + H_2(t,t')C_t(t,t')]dt' \qquad (2.20)$$

where $C_t(t,t')$ is the relative Cauchy strain tensor. The Finger tensor $C_t^{-1}(t,t')$ and the Cauchy tensor are both multiplied with a nonlinearity function, respectively $H_1(t,t')$ and $H_2(t,t')$. Because of the incorporation of the Cauchy tensor, a second normal stress difference arises in shear flow. However, the problem that shear and planar elongation cannot be described with the same set parameters is not solved.

Differential models. Here the results of the finite element simulations of the flow through the tapered duct, using the differential models, are discussed. In figure 2.20, the stresses calculated are depicted along with the experimental data, at various cross-sections.

At the cross-section $x = 7.32$ mm the calculations for the PTT model exhibit some slight oscillations. This is due to convergence problems in the numerical code of SEPRAN at high Weissenberg numbers We, defined as

$$We = \frac{N_1}{2\sigma}\Big|_{\dot{\gamma}_a} \quad \text{with} \quad \dot{\gamma}_a = \frac{6Q}{WH^2} \qquad (2.21)$$

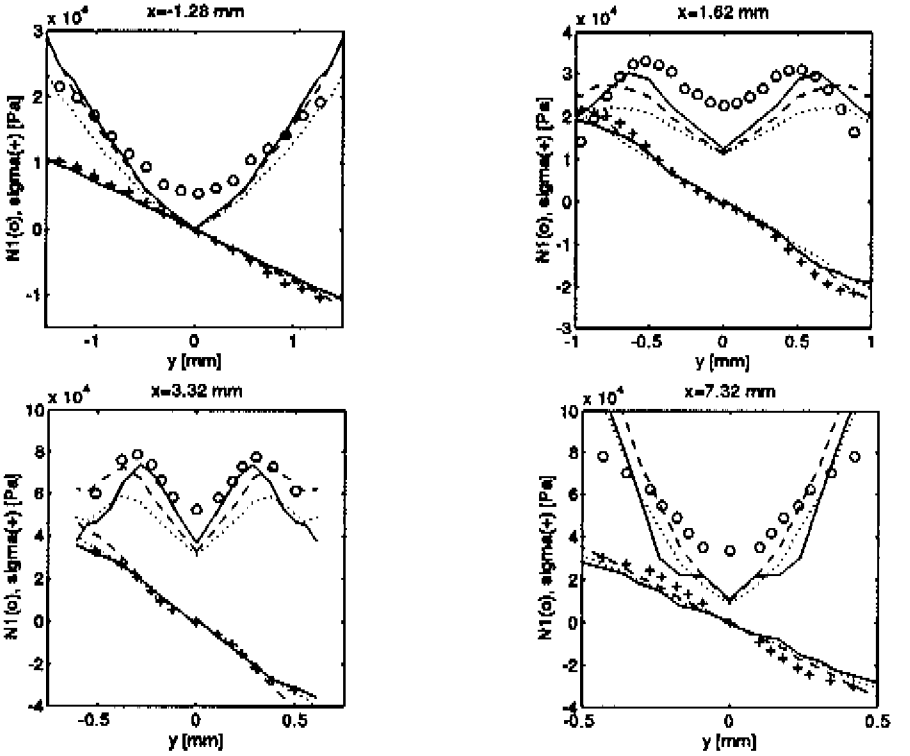

Figure 2.20: Measured and calculated normal stresses (N_1) and shear stresses (σ) at various cross-sections in the tapered duct for Q= 17.2 mm^3/s. Measurements of N_1 (o), measurements of σ (+), Giesekus (- -), Leonov (..),S PTT (—).

with $\dot{\gamma}_a$ is the apparent shear rate in the downstream channel, Q the flow rate, W the depth of the slit and H the width of the downstream slit. The value of We in this experiment was $We = 2.2$. From a paper by Gotsis *et al.* [1990] it is known that the Phan Thien Tanner equation is most sensible to numerical instabilities.

At the cross-section $x = -1.28$ mm, the measured normal stress N_1 does not equal to 0 at $y = 0$, which should be the case for a fully developed two dimensional shear flow. Apparently, in the upstream part before the contraction, the flow is not fully two dimensional. The contribution of the shear flow between the front and back wall to the normal stress cannot be neglected.

From figure 2.20, it is clear that all three models predict the shear stress

quite well and the major differences are demonstrated in the calculations of the normal stresses in the converging part. Obviously, the Leonov model underpredicts the experimentally determined normal stresses. Phan Thien and Tanner's and Giesekus' equations seem to give the best results.

2.4.5 Conclusions

The main conclusions of this section are:

- All four constitutive equations (Wagner, Leonov, Phan Thien and Tanner and Giesekus) predict the experimental results in shear satisfactory, at least in the investigated range of shear rates. Differences are most notable in the relaxation of the first normal stress coefficient after steady shear flow. At high shear rates, the predictions of the first normal stress difference N_1 differ considerably. Unfortunately, no experimental data were available in this shear rate range.

- Although no extra parameters are available in Leonov's and Giesekus' models to fit the experiments in elongation, the predictions for all four models match the experiments fairly well. As in shear, considerable differences between the models are observed at high elongation rates. Measurements by Laun [1984] suggest that Phan Thien and Tanner's and Wagner's equations should be most suitable to describe uniaxial elongation at high strain rates.

- Major differences between the four models are observed in the prediction of the normal stresses in the converging flow through the tapered duct. Wagner's model underpredicts the experimentally determined stresses at the centerline of the die (planar elongation). This indicates that Wagner's model with nonlinearity parameters obtained from shear fails in planar elongation. At different cross-sections in the converging part, predictions with the models of differential form are qualitatively in agreement with experiments. Quantitatively, however, the Giesekus' and especially the Phan Thien and Tanner's models match the experiments fairly well, while Leonov's model fails.

2.5 Discussion

To investigate the capability of viscoelastic constitutive models to describe the rheological behaviour of polymer melts, standard rheological experiments

are inadequate. Measurements of normal stresses in shear and elongational viscosities at high strain rates are highly desirable. Furthermore, a promising technique to determine the rheological behaviour of polymer melts and distinguish between various constitutive equations is represented by measurements of flow induced birefringence in complex flow geometries. However, more attention should be payed to an accurate determination of the stress optical coefficient. Moreover, existing numerical techniques should be improved to be able to simulate the flow of viscoelastic liquids at high Weissenberg numbers.

Chapter 3

Stresses during film blowing

3.1 Introduction

Stresses in the film at the freeze line height have a great influence on the final properties, as was indicated in the introduction of this thesis. In this chapter the experimental and the theoretical determination of the stresses in the film during processing are treated. The basic set of equations describing the film blowing process are summarized in section 3.2. The dynamics and kinematics of the film blowing process have been measured from which the stresses are determined. This is the subject of section 3.3. Using the constitutive equations discussed in Chapter 2 and the kinematics measured, the stresses have been calculated and comparison is made with the experiments in section 3.4. Finally, a discussion of the results obtained is given in section 3.5.

3.2 Basic equations

The basic set of equations describing the film blowing process was derived by Pearson and Petrie [1970a,1970b,1970c]. In this chapter this derivation will be followed. Basic assumptions are:

- the flow is time stationary
- the thickness of the film is an order of magnitude smaller than the radius.
- the flow is rotational symmetric
- inertia and surface tensions can be neglected.

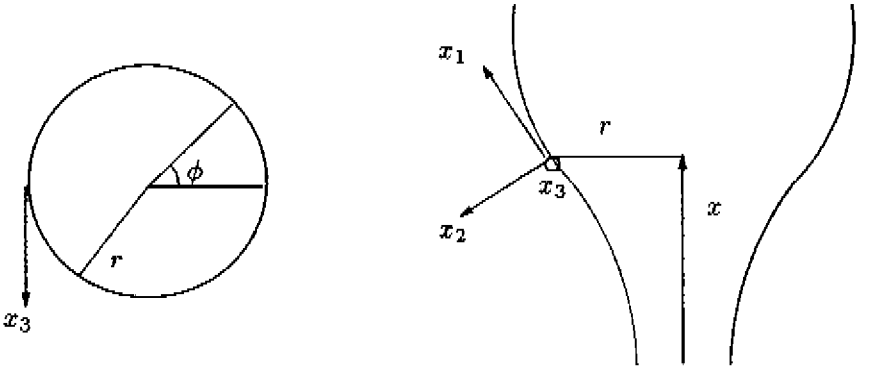

Figure 3.1: The Cartesian coordinate system.

A local Cartesian coordinate system is introduced with x_1 in the tangential direction (in the x-r plane), x_2 in the thickness direction and x_3 in the transverse (or circumferential) direction (see figure 3.1). If the continuity equation is integrated over the thickness, the following equation is obtained

$$Q = 2\pi r(x)h(x)v(x)\rho(T(x)) \tag{3.1}$$

where Q is the mass flow rate, $r(x)$ the radius of the bubble, $h(x)$ the thickness of the film, $v(x)$ the velocity and $T(x)$ the temperature, all as functions of the distance from the die x. The point $x = 0$ is taken to be the point where the polymer leaves the die. The density is given by $\rho(T)$. According to Spencer and Gilmore [1950], the density of many polymers in the molten state can be described with

$$\rho(T) = \frac{1}{\frac{R_g T}{P^* w} + b'} \tag{3.2}$$

where T is temperature in K, R_g the universal gas constant (R_g=8.314 $J.K^{-1}.mol^{-1}$), w the molecular weight of a monomer in kg/mol, P^* the cohesion pressure in Pa, and b' the specific volume in m^3/kg. Hellwege *et al.* [1962] determined these values for PE (w=28 10^{-3} kg/mol, b'=8.75 10^{-4} m^3/kg and P^*=3.18 $10^8 Pa$). Substitution of these values in equation (3.2) yields

$$\rho(T(x)) = \frac{10^3}{0.934\ 10^{-3}T(x) + 0.875} \tag{3.3}$$

Rewriting the momentum equation and using membrane theory leads to the following expression

$$\Delta P = \frac{h\sigma_{11}}{R_m} + \frac{h\sigma_{33}}{R_t} \tag{3.4}$$

where ΔP is the internal bubble pressure, σ_{11} is the stress in the 11 or machine direction, σ_{33} the stress in the 33 or transverse direction, R_m the radius of curvature in the machine direction and R_t the radius of curvature in the transverse direction. These radii of curvature can be calculated according to the formulae

$$R_t = \frac{r}{cos(\theta)} \tag{3.5}$$

$$R_m = \frac{-1}{\frac{d^2r}{dx^2}cos^3(\theta)} \tag{3.6}$$

where $cos(\theta)$ is given by

$$cos(\theta) = \frac{1}{\sqrt{1 + (\frac{dr}{dx})^2}} \tag{3.7}$$

The force balance in the vertical direction, taking into account the fourth assumption, is given by

$$2\pi r h\sigma_{11}cos(\theta) = F_e - \pi\Delta P({r_f}^2 - r^2) - G + H \tag{3.8}$$

where r_f is the radius of the bubble at the freeze line height, F_e the take-up force, G the gravity and H the upward force due to the airflow. In agreement with Fisher [1983] it is assumed that G and H are equal. So the contribution of these two forces is neglected. Equation (3.8) now becomes

$$2\pi r h\sigma_{11}cos(\theta) = F_e - \pi\Delta P({r_f}^2 - r^2) \tag{3.9}$$

If equation (3.9) is rewritten, an expression for the stress σ_{11} as a function of x is obtained

$$\sigma_{11}(x) = \frac{F_e - \pi\Delta P({r_f}^2 - r(x)^2)}{2\pi r(x)h(x)cos(\theta(x))} \tag{3.10}$$

Using equation (3.4), the following expression for the stress in the transverse direction σ_{33} is obtained

$$\sigma_{33}(x) = \frac{R_t(x)}{h(x)}(\Delta P - \frac{h(x)}{R_m(x)}\sigma_{11}(x)) \tag{3.11}$$

Note that in equations (3.10) and (3.11) all variables on the right hand side are written as functions of the distance x.This means that if these variables are known, the stresses in both directions can be calculated.

Since stresses calculated by constitutive equations are the extra stresses τ, a correlation between τ and the total stress σ is still necessary. Taking into account the second assumption ($h \ll r$), it can be shown that $|\sigma_{22}| \ll |\sigma_{33}|$ and $|\sigma_{22}| \ll |\sigma_{11}|$. Setting $\sigma_{22} = 0$ and taking into consideration $\sigma = -pI + \tau$, the correlation between the total stresses and the extra stresses can be written as

$$\begin{aligned} \sigma_{11} &= \tau_{11} - \tau_{22} \\ \sigma_{22} &= 0 \\ \sigma_{33} &= \tau_{33} - \tau_{22} \end{aligned} \tag{3.12}$$

3.3 Experimental determination of stresses

In this section, the experimental determination of the stresses in the film during processing will be discussed. From equations (3.10) and (3.11) the stresses in machine and transverse direction can be derived as functions of the distance from the die, once the radius, the velocity, the internal bubble pressure, the take-up force, the temperature and the mass flow rate are known. Measurement of these quantities is subject of this section. In section 3.3.1 the experimental set-up is reported, in section 3.3.2 the measuring equipment is briefly discussed and, finally, the results are given in section 3.3.3.

3.3.1 Experimental set-up

In order to investigate the influence of the type of LPDE and the processing parameters on the stresses at the freeze line (and ultimately on the film properties which will be dealt with in Chapter 5), various experiments have been performed. During these experiments bubble radii, velocities, temperatures, bubble pressures and take-up forces have been measured. To be able to measure temperature, velocity and radius close to the die, the air ring was

LDPE	L1o & L1	L8
Inner diameter	38.4 mm	35.6 mm
Outer diameter	40 mm	40 mm
Gap width	.8 mm	2.2 mm

Table 3.1: Characteristics of the annular die for film blowing experiments.

lowered to the same level as the die exit. All experiments were performed at a Schwabentan 6 extruder with diameter 30 mm. The distance from the die to the nip rolls was 136 cm. The settings of the annular die are given in table 3.1.

For each material, nine experiments were performed, for which the mass flow rate and freeze line height were kept constant. The draw ratio DR, defined as the ratio of the velocity of the film at the freeze line to the velocity at the die exit, and the blow up ratio BUR, defined as the ratio of the radius at the freeze line to the radius of the die, were varied. The BUR and DR were chosen such that films were made with three different thicknesses. The settings of the process parameters for all experiments are given in tables 3.2, 3.3 and 3.4. Here, T_0 is the temperature of the die, N is the screw speed of the extruder (in rpm), Q is the resulting mass flow rate, x_e is the freeze line height, v_e is the take-up speed and h_e is the resulting film thickness. For the freeze line height x_e, the position is taken where the film becomes opaque.

Because of the lower viscosity, the die temperature for LDPE L8 had to be set lower than for the other two LDPE's, while the die gap had to be widened. Therefore, the Draw Ratio's achieved for this melt are much higher than for the other two melts. Differences between final thicknesses, freeze line height and output are explained by the processability of the various melts.

Exp.	T_0	N	Q	x_e	v_e	h_e	BUR	DR
	C	rpm	g/min	cm	m/min	μm		
2	175	20	68	15	8.4	45	1.5	8.8
3	175	20	69	15	6.4	60	1.5	6.7
4	175	20	70	15	5.4	75	1.5	5.6
5	175	20	68	15	6.1	45	2	6.4
6	175	20	70	15	5.0	60	2	5.2
7	175	20	70	15	4.1	75	2	4.3
8	175	20	70	15	5.3	45	2.5	5.5
9	175	20	70	15	4.2	60	2.5	4.4
10	175	20	70	15	3.3	75	2.5	3.4

Table 3.2: Settings for film blowing experiments for LDPE L1o.

Exp.	T_0	N	Q	x_e	v_e	h_e	BUR	DR
	C	rpm	g/min	cm	m/min	μm		
11	175	20	68	15	8.4	45	1.5	8.8
12	175	20	68	15	6.4	60	1.5	6.7
13	175	20	68	15	5.4	75	1.5	5.6
14	175	20	70	15	6.7	45	2	7.0
15	175	20	70	15	5.2	60	2	5.4
16	175	20	70	15	4.2	75	2	4.4
17	175	20	70	15	5.4	45	2.5	5.6
18	175	20	70	15	4.2	60	2.5	4.4
19	175	20	70	15	3.4	75	2.5	3.6

Table 3.3: Settings for film blowing experiments for LDPE L1.

Exp.	T_0	N	Q	x_e	v_e	h_e	BUR	DR
	C	rpm	g/min	cm	m/min	μm		
26	145	15	60	10	12.5	30	1.5	35
20	145	15	57	10	7.4	45	1.5	21
21	145	15	57	10	5.8	60	1.5	16.2
27	145	15	60	10	9.5	30	2	26.3
23	145	15	60	10	6.0	45	2	16.7
24	145	15	60	10	4.6	60	2	12.8
28	145	15	60	10	8.4	30	2.5	23.3
29	145	15	60	10	5.4	45	2.5	15
30	145	23	96	10	5.9	60	2.5	16.3

Table 3.4: Settings for film blowing experiments for LDPE L8.

3.3.2 Measuring equipment

In subsection 3.2 the equations to calculate stresses in the film were given. In order to calculate these stresses as functions of the distance from the die, the radius, velocity and temperature were measured in each experiment, along with the internal bubble pressure and the take-up force. Here, the measuring methods are briefly outlined.

Radius

During the experiments photographs were taken. A measuring rod, indicating the distance from the die, was placed aside of the bubble. From the photographs, the radius at each position, at regular intervals, was determined.

Velocity

Laser Doppler velocity measurements were carried out with the 488nm line of a Lexel 85 Argon-ion laser operating at 1W. The optical train was built up by Dantec modular optics, consisting of two quarter wave plates, a beam waist adjuster, a polarizing beam splitter prism, a Bragg cell in one of the two beams introducing a 40MHz optical frequency shift, a beam expander and a 310mm focal lens. The system operated in the back-scattering geometry and detection was performed with a RCA 4526 photomultiplier tube. The signal was electronically shifted down to 10 kHz and fed into a Dantec 57N10 Burst Spectrum Analyzer. Data were collected in a PC and the average velocity was calculated from the frequency distribution. Only velocities in the x direction were measured.

Temperature

An Infrared Radiation camera was used to record the temperatures. In the Ph.D. thesis of Ast [1976] it has been shown that the specific emissivity coefficient ϵ_{sp} of PE is a function of film thickness. To average the error in temperature measurement due to changing film thickness it was recommended to use $\epsilon_{sp} = 0.65$, which corresponds to a film thickness of $100\mu m$. According to Ast, the total error in the measured temperature is in this way reduced to 4 percent, where the largest error is made in the region of the die.

Moreover, close to the die, radiation of the cooling ring is received, so temperature measurements close to the die are not evaluated in this research. The wavelength was set to 3.43 μ, which, according to Cao, Sweeney and Campbell [1990], implies that the surface temperature was measured.

Internal bubble pressure

A water manometer was used to record the pressure difference inside the bubble and the surroundings.

Take-up force

The wage, specially constructed to measure the take-up force, is shown in figure 3.2. The force acting on the nip roll on the right hand side equals $2F_e$, with F_e the force acting on the film. Now, F_e is obtained by solving the balance of momentum, leading to $F_e = \frac{F_p}{4}$. The force F_p was recorded by a force transducer.

It should be mentioned that by measuring the take-up forces this way, no correction is made for friction between the two nip rolls. Therefore, the nip rolls were pressed together slightly by a spring. To get an idea what the influence of friction might be, several runs were made with the nip rolls pressed tight together. Deviations were less than 10 %.

Thickness

To calculate the stresses according to equations (3.10) and (3.11), the thickness of the film should be known. No direct measurement of the thickness was to our disposal. However, from temperature measurements and equations (3.1) and (3.3), the thickness could be calculated.

3.3.3 Results

The results of the measurements described above are discussed now. First the measurements on the temperature and dynamics are dealt with. For the LDPE's L1o, L1 and L8, the velocities, radii and temperatures for various experiments are shown in figures 3.3, 3.4 and 3.5. Velocities and radii were fitted with fifth order polynomials, the elongation rates were determined by taking the derivative of these polynomials. In figures 3.6, 3.7 and 3.8 the elongation rates in machine and transverse direction are depicted. After dealing with the force and bubble pressure measurements, finally the experimentally determined stresses are discussed.

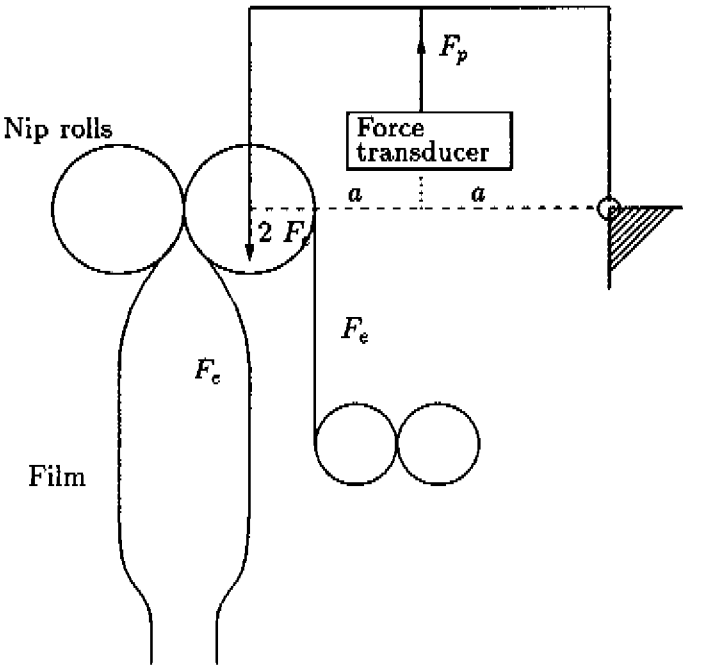

Figure 3.2: The wage-like construction used to measure the take-up forces.

Temperature

Along the film blowing line, in a broad region between the die exit and freeze line, a linear decrease of temperature as a function of distance from the die is observed. For all experiments on one material, a plateau in the temperature is reached which does not seem to depend on the deformation history (DR and BUR). For L1 and L1o, the temperature at this plateau is in between 95 ^oC and 100 ^oC, for L8 between 92 ^oC and 96 ^oC. These values do not differ much from the crystallization temperatures reported as measured by means of DSC (see section 1.2). Apparently, the effect of undercooling is anticipated by the appearance of orientation induced crystallization. For example, if the Draw Ratio is increased, the cooling rate is increased (in an attempt to keep the freeze line height constant), so one might expect a lower plateau temperature due to the undercooling effect. Increasing the DR, however, also increases the stress in the machine direction. Because of these higher stresses (or higher orientation), the crystallization temperature will increase and this effect eliminates the undercooling effect.

A linear decrease in temperature and the existence of a plateau region is also found in literature data (see e.g. Wagner [1976b], Fisher [1983], Cao, Sweeney and Campbell [1990], Winter [1983], Kanai and White [1984] and Ast [1976]). Dependent on the type of PolyEthylene, plateau temperatures ranging between 95 ^oC and 120 ^oC were reported. In studies by Wagner [1976b] and Ast [1976] on the effect of freeze line height on the plateau temperature, no dependence was found.

Dynamics

In figures 3.6, 3.7 and 3.8 it can be seen that the film is stretched in the machine direction, immediately after the die-exit. The elongation in the transverse direction seems to start later than the elongation in the machine direction. Experiments with low Blow Up Ratio (BUR=1.5) even show that initially a negative elongation rate is obtained in the TD.

An important conclusion from the measurements of temperature, radii and velocities is that after a plateau in temperature is reached, the elongation rates are still positive. This means that even when crystallization starts, there is still some deformation going on. As is known, this might have a great effect on the ultimate film properties. However, this does not imply, as originally thought by a great number of people, that the deformation and temperature history in the region before the plateau is not of any importance. It might well be that the total deformation of the film in the plateau region is determined by the orientation (or stresses) at the onset of crystallization. Moreover, in Chapter 5 it will be shown that the stresses calculated at the freeze line, without incorporation of the deformation in the temperature plateau region, have a high impact on the ultimate film properties.

In modelling the film blowing process, most researchers (e.g. Wagner [1976b], Kanai and White [1985], Kanai [1987], Petrie [1975], Cain and Denn [1988], Yamane and White [1987], Luo and Tanner [1985]) assumed that the deformation stops when crystallization starts. As might be clear from the measurements shown here, this assumption is not justified. Cao and Campbell [1990], Ashok and Campbell [1992] and Babel and Campbell [1993] also met with this problem and they introduced a viscoelastic plastic model, only to be able to model this important area of the film blowing process in more detail. The tradionally kinematic boundary conditions were replaced by a rheological boundary condition, the so-called plastic elastic transition (PET). The merits and demerits of their model were already discussed in the introductionary chapter.

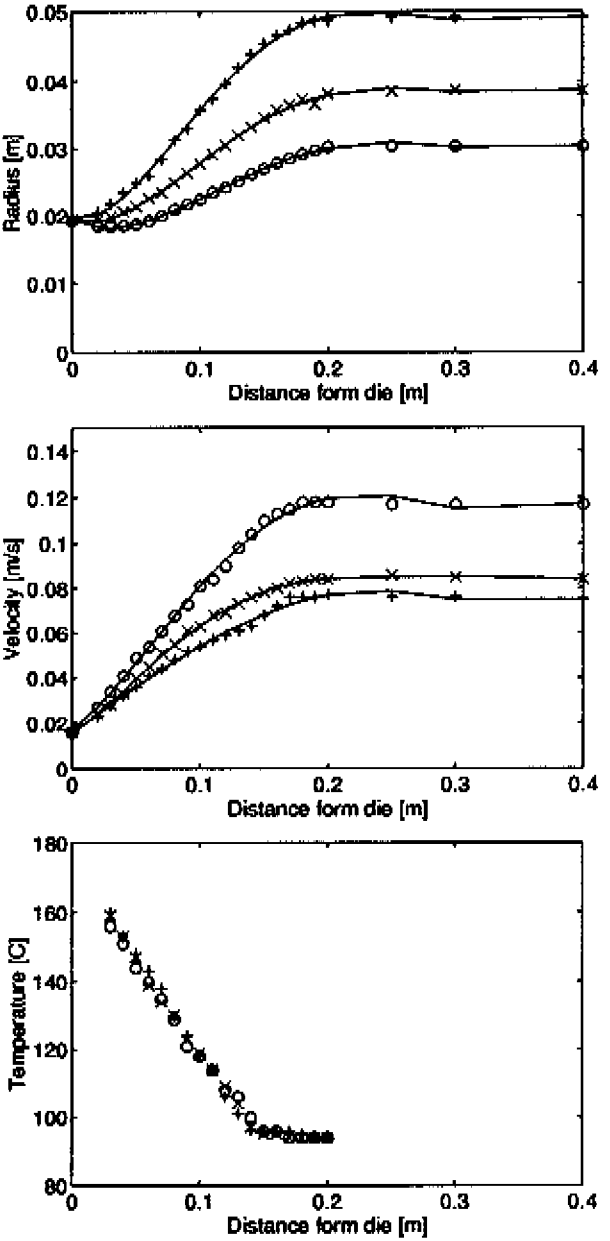

Figure 3.3: Measured radius, velocity and temperature for LDPE L1o. exp. 3 (o), exp. 6 (x), exp. 9 (+).

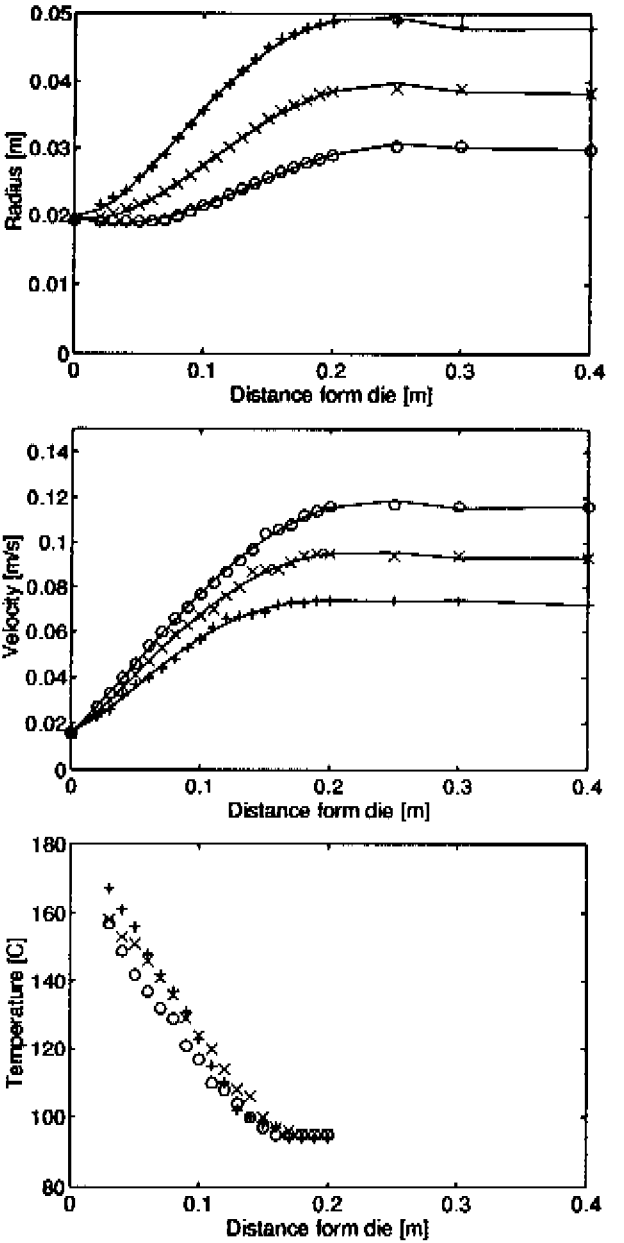

Figure 3.4: Measured radius, velocity and temperature for LDPE L1. exp. 12 (o), exp. 15 (x), exp. 18 (+).

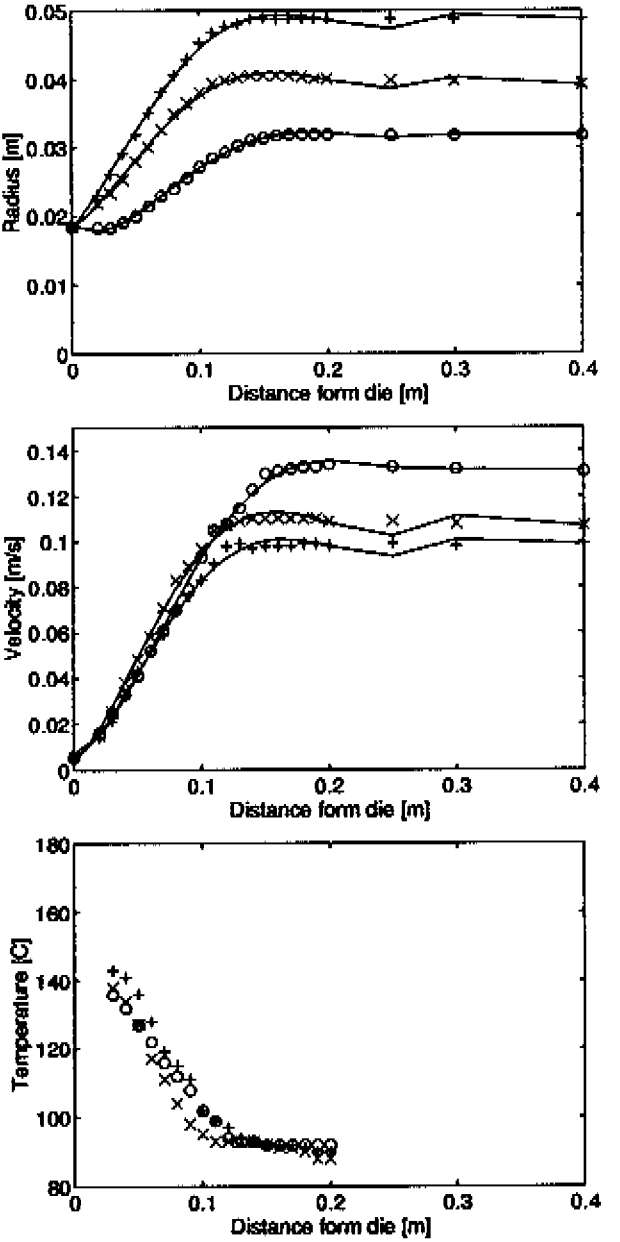

Figure 3.5: Measured radius, velocity and temperature for LDPE L8. exp. 20 (o), exp. 23 (x), exp. 29 (+).

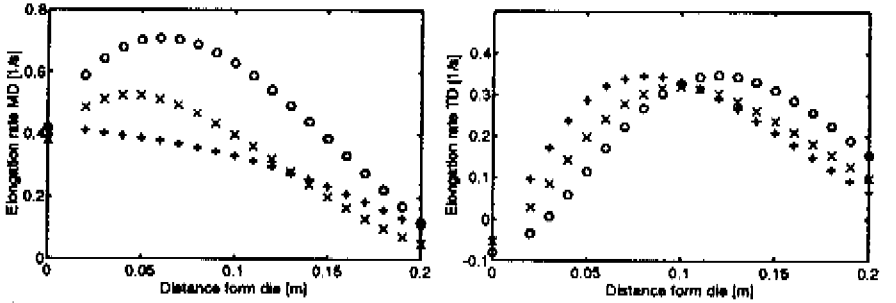

Figure 3.6: Elongation rates in machine (MD) and transverse direction (TD) for LDPE L1o. Exp. 3 (o), exp. 6 (x), exp. 9 (+).

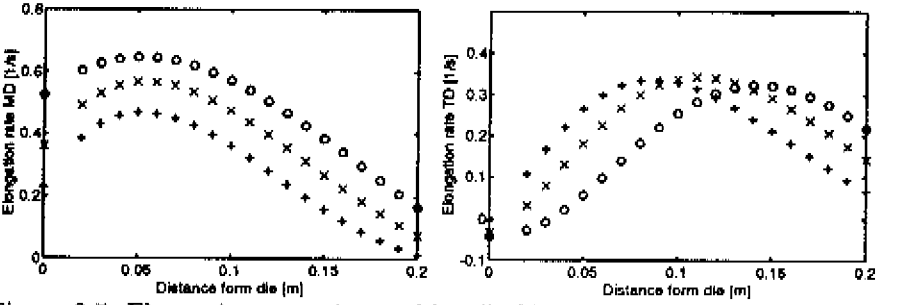

Figure 3.7: Elongation rates in machine (MD) and transverse direction (TD) for LDPE L1. Exp. 12 (o), exp. 15 (x), exp. 18 (+).

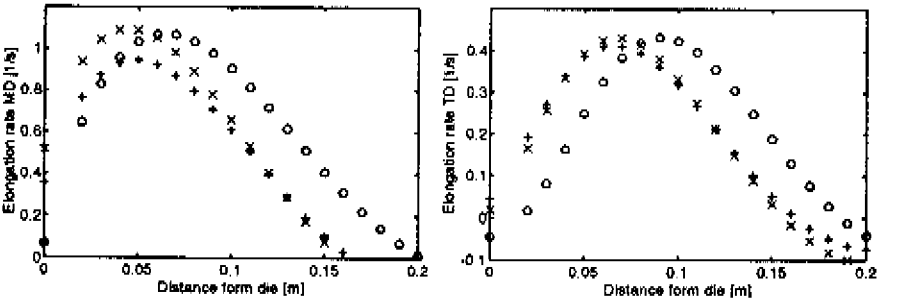

Figure 3.8: Elongation rates in machine (MD) and transverse direction (TD) for LDPE L8. Exp. 20 (o), exp. 23 (x), exp. 29 (+).

Bubble pressure and take-up force

In table 3.5 the measured bubble pressures and take-up forces for all experiments are listed. It is observed that if the BUR is kept constant and the DR is decreased, the bubble pressure ΔP slightly increases. A possible explanation for this behaviour is that for constant BUR and decreasing DR the overall film thickness increases, therefore the bubble pressure should increase because more material has to be blown up.

If the film thickness is kept constant and the BUR is increased ΔP decreases. This follows straightforward from the well-known pressure vessel equation.

The take-up forces measured do not show a clear correlation with BUR or DR. This does not mean that the take-up force is not important, since it determines the stress in the machine direction. If the take-up forces for L1o and L1 are compared, those for L1 prove to be higher. Since the conditions were the same, it might be concluded that L1 exhibits a more pronounced strain hardening behaviour in film blowing than L1. This is in accordance with the behaviour of these two materials in uniaxial elongation.

A comparison with literature data (Gupta [1980], Wagner [1976b], Fisher [1983], White and Cakmak [1988], Han and Kwack [1983], Kwack, Han and Vickers [1988]) is difficult to make since in all those experiments also output rates and freeze line heights were altered. It might be clear that these processing parameters also influence the forces and pressures, and therefore also the stresses, to a great extent.

L1o			L1			L8		
Exp.	ΔP *Pa*	F_e *N*	Exp.	ΔP *Pa*	F_e *N*	Exp.	ΔP *Pa*	F_e *N*
2	115	5.8	11	110	7.7	26	85	4.0
3	135	6.6	12	118	7.6	20	78	3.8
4	130	6.9	13	128	7.5	21	88	3.9
5	113	6.5	14	103	7.5	27	75	4.5
6	120	6.7	15	108	7.7	23	85	4.3
7	123	6.5	16	113	7.7	24	85	3.6
8	100	6.0	17	95	6.9	28	65	3.8
9	105	5.7	18	95	6.9	29	70	3.5
10	110	6.4	19	105	7.3	30	80	3.9

Table 3.5: Take-up forces and bubble pressures measured.

Stresses

From equations (3.10) and (3.11) the stresses in the machine and transverse direction can be calculated. If the point of interest is the ultimate stresses in the film, i.e. when the film does not deform anymore, the expression for the stresses can be simplified. After all, R_m goes to infinity if the radius is constant. Let r_e be the final radius, h_e the final thickness, $\sigma_{11,E}$ the final stress in the machine direction and $\sigma_{33,E}$ the final stress in the transverse direction. The following equations are then obtained

$$\sigma_{11,E} = \frac{F_e}{2\pi r_e h_e} \tag{3.13}$$

$$\sigma_{33,E} = \frac{r_e}{h_e}\Delta P \tag{3.14}$$

In table 3.6, the stresses calculated using these expressions are listed. Note that these stresses are calculated at a point **beyond** the freeze line.

L10		
Exp.	$\sigma_{11,E}$ $10^5 Pa$	$\sigma_{33,E}$ $10^5 Pa$
2	7.0	0.73
3	6.0	0.64
4	5.0	0.49
5	5.9	0.95
6	4.6	0.76
7	3.6	0.62
8	4.4	1.05
9	3.1	0.83
10	2.8	0.70

L1		
Exp.	$\sigma_{11,E}$ $10^5 Pa$	$\sigma_{33,E}$ $10^5 Pa$
11	9.4	0.70
12	6.9	0.56
13	5.5	0.49
14	6.8	0.87
15	5.3	0.68
16	4.2	0.57
17	5.0	1.00
18	3.8	0.75
19	3.2	0.66

L8		
Exp.	$\sigma_{11,E}$ $10^5 Pa$	$\sigma_{33,E}$ $10^5 Pa$
26	7.6	0.77
20	4.8	0.47
21	3.7	0.40
27	6.5	0.91
23	4.1	0.68
24	2.6	0.51
28	4.4	0.98
29	2.7	0.70
30	2.2	0.60

Table 3.6: Experminentally determined stresses above the freeze line.

In figures 3.9, 3.10 and 3.11 these stresses are shown as functions of the BUR, with the film thickness as a parameter. If the BUR is increased and the film thickness is kept constant, the stress in the machine direction decreases while the stress in transverse direction increases. The decrease of the stress in machine direction is understandable because with increasing BUR and constant thickness the draw ratio decreases. For all experiments, the stress in MD is always higher than the stress in TD. Although with increasing BUR the stress ratio (MD/TD) may become smaller, it will always be considerably larger than unity. As was pointed out by Kwack, Han and Vickers [1988], this stress ratio is an important factor in determining the film anisotropy.

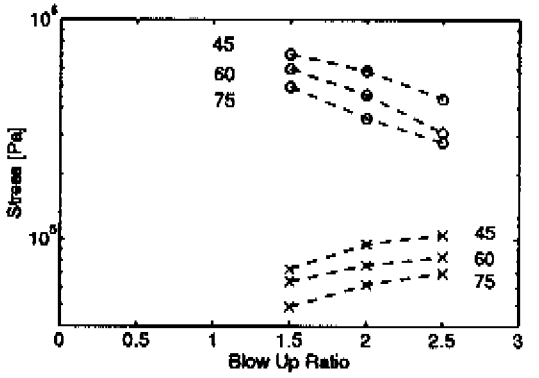

Figure 3.9: $\sigma_{11,E}$ (o) and $\sigma_{33,E}$ (x) vs. BUR for LDPE L1o. Parameter is film thickness in μm.

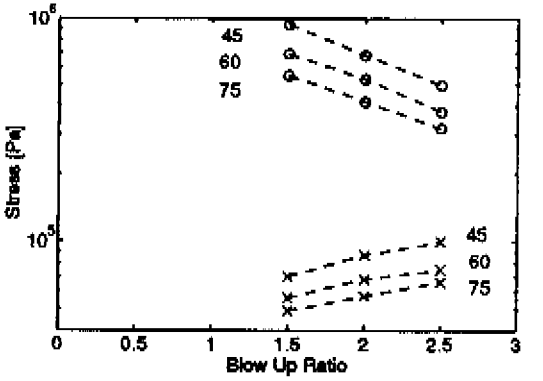

Figure 3.10: $\sigma_{11,E}$ (o) and $\sigma_{33,E}$ (x) vs. BUR for LDPE L1. Parameter is film thickness in μm.

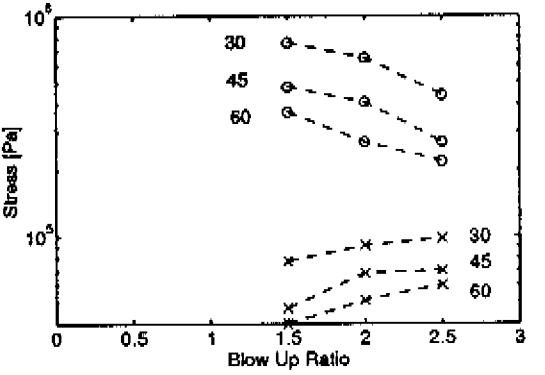

Figure 3.11: $\sigma_{11,E}$ (o) and $\sigma_{33,E}$ (x) vs. BUR for LDPE L8. Parameter is film thickness in μm.

In figure 3.12 the stress in transverse direction $\sigma_{33,E}$ is plotted against the stress in machine direction $\sigma_{11,E}$. The lowest ratio is reached for experiment nr. 29, and amounts 3.67. For this experiment (with LDPE L8) the DR was 16.3 and the BUR was 2.5. For experiment nr. 10 (with LDPE L1o) the stress ratio is 4.0 while the BUR=2.5 and the DR=3.4. The more elastic behaviour of LDPE L1o and L1 is responsible for long relaxation times and, therefore, these materials will still exhibit stresses in the machine direction induced by the flow in the die. The high melt index material (L8) has a short memory and, therefore, it can happen that the stress ratio for exp. 29 is smaller than for exp. 10, even though the ratio $\frac{\mathrm{DR}}{\mathrm{BUR}}$ is larger.

A more balanced film (Stress ratio$\rightarrow$1) can be achieved by increasing the BUR and decreasing the DR, as can be concluded from figures 3.9, 3.10 and 3.11. However, this is not so much caused by the increase of $\sigma_{33,E}$ but more the result of the sharp decrease of $\sigma_{11,E}$. Furthermore, the choice of the material plays an important role. It seems that for LDPE L8, with its extremely short memory, films which are in balance can be made more easier than for LDPE's L1o and L1.

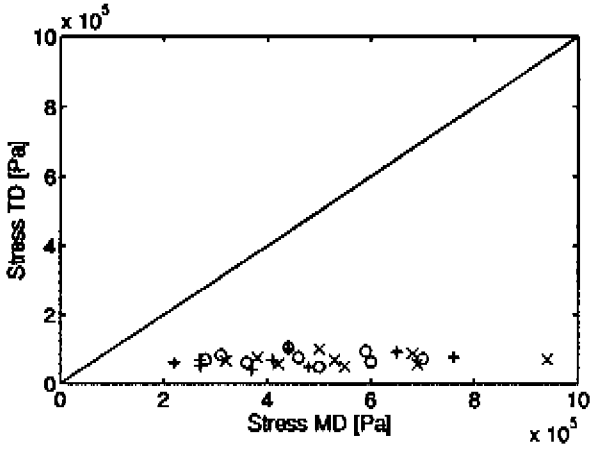

Figure 3.12: Experimental $\sigma_{33,E}$ vs. experimental $\sigma_{11,E}$ for grades L1o (o), L1 (x) and L8 (+).

3.3.4 Conclusions

To finish this section the main conclusions are listed below.

- The temperature decreases almost linearly between die and freeze line.
- The temperature at which crystallization starts does not seem to depend on the blow-up ratio and the draw ratio. The effect of undercooling and orientation induced crystallization seem to counterbalance each other.
- Considerable deformation in machine and transverse direction is observed after the film starts to crystallize.
- Though the ratio $(\frac{\mathrm{DR}}{\mathrm{BUR}})$ can be almost 1, the stress ratio $\frac{\sigma_{11,E}}{\sigma_{33,E}}$ is still considerably deviating from unity, especially for the higher molecular weight materials.
- Increasing the BUR while keeping the film thickness and freeze line height constant results in films for which the stress ratio goes to 1. This is more a result of the decrease of $\sigma_{11,E}$ than the increase of $\sigma_{33,E}$.

3.4 Theoretical determination of stresses

In this section the determination of the stresses acting in the film are calculated. The question to be answered is

> *Is any rheological constitutive equation able to predict stresses in machine and transverse direction in the film during film extrusion, using parameters as determined from standard rheological experiments and macroscopically determined processing conditions.*

All four constitutive equations will be used. As Wagner's equation is of integral type, it will need a different numerical procedure to calculate the stresses than the other three models that all are of differential type. In section 3.4.1, Wagner's integral equation will be discussed and in 3.4.2 the other three models are treated. Since the viscoelastic constitutive equations are only valid in the region where no crystallization takes place, calculations are stopped at the point where a plateau in temperature is reached. Using equation (3.12) the calculated stresses can be converted into the total stresses, that were determined experimentally. A comparison between calculated and measured stresses is made in section 3.4.3. Finally, conclusions are drawn in section 3.4.4.

3.4.1 Integral models

To calculate stresses using an integral constitutive equation, the Finger tensor should be known. Fisher [1983] gives an extensive derivation of this tensor for the film blowing process. It is composed of the elongational deformation in the bubble forming region and the shear deformation inside the die

$$C_t^{-1}(t') = \begin{pmatrix} (1+\gamma_{t,t'}{}^2)\frac{v(t)^2}{v(t')^2} & -\gamma_{t,t'}\frac{v(t)}{v(t')}\frac{h(t)}{h(t')} & 0 \\ -\gamma_{t,t'}\frac{v(t)}{v(t')}\frac{h(t)}{h(t')} & \frac{h(t)^2}{h(t')^2} & 0 \\ 0 & 0 & \frac{r(t)^2}{r(t')^2} \end{pmatrix} \tag{3.15}$$

where the relative shear is given by

$$\gamma_{t,t'} = \gamma(t) - \gamma(t') \tag{3.16}$$

For the shear in the die the intermediate shear rate for a Newtonian flow has been chosen to be characteristic, given by

$$\dot{\gamma} = \frac{2Q}{3\,\pi\, r_0\, {h_0}^2\, \rho(T_0)} \tag{3.17}$$

with r_0 the inner die radius, h_0 the die gap and T_0 the temperature of the melt in the die. It is assumed that the die does not contain a convergent or divergent part. Since stresses are calculated as functions of the distance from the die, the integration over the time is replaced by an integration over place, using

$$dx = v(x)dt \tag{3.18}$$

For a material point which is at time t at height x outside the die and at time t' at height ξ inside the die, the Finger tensor (equation (3.15)) reads

$$C_x^{-1}(\xi) = \begin{pmatrix} (1+\gamma_{x,\xi}^2)\frac{v(x)^2}{v(\xi)^2} & -\gamma_{x,\xi}\frac{v(x)}{v(\xi)}\frac{h(x)}{h(\xi)} & 0 \\ -\gamma_{x,\xi}\frac{v(x)}{v(\xi)}\frac{h(x)}{h(\xi)} & \frac{h(x)^2}{h(\xi)^2} & 0 \\ 0 & 0 & \frac{r(x)^2}{r(\xi)^2} \end{pmatrix} \tag{3.19}$$

where

$$\gamma(x,\xi) = \gamma(x) - \gamma(\xi) \tag{3.20}$$

Note that for x and ξ both positive, i.e. above the die ($\gamma(x) = \gamma(\xi)$), the Finger tensor reduces to

$$C_x^{-1}(\xi) = \begin{pmatrix} \frac{v(x)^2}{v(\xi)^2} & 0 & 0 \\ 0 & \frac{h(x)^2}{h(\xi)^2} & 0 \\ 0 & 0 & \frac{r(x)^2}{r(\xi)^2} \end{pmatrix} \tag{3.21}$$

The irreversibility condition (2.5) can be rewritten to

$$h(x,\xi) = \text{ minimum } h(\zeta,\xi),\ \xi \le \zeta \le x \tag{3.22}$$

Taking into account the variation of the temperature with the height, and $T = T(\xi)$, the memory function (equation (2.2)) becomes

$$m(x-\xi) = \int_{-\infty}^{\infty} \frac{c_{T,x} G(\lambda)}{a_{T,\xi}\lambda} e^{\frac{-1}{\lambda}\int_{\xi}^{x} \frac{d\zeta}{a_{T,\zeta} v(\zeta)}} d(ln a_{T,\xi}\lambda) \tag{3.23}$$

or, alternatively, in a discrete form

$$m(x-\xi) = \sum_{i=1}^{N} \frac{c_{T,x} G(\lambda)}{a_{T,\xi}\lambda} e^{\frac{-1}{\lambda}\int_{\xi}^{x} \frac{d\zeta}{a_{T,\zeta} v(\zeta)}} \tag{3.24}$$

where $c_{T,x}$ is the vertical shift factor for the temperature at height x, $a_{T,\xi}$ the horizontal shift factor for the temperature at height ξ. With equations (3.19), (3.20), (3.22) and (3.23) or (3.24), the stresses in the film can be calculated as functions of the height according to

$$\tau(x) = \int_{-\infty}^{x} m(x-\xi) h(x,\xi) C_x^{-1}(\xi)\, d\xi \tag{3.25}$$

Equation (3.25) is evaluated using the trapezium rule. In order to take into account the fading memory of the melt, the term $x - \xi$ is split into N parts, using logarithmic steps. The limit $-\infty$ is replaced by -20 cm, i. e. 20 cm inside the die. The number N was determined such that no dependence on N was observed.

3.4.2 Differential models

Now, the equations to be solved for the differential models are treated in somewhat more detail. The strain rate tensor D in the bubble forming region is given by

$$D = \begin{pmatrix} \frac{1}{v}\frac{dv}{dt} & 0 & 0 \\ 0 & \frac{1}{h}\frac{dh}{dt} & 0 \\ 0 & 0 & \frac{1}{r}\frac{dr}{dt} \end{pmatrix} \tag{3.26}$$

The derivatives with respect to the time t can be replaced by derivatives to the height x:

$$D = \begin{pmatrix} \frac{dv}{dx} & 0 & 0 \\ 0 & \frac{v}{h}\frac{dh}{dx} & 0 \\ 0 & 0 & \frac{v}{r}\frac{dr}{dx} \end{pmatrix} \tag{3.27}$$

Now, for the ith relaxation mode of the Phan Thien and Tanner model we must solve

$$\begin{aligned}
a_T v\lambda_i \frac{d\tau_{11}}{dx} &= 2a_T\eta_i \frac{dv}{dx} - e^{\frac{\epsilon\lambda_i}{\eta_i}(\tau_{11}+\tau_{22}+\tau_{33})}\tau_{11} \\
&\quad +2a_T\lambda_i(1-\xi)\frac{dv}{dx}\tau_{11} \\
a_T v\lambda_i \frac{d\tau_{22}}{dx} &= 2a_T\eta_i \frac{v}{h}\frac{dh}{dx} - e^{\frac{\epsilon\lambda_i}{\eta_i}(\tau_{11}+\tau_{22}+\tau_{33})}\tau_{22} \\
&\quad +2a_T\lambda_i(1-\xi)\frac{v}{h}\frac{dh}{dx}\tau_{22} \\
a_T v\lambda_i \frac{d\tau_{33}}{dx} &= 2a_T\eta_i \frac{v}{r}\frac{dr}{dx} - e^{\frac{\epsilon\lambda_i}{\eta_i}(\tau_{11}+\tau_{22}+\tau_{33})}\tau_{33} \\
&\quad +2a_T\lambda_i(1-\xi)\frac{v}{r}\frac{dr}{dx}\tau_{33} \\
a_T v\lambda_i \frac{d\tau_{12}}{dx} &= a_T\lambda_i\frac{dv}{dx}(1-\xi)\tau_{12} + a_T\lambda_i\frac{v}{h}\frac{dh}{dx}(1-\xi)\tau_{12} - \\
&\quad e^{\frac{\epsilon\lambda_i}{\eta_i}(\tau_{11}+\tau_{22}+\tau_{33})}\tau_{12}
\end{aligned} \tag{3.28}$$

Since the velocity v and the radius r have been measured, the deformation rates $\frac{dv}{dx}$ and $\frac{v}{r}\frac{dr}{dx}$ can be determined. The deformation rate in the thickness direction, given by $\frac{v}{h}\frac{dh}{dx}$, is obtained from the incompressibility constraint $tr(D) = 0$, and reads

$$\frac{v}{h}\frac{dh}{dx} = -\frac{v}{r}\frac{dr}{dx} - \frac{dv}{dx} \tag{3.29}$$

In equation (3.29) no thermal effects are taken into consideration.

Because the set of equations (3.28) yields a set of stiff differential equations, they are solved using a backward difference scheme with the help of the D02EBF routine from the NAG Fortran library (see NAG Fortran Library Manual-Mark 13, 1988, 1st Edition). Initial values for the stresses τ_{11}, τ_{22}, τ_{33} and τ_{12} are such that they belong to the steady state values for a shear

flow with the intermediate Newtonian shear rate (see equation (3.17)). The total extra stress tensor is calculated by a summation over all the relaxation modes (see equation (2.8).

The equations to be solved for the i^{th} mode of the Giesekus equation are given by

$$
\begin{aligned}
a_T v\lambda_i \tfrac{d\tau_{11}}{dx} &= 2a_T\eta_i \tfrac{dv}{dx} - \tfrac{\alpha}{G_i}\tau_{11}{}^2 - \tau_{11} + \\
&\quad 2a_T\lambda_i \tfrac{dv}{dx}\tau_{11} - \tfrac{\alpha}{G_i}\tau_{12}{}^2 \\
a_T v\lambda_i \tfrac{d\tau_{22}}{dx} &= 2a_T\eta_i \tfrac{v}{h}\tfrac{dh}{dx} - \tfrac{\alpha}{G_i}\tau_{22}{}^2 - \tau_{22} + \\
&\quad 2a_T\lambda_i \tfrac{v}{h}\tfrac{dh}{dx}\tau_{22} - \tfrac{\alpha}{G_i}\tau_{12}{}^2 \\
a_T v\lambda_i \tfrac{d\tau_{33}}{dx} &= 2a_T\eta_i \tfrac{v}{r}\tfrac{dr}{dx} - \tfrac{\alpha}{G_i}\tau_{33}{}^2 - \tau_{33} + \\
&\quad 2a_T\lambda_i \tfrac{v}{r}\tfrac{dr}{dx}\tau_{33} \\
a_T v\lambda_i \tfrac{d\tau_{12}}{dx} &= -\tau_{12} + a_T\lambda_i \tfrac{dv}{dx}\tau_{12} + a_T\lambda_i \tfrac{v}{h}\tfrac{dh}{dx}\tau_{12} - \\
&\quad \tfrac{\alpha}{G_i}\tau_{12}(\tau_{11} + \tau_{22})
\end{aligned}
\tag{3.30}
$$

Apparently, the derivatives of the stresses τ_{11} and τ_{22} in equations (3.30) are dependent on the shear stress τ_{12}, while for the Phan Thien and Tanner model (equations (3.28) the shear stress does not appear in the equations determining the stresses τ_{11} and τ_{22}. This difference between these two models originates from the presence of a quadratic term in the Giesekus model. This implies that for the Leonov model, in which also a quadratic term is present, a similar dependence on the shear stress is found as for the Giesekus model.

Finally, the equations to be solved for the Leonov model, where for convenience the Finger tensor C^{-1} is replaced by B, read

$$
\begin{aligned}
v\tfrac{dB_{11}}{dx} &= 2\tfrac{dv}{dx}B_{11} - \tfrac{1}{2a_T\lambda_i}(B_{11}{}^2 + B_{12}{}^2 - 1 \\
&\quad + \tfrac{1}{3}(\mathrm{tr}B - B_{11} - B_{22} - B_{33})B_{11}) \\
v\tfrac{dB_{22}}{dx} &= 2\tfrac{v}{h}\tfrac{dh}{dx}B_{22} - \tfrac{1}{2a_T\lambda_i}(B_{22}{}^2 + B_{12}{}^2 - 1 \\
&\quad + \tfrac{1}{3}(\mathrm{tr}B - B_{11} - B_{22} - B_{33})B_{22}) \\
v\tfrac{dB_{33}}{dx} &= 2\tfrac{v}{r}\tfrac{dr}{dx}B_{33} - \tfrac{1}{2a_T\lambda_i}(B_{33}{}^2 - 1 \\
&\quad + \tfrac{1}{3}(\mathrm{tr}B - B_{11} - B_{22} - B_{33})B_{33}) \\
v\tfrac{dB_{12}}{dx} &= \tfrac{dv}{dx}B_{12} + \tfrac{v}{h}\tfrac{dh}{dx}B_{12} - \tfrac{1}{2a_T\lambda_i}(B_{12}(B_{11} + B_{22}) - 1 + \\
&\quad \tfrac{1}{3}(\mathrm{tr}B - B_{11} - B_{22} - B_{33})B_{12})
\end{aligned}
\tag{3.31}
$$

where $\mathrm{tr}B$ is the trace of the inverse of the tensor B which is given by

$$
\mathrm{tr}B = \frac{B_{11}B_{22} + B_{11}B_{33} + B_{22}B_{33} - B_{12}{}^2}{B_{11}B_{22}B_{33} - B_{33}B_{12}{}^2} \tag{3.32}
$$

The equations (3.30) and (3.31) are solved using the same numerical method as for the PTT equation.

3.4.3 Results

For experiment 3 (DR=6.7, BUR=1.5) on LDPE L1o the stress build-up in the bubble forming region is shown in figure 3.13. It is seen that the experimentally observed stresses in the machine direction are underpredicted by the Wagner model and overpredicted by the Giesekus model. The PTT and the Leonov model seem to predict these stresses fairly well. For all four

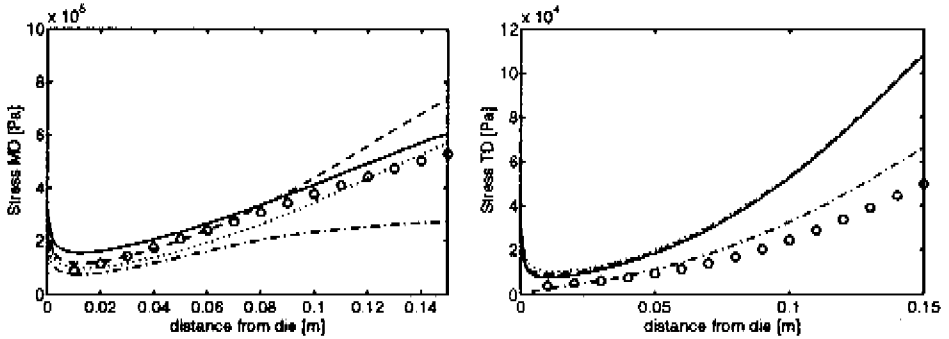

Figure 3.13: Experimentally determined and calculated stress in the machine and the transverse direction versus distance from the die for experiment 3 (L1o). PTT (—), Giesekus (- -), Leonov (..), Wagner (-.) and experimental (o).

models it is observed that the stress induced by the shear deformation in the die first partly relaxes, and only a few centimeters after the die, the stress is build up by the elongational flow caused by the deformation by drawing and blowing up of the film.

The stresses in the transverse direction are overpredicted by all three differential models, whereas the Wagner model predicts these stresses satisfactory. It should be mentioned, however, that the experimental determination of σ_{TD} is rather dubious because the second derivative of the radius is needed to obtain this stress (see equation (3.6)). Since a fifth order polynomial was fitted on the radius, it is not clear whether the second derivative of this polynomial is a good approximation. Therefore, the calculated radius of curvature R_m could contain mistakes leading to an inaccurate determination of σ_{TD}.

Note the difference in the stress build-up in the transverse direction. Due to the shear flow in the die, the three differential models have built up a second normal stress difference, leading to a non zero transverse directional stress at the die. Since for the Wagner model no second normal stress difference in shear is obtained, the transverse directional stress for this model is zero here.

For experiment 9 (DR=4.4, DR=2.5) the stress build-up is shown in figure 3.14. Here, it is observed that the stress in the machine direction is slightly underpredicted by the Wagner and the Leonov model and overpredicted by the PTT and the Giesekus model. The stress in the transverse direction is predicted well by the Wagner model and overestimated by the

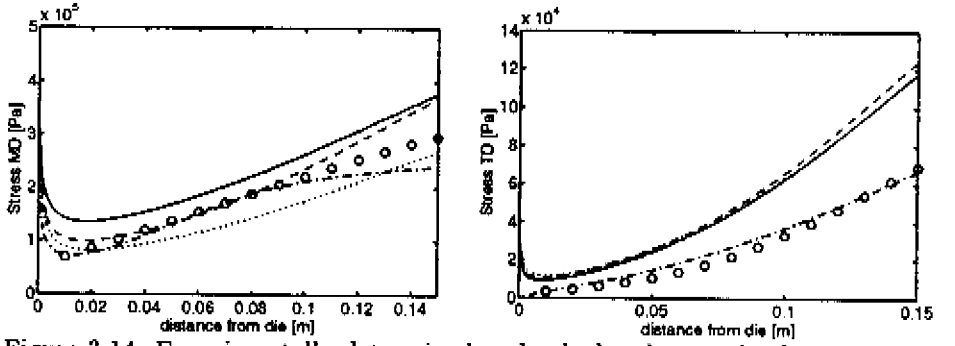

Figure 3.14: Experimentally determined and calculated stress in the machine and transverse direction versus distance from the die for experiment 9 (L1o). PTT (—), Giesekus (- -), Leonov (..), Wagner (-.) and experimental (o).

differential models.

As was indicated in Chapter 1, the stresses at the freeze line might be of great importance in the prediction of the ultimate film properties. Therefore, it is of interest to compare the calculated stresses at the freeze line height with the experimentally determined stresses. Since for all experiments the stress in the machine direction is at least 3.67 higher than the stress in the transverse direction, the most important stress is σ_{MD}, as will be shown in Chapter 5. In figure 3.15, the experimentally determined σ_{MD} is compared to the calculated σ_{MD}. Note that the experimental σ_{MD} are slightly lower than the stresses given in table 3.6. This is because the tabulated stresses are calculated beyond the freeze line, while the stresses in figure 3.15 are calculated at the freeze line.

From these figures, it is easily concluded that the stresses are underpredicted by the Wagner model, especially for LDPE L8. Note that for this material the elongation rates are much higher than for the other two materials, as can be seen in figures 3.6, 3.7 and 3.8. Apparently, the Wagner model is not able to predict the stress in the machine direction with parameters obtained from shear and uniaxial elongation only. Deviations from experiments become larger if the elongation rates increase. The results for the Wagner model are in agreement with those obtained by Fisher [1983]. He made a modification to the Wagner model to be able to predict the stresses satisfactory. In this modification the nonlinearity has to be left intact inside the die, while a linear viscoelastic integral model has to be used for the melt that has left the die. It should be mentioned that by making such a

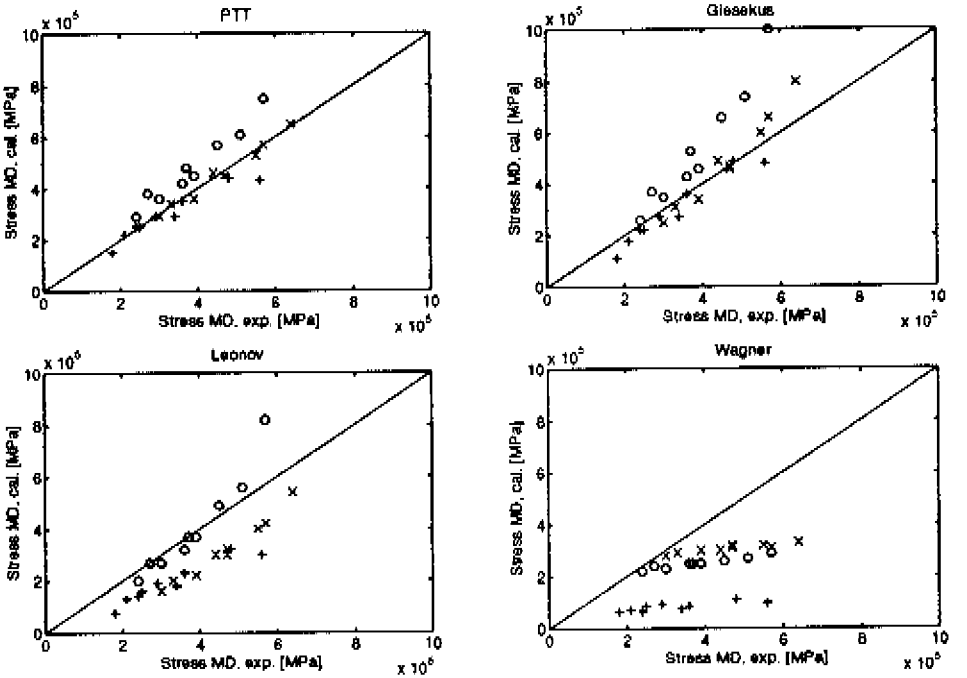

Figure 3.15: Experimentally determined stresses at the freeze line height versus calculated stresses with various constitutive equations. L1o (o), L1 (x), L8 (+).

modification an inconsistent constitutive relation is obtained.

The Leonov model also shows a too pronounced strain thinning behaviour. For LDPE's L1 and L8 the stresses predicted are too low, for LDPE L1o reasonable results are obtained. Luo and Tanner [1985] also concluded that the Leonov model was not stiff enough to model the film blowing process.

The Giesekus model tends to predict stresses which are too high, especially for the materials with melt index 1 (L1o and L1) at high elongation rates. This is due to the fact that the Giesekus model is not able to predict strain thinning behaviour at relatively high elongation rates in planar and biaxial elongation.

For the PTT equation fairly good predictions of the stresses are obtained. Only for LDPE L1o the calculated stresses are slightly higher than the experimental stresses.

Since strange enough, in many simulations of the film blowing process the shear flow inside the die is ignored, it is of interest to see what would be the

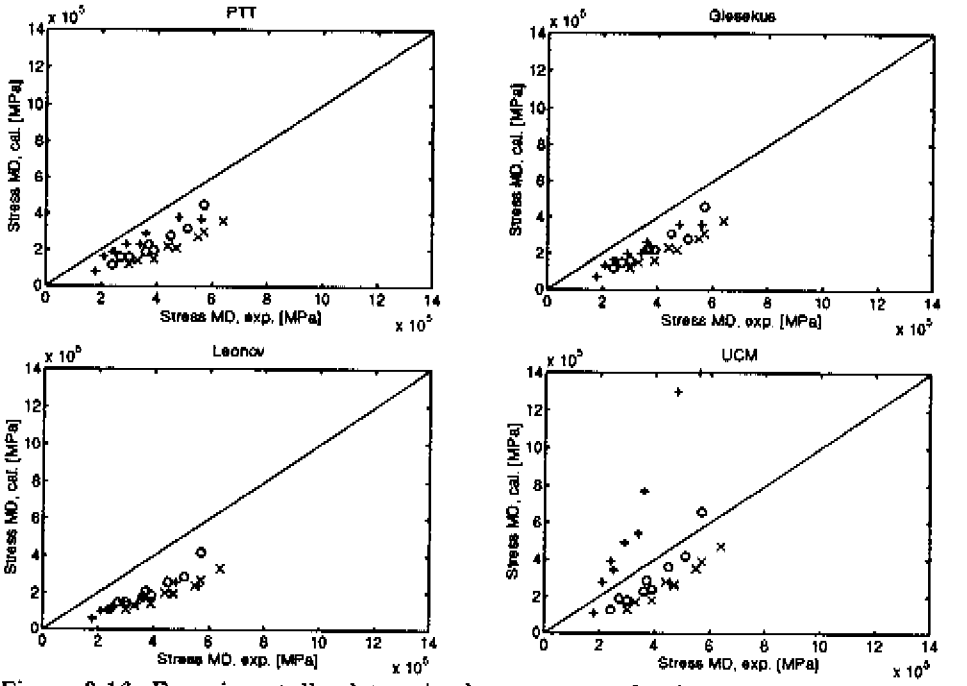

Figure 3.16: Experimentally determined stresses at the freeze line height versus calculated stresses with various constitutive equations without taking into account the shear in the die. L1o (o), L1 (x), L8 (+).

stress predictions of the constitutive models without taking the intermediate shear rate into account. Figure 3.16 shows the experimental stresses σ_{MD} versus the the stresses at the freeze line height, calculated without shear in the die. In this figure the predictions of the Wagner model are replaced by the predictions of the Upper Convected Maxwell model, i.e. the nonlinearity function is set to unity. Even though, results are not satisfactory. The three nonlinear models underpredict the experimentally observed stresses for all three materials. Apparently, in modelling the film blowing process with nonlinear viscoelastic models, the incorporation of shear flow in the die is indispensable. Moreover, from experimental experience, it is known that the flow in the die also influences the final properties of the film.

The Upper Convected Maxwell model shows an interesting feature. For the two materials with melt index 1, the stresses are slightly underpredicted while for the melt index 8 material the stresses are strongly overpredicted. This is explained by the fact that for L8 the elongation rates are much higher than for the other two materials. Apparently, in this elongation rate regime

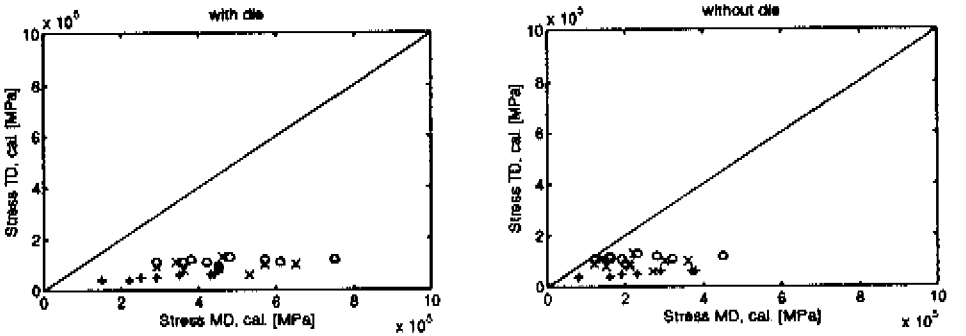

Figure 3.17: Calculated σ_{TD} versus calculated σ_{MD} at freeze line for PTT model, with and without incorporation of the shear flow in the die. L1o (o), L1 (x) and L8 (+).

a nonlinear model is required.

The most remarkable difference in calculating stresses with or without incorporation of the shear flow in the die, is demonstrated in the stress ratio (σ_{MD}/σ_{TD}). For the PTT model, the calculated stress σ_{TD} at the freeze line is plotted against the calculated σ_{MD} in figure 3.17. Similar results are obtained for the Leonov and the Giesekus model. The calculated σ_{TD} does not depend on the shear flow in the die. Moreover, the calculated σ_{TD} for the nonlinear differential models equals the calculated σ_{TD} for the Upper Convected Maxwell model. Apparently, the elongation rates in the transverse direction are not high enough to differentiate between these models. The σ_{MD} calculated without the flow in the die is, however, lower than σ_{MD} with incorporation of this flow. As a result, the stress ratio for calculations without shear flow becomes smaller and tends to go to unity. This is not in agreement with the experimental observations (see figure 3.12). So, to obtain a stress ratio which is in accordance with the experimentally determined ratio, the incorporation of the shear flow in the die is essential.

3.4.4 Conclusions

The main conclusions of this part of the research are listed below.

- In calculating the stresses in the film, various constitutive equations with parameters fitted on standard rheological experiments give different results.
  - The Wagner model exhibits a too pronounced strain thinning behaviour, resulting in an underprediction of the experimentally

determined stresses in the machine direction.

- The Leonov model is not stiff enough to predict the experimental stresses in the machine direction quantitatively correct.
- The Giesekus model does not show strong enough strain thinning behaviour in planar and biaxial elongation, at least at elongation rates which are typical for the film blowing process. Consequently, the experimental stresses are overpredicted.
- The PTT model gives fairly good agreement between calculated and experimentally determined stresses.

- In modelling the film blowing process the incorporation of the shear flow is essential.
  - Stresses in the machine direction, calculated without incorporation of the die, are too low if compared to the experimental stresses, at least for nonlinear viscoelastic models. Depending on the elongation rates, the predictions with the Upper Convected Maxwell model can become far too high.
  - The stress ratio (σ_{MD}/σ_{TD}) tends to go to unity for calculations where the flow in the die is neglected. This is not in agreement with experimental observations. Incorporation of the die gives qualitatively better results.

Returning to the key question posed in the beginning of this section, our results lead to the following answer:

> *To calculate the stresses in the film during film extrusion, a nonlinear viscoelastic material model is needed, and the incorporation of the flow in the die is essential. Comparison between calculations with the constitutive relations investigated and experimental results, leads to the conclusion that the PTT model is the most suitable.*

3.5 Discussion

In modelling the film blowing process it seems to be crucial to be able to determine stresses in the film correctly. Unfortunately, not many researchers have looked upon the film blowing process as a stress problem.

In this chapter it has been shown that a thorough measurement of stresses can lead to some interesting results. The stress ratio (σ_{MD}/σ_{TD}) for LDPE seems to be always higher than unity, even when the total deformation in the machine direction equals the total deformation in the transverse direction (DR=BUR). In modelling the film blowing process, the calculation of the stresses is not as straightforward as one may expect. Apparently, to obtain a reasonable stress ratio, the shear flow in the die should be incorporated. Furthermore, the choice of the constitutive equation is of great importance. Amongst the constitutive relations investigated, the PTT equation seems to give the best results, when calculated stresses are compared to experimentally determined stresses.

In Chapter 5 it will be shown that the stresses at the freeze line play a crucial role in predicting the ultimate film properties. Therefore, the results obtained in this chapter are of great value.

Chapter 4

Film Morphology

4.1 Introduction

In this thesis, the theory of flow induced crystallization is discussed aimed at getting a better understanding of the impact of processing conditions on the resulting structures of blown films in order to predict the film properties. In section 4.2 the basic concepts of orientation induced crystallization are dealt with and in section 4.3 the influence of flow induced orientation on the resulting blown film morphology is discussed.

4.2 Orientation induced crystallization

Crystallization characteristics of flowing polymer melts differ considerably from those of quiescent melts. Because the (segmental) orientation of the macromolecules in flowing melts results in a larger number of nuclei, the crystallization rates increase notably and even the crystallization temperature can rise. Apart from these phenomena, the micro-structure may be influenced by orientation induced crystallization and, consequently, the final properties of a product are affected.

A clear description of the influence of orientation of the macromolecules in the flowing melt on the crystallization kinetics is given by e.g. Ziabicki and Jarecki [1985]. Following their approach, first the basic concepts of crystallization are discussed, and, subsequently, the effect of orientation on crystallization is, shortly, reviewed.

4.2.1 Basic concepts of crystallization

Classical theories are based on equilibrium quantities only, such as the enthalpy Δh and the entropy Δs of crystallization, given by

$$\Delta h = h_c - h_a \quad \text{and} \quad \Delta s = s_c - s_a \tag{4.1}$$

where h is the enthalpy per segment and s the entropy per segment, while the subscript a denotes the amorphous and c the crystalline phase. The (equilibrium) crystallization temperature T_m can be obtained from the ratio

$$T_m = \frac{\Delta h}{\Delta s} \tag{4.2}$$

In crystallization kinetics, two main processes can be distinguished: the formation of nuclei and their growth to crystals. Because the latter process is often considered to be controlled by formation of surface nuclei, which implies that the crystal growth speed also depends on the nucleation rate, attention is focused on nucleation in general.

From e.g. Turnbull and Fisher [1949] and Frank and Tossi [1961] it is known that the basic driving force for nucleation is the Gibb's free energy ΔF of the transformation of g kinetic segments into a crystalline cluster of size g

$$\Delta F(g) = F_{cl}(g) - gF_1 \tag{4.3}$$

where F_{cl} is the free energy of the cluster and F_1 the free energy of a single isolated kinetic segment. For $g = 1$, $F_{cl} = F_1$ and so $\Delta F(1) = 0$. Since the free energy of a cluster is a combination of the bulk contribution, proportional to the size of the cluster g, and the surface energy, proportional to $g^{2/3}$, $\Delta F(g)$ reads

$$\Delta F(g) = \Delta f(g-1) + a(g^{2/3} - 1) \tag{4.4}$$

where a is the interface free energy per kinetic segment and Δf the bulk free energy per kinetic segment, which is a function of temperature T, Δh and Δs. Usually, a linear approximation, which is valid in the neighbourhood of the melting temperature, is taken to be representative

$$\Delta f = \Delta h - T\Delta s \tag{4.5}$$

Combining equations (4.2) and (4.5) yields

$$\Delta f = \Delta h \frac{T_m - T}{T_m} \tag{4.6}$$

Prerequisite for crystallization is that $d\Delta F(g)/dg < 0$. Because the term providing the free surface energy is positive, this implies that Δf has to be negative (see equation (4.4)). In the process of crystallization both the entropy s and the enthalpy h decrease and, therefore, Δs and Δh are negative. Consequently, Δf can only become negative if $T < T_m$, and thus this is a necessary condition for crystallization.

The critical cluster size g^* for which a nucleus can grow into a macroscopic crystal and the corresponding maximum of the free energy $\Delta F(g^*)$ is now introduced. Setting the derivative with respect to g of the free energy function $\Delta F(g)$ equal to zero, values for g^* and $\Delta F(g^*)$ are obtained

$$\begin{aligned} g^* &= -\left(\frac{2a}{3\Delta f}\right)^3 \\ \Delta F(g^*) &= \frac{4a^3}{27(\Delta f)^2} - (a + \Delta f) \end{aligned} \tag{4.7}$$

The first characteristic of crystallization, the crystallization temperature T_m, is given in equation (4.2). The second one, the nucleation rate $\dot{N}$, is controlled by the function $\Delta F(g)$ in the vicinity of its maximum $\Delta F(g^*)$ and is given by (Ziabicki and Jarecki [1985])

$$\dot{N} = C\left(\int_1^\infty \exp(\Delta F(g))dg\right)^{-1} \tag{4.8}$$

where C is an unknown constant. If the maximum in ΔF is sharp, equation (4.8) can be approximated by (Ziabicki and Jarecki [1985])

$$\dot{N} \approx C \exp\left(\frac{-\Delta F(g^*)}{kT}\right) \tag{4.9}$$

where k is the Boltzmann constant.

Obviously, the critical cluster size g^* and the nucleation energy $\Delta F(g^*)$ play an important role in the nucleation kinetics. For instance, an increasing bulk free energy per kinetic segment Δf or a decreasing interface free energy per kinetic segment a result in a decreasing critical cluster size g^*

and nucleation energy $\Delta F(g^*)$ and, consequently, the nucleation process accelerates and, because crystal growth is often considered to be controlled by formation of surface nuclei, also the crystallization rate increases.

At this point it becomes interesting to show the influence of orientation on the crystallization characteristics.

4.2.2 Basic concepts of orientation induced crystallization

Ziabicki and Jarecki [1985] investigated both the effect of molecular orientation on the crystallization of an 'average' macromolecule and the effect of segmental orientation on the crystal nucleation involving individual chain segments. Because a detailed analysis of the crystallization process is beyond the scope of this thesis, we will only deal with the first effect.

In general, orientation of macromolecules in a flowing polymer affects the enthalpy and entropy of both the crystalline and amorphous fractions. Denote the changes in Δh and Δs with δh and δs, then

$$\Delta h = \Delta h_0 + \delta h \quad \text{and} \quad \Delta s = \Delta s_0 + \delta s \tag{4.10}$$

where the subscript 0 refers to the situation of a quiescent melt (see equation (4.1)). Obviously, this modification of enthalpy and entropy results in a modification of the crystallization temperature, which becomes

$$T_m = \frac{\Delta h_0 + \delta h}{\Delta s_0 + \delta s} = \frac{T_m{}^0(1 + \delta h/\Delta h_0)}{1 + \delta s/\Delta s_0} \tag{4.11}$$

where $T_m{}^0$ is the (equilibrium) crystallization temperature of a quiescent melt as given by equation (4.2).

Furthermore, the bulk free energy per kinetic segment Δf is affected by the changes in enthalpy and entropy according to

$$\Delta f = \Delta f_0 + \delta h - T\delta s = \Delta f_0 + \delta f \tag{4.12}$$

where Δf_0 is given by equation (4.5). Substitution of equation (4.12) in equation (4.7) yields

$$\begin{aligned} g^* &= g^*{}_0(1 + \tfrac{\delta f}{\Delta f_0})^{-3} \\ \Delta F(g^*) &= \Delta F(g^*)_0(1 + \tfrac{\delta f}{\Delta f_0})^{-2} \end{aligned} \tag{4.13}$$

with $g^*{}_0$ and $\Delta F(g^*)_0$ given by equation (4.7).

From equations (4.8) or (4.9), and (4.13), it is easily concluded that the critical cluster size leading to crystal growth and the nucleation rate are affected by the change in enthalpy and entropy due to molecular orientation. To determine whether g^* and $\Delta F(g^*)$ increase or decrease, and so consequently the nucleation rate $\dot{N}$ (equations (4.8) and (4.9)), it is necessary to know the sign of δf.

The largest contribution to δf originates from the entropy change of the amorphous phase (Ziabicki and Jarecki [1985]). Obviously, molecular orientation in the melt reduces the entropy s_a and, neglecting all other orientation dependent contributions, it is obtained that

$$\begin{aligned} &\delta s_a < 0, \quad \delta s = -\delta s_a, \quad \tfrac{\delta s}{\Delta s_0} < 0 \\ &\delta f = -T\delta s = T\delta s_a < 0, \quad \tfrac{\delta f}{\Delta f_0} > 0 \end{aligned} \tag{4.14}$$

From equation (4.11) it is concluded that, because of the change of entropy, the crystallization temperature increases and raises above the crystallization temperature ${T_m}^0$ of a quiescent melt. Moreover, g^* and ΔF^* increase with molecular orientation resulting in an enhanced nucleation rate and, consequently, an enhanced crystallization rate.

Ziabicki [1973], Jarecki [1974,1979] and Jarecki and Ziabicki [1977] also investigated the influence of other contributions to δf, including enthalpy change of the amorphous phase and strain energy of crystals, on the crystallization characteristics. They concluded that each of these contributions raised the crystallization temperature and increased the nucleation rate.

To demonstrate the dependency of δs_a on the macromolecular orientation, the analogy between a polymer melt and a rubber is assumed, as was already proposed by e.g. Peterlin [1976]. In general, the average change of entropy per segment of the amorphous phase equals

$$\delta s_a = \frac{1}{N} k \int (W(\vec{R} \,.\, \vec{R}) - W_0(\vec{R} \,.\, \vec{R})) \ln W_0(\vec{R} \,.\, \vec{R}) d\,\vec{R} \,.\, \vec{R} \tag{4.15}$$

where $\vec{R} \,.\, \vec{R}$ is the end-to-end vector, $W_0(\vec{R} \,.\, \vec{R})$ the end-to-end vector distribution for a quiescent melt and $W(\vec{R} \,.\, \vec{R})$ the end-to-end vector distribution for the deformed melt. The factor $\frac{1}{N}$ accounts for the fact that δs_a is the

entropy increment per segment. For a rubber network subjected to uniaxial elongation, this equation yields

$$\delta s_a = -\frac{k}{2N}(\lambda^2 + \frac{2}{\lambda} - 3) \tag{4.16}$$

where λ is the elongation ratio. Setting $T\delta s_a$ equal to δf, the effect of elongation on the crystallization temperature, equation (4.11), and on the nucleation rate, equations (4.9) and (4.13), can easily be deduced. Ziabicki and Jarecki [1985] showed examples of the theoretical increase of T_m and $\dot{N}$ with increasing λ for PET high speed melt spinning. For T_m a maximum increase of 60 K was reported, while the nucleation rate can even become 10^{20} times the nucleation rate of a quiescent melt. It should be mentioned, however, that in high speed melt spinning, stresses are reached in the order of 10 MPa, while in e.g. film blowing maximum stresses of approximately 1 MPa are found. So, the effect of orientation in film blowing, induced by the deformation in the bubble forming region, is expected to be much less pronounced.

Furthermore, Ziabicki and Jarecki [1985] concluded that it should be reasonable to present the thermodynamic and kinetic characteristics of crystallization in terms of the stress applied to the deforming polymer melt. After all, if the stress optical law is applied (which is permitted if the stresses are relatively low like in e.g film blowing) this stress is a direct measure of the orientation, independent of the type of flow and the molecular weight or molecular weight distribution of the polymer.

Without going into further detail, it is worthwhile to mention that a considerable amount of studies has been performed to the effect of orientation on crystallization. Extensive reviews are given by e.g. White and Cakmak [1986] and Ziabicki and Jarecki [1985] on the structure development in melt spinning of fibres, and by Eder *et al.* [1990] on shear induced crystallization, while the Bristol group mainly focused on the homogeneous flow of pressure quenched or supercooled, relatively high molecular weight linear PE's which resulted in interesting morphologies (see e.g. the review of Keller and Kolnaar [1993]). Especially the work of the group of Janeschitz-Kriegl at the Johannes Kepler University (Eder *et al.*) in Linz is of interest. They were able to unravel some of the mysteries of orientation induced crystallization by setting up a new theory in which the nucleation rate was made dependent on the complete flow- and temperature-history. In later work of this group the theory was extended (Liedauer *et al.* [1993,1994]).

Furthermore, the results obtained by Lagasse and Maxwell [1976] are also worth mentioning. For three linear (high molecular weight) PE's they reported that at a shear rate of only 10 s^{-1} the crystallization induction time reduced by a factor 100. Apparently, crystallization of these materials is very sensitive to a relatively small orientation in the melt.

4.3 Blown films

From the preceding section, it became clear that orientation induced crystallization also plays an important role in the film blowing process. As was already mentioned in Chapter 3, the effect of undercooling of the melt seems to be counterbalanced by the enhanced crystallization due to the orientation of the macromolecules in the bubble forming region. Therefore, the crystallization temperature in the film is approximately equal to the crystallization temperature as obtained from DSC measurements at a cooling rate of 1 C^o/min. This does not mean, however, that the crystallization kinetics in the film and in the DSC sample are identical, and film morphologies will differ notably.

From the films made during the experiments described in Chapter 3, those which exhibit the most extreme orientation were subjected to a transmission electron microscope (TEM) investigation. In order to understand the results obtained, first some existing ideas about the expected film morphology are discussed. For an extensive review on the structure development in blown films, the reader is referred to White and Cakmak [1988].

4.3.1 Ideas about morphology

Based on experimental observations on fibres in a stirred undercooled dilute UHMW-PE solution, Pennings [1967] proposed a model for a crystalline structure consisting of (so-called) shish-kebabs: highly oriented chain segments in the flow direction form a long (and thin) central nucleus (shish) from which folding chain lamellae (kebabs) grow in the perpendicular direction. Since the extreme shish-kebab structure has never been found for LDPE blown films, apparently because the orientation is not extremely high (see Chapter 3) and the polymer concentration is much higher, it is not likely to suppose that this shish-kebab structure is representative for these films. Keller and Machin [1967] proposed a model which is more relevant for the orientation induced crystalline structures in more concentrated systems. They made a distinction between polymers crystallized at a high and a low stress

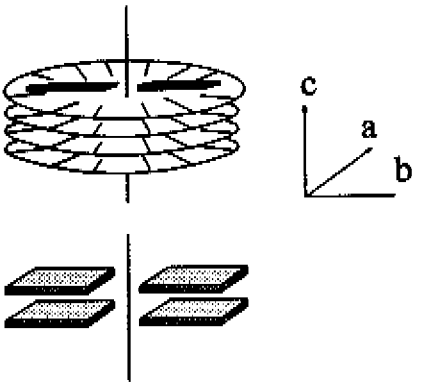

Figure 4.1: Model of Keller and Machin [1967] of crystallization at high stresses.

state. At high stresses, stacked lamellae are formed with their normals in the direction of stress (see figure 4.1). The c-axis is in the stress direction, while the a- and b-axes grow perpendicular to this direction.

Low stresses (see figure 4.2) also result in the formation of stacked lamellae with their normals in the stress direction. The difference with the high stress case is seen in the orientation of the a- and c-axes. The b-axis orientation is again perpendicular to the stress direction, but now the a- and c-axes are twisting around the b-axis. The morphology thus obtained can be seen as a row nucleated structure, with the lamellae growing perpendicular to the stress direction in a twisted manner.

From experimental findings (Nagasawa *et al.* [1973], Choi *et al.* [1982] and Kwack *et al.* [1988]) it seems that the latter model is the most suitable

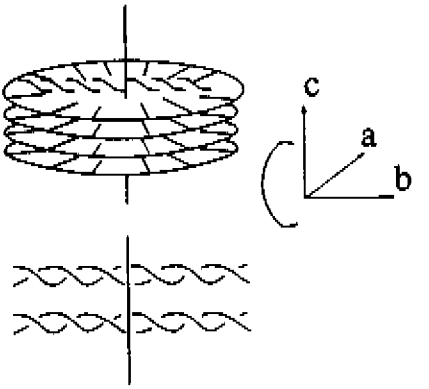

Figure 4.2: Model of Keller and Machin [1967] of crystallization at low stresses.

to describe the morphologies observed for LPDE blown films.

In a series of papers, Nagasawa *et al.* [1973] investigated the development of molecular orientation and the microstructure in tubular blown films. On-line measurements of film birefringence were reported for three semi-crystalline polymers, including a HDPE. In order to avoid problems with the birefringence measurements, the blow up ratios in their experiments were equal to unity. It was concluded that no extreme orientation was build up in the bubble forming region, but that this slight orientation of macromolecules in the molten state enhanced the crystallization rate to a great extent and, moreover, controlled the growth direction of the crystals. The microstructure was investigated with X-ray diffraction and electron microscopy. Two stages in the crystallization process could be distinguished. In the first stage, lamellar crystals, having c-axis orientation along the direction of the principal stress, grew in a direction perpendicular to the stress along the b-axis, indicating a shish kebab-like structure. In the second stage, the lamellae grew with twisting around the b-axis, where the size of the lamellar crystals in the b-axis direction was small because of the large number of nuclei. Consequently, the number of twists was small. Furthermore, they concluded that the surfaces of PE blown films were composed of fine lamellae piled up one on top of another with their normals aligned parallel to the extrusion direction. For an interpretation of the microstructure found, they proposed a model based on a rod having a central core with c-axis orientation and twisted lamellae originating from the core in which the a-axis is oriented preferentially along the extrusion direction.

Choi, Spruiell and White [1982] reported a study on the orientation and morphology of a HDPE film produced by film blowing and its relationship to processing conditions. The orientation and crystallization was measured by film birefringence and wide angle X-ray scattering (WAXS). The data obtained were used to compute biaxial orientation factors, which are modifications of the well-known Hermans' orientation factor. Also, the take-up force was recorded by a tensiometer and the bubble pressure by a manometer, from which the stresses at the freeze line were calculated. It appeared that both biaxial crystalline orientation factors were unique functions of these stresses, independent of the blow up ratio.

As a matter of fact, in an earlier paper by Choi *et al.* [1980] it was found that the birefringence of PolyStyrene films was a linear function of the stresses at the freeze line, as may be expected for an amorphous polymer if the stresses are not extremely high (White and Cakmak [1986], Yilmaz and Cakmak

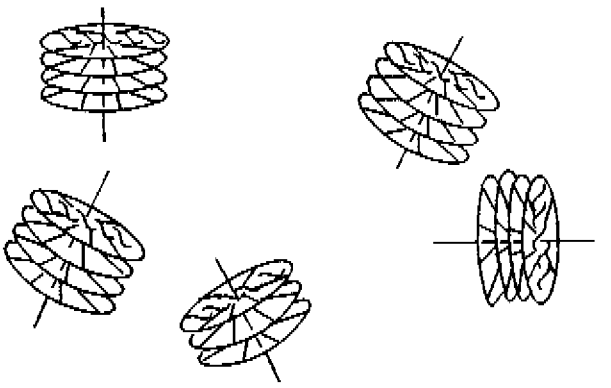

Figure 4.3: Model for crystalline morphology proposed by Choi *et al.* [1982]

[1994]).

Furthermore, from small angle X-ray scattering (SAXS) experiments it was concluded that lamellar structures exist in both uniaxally and biaxially oriented PE films. A closer examination of the uniaxally oriented films indicated a row structure or cylindrite morphology of the low stress type proposed by Keller and Machin [1967] (see figure 4.2)

To obtain a model which is also consistent with the data of the more biaxial films, Choi *et al.* [1982] proposed a modification of Keller and Machin's model, which is depicted in figure 4.3. Packages of stacked lamellae (exhibiting a twisted ribbon texture), with a mean orientation distribution function depending on the direction of the principal stress are embedded in a matrix of amorphous PE.

Results obtained by Kwack *et al.* [1988] more or less supported this morphological model of blown films. In their study, the development of crystalline structure during film blowing of a LDPE and a LLDPE was investigated using WAXS, low angle light scattering (LALS) and scanning electron microscopy (SEM).

An interesting difference between LDPE and LLDPE film morphologies was observed. For LLDPE, the imposition of relatively low stresses accompanied with a low value of the ratio of the stress in the machine direction to the stress in the transverse direction seemed to bring about a more or less spherulitic structure. For LDPE, at similar processing conditions as for LLDPE, higher values for the stress in the machine direction were obtained, while the stress ratio was deviating notably from unity. Film morpholo-

gies obtained for LDPE were similar to those reported by Choi *et al.* [1982]. Apparently, the structural development could not be described solely by processing parameters like BUR and DR. Instead, one must use the magnitude and direction of stresses to predict the resulting film morphology.

4.3.2 Experimental: stresses and morphology

Experimental. For each grade the most uniaxally oriented and the most biaxially oriented films were investigated by means of Transmission Electron Microscopy (TEM) at DSM Research. The films investigated correspond with the experiments 2 and 10 (L1o), 11 and 19 (L1) and 26 and 30 (L8) (see Chapter 3, section 2). To obtain a visual contrast between amorphous and crystalline regions of the films, they were stained for 8 hours in RuO_4 at room temperature. Subsequently, they were embedded in an epoxy resin, trimmed and cut into slices of 70 nm thickness by means of ultra microtome at room temperature. The slices were cut in the M-N plane (the plane normal to the film surface and the machine direction, see figure 4.4). Next, the slices were investigated using a Philips TEM CM 200 with a beam current of 120 kV.

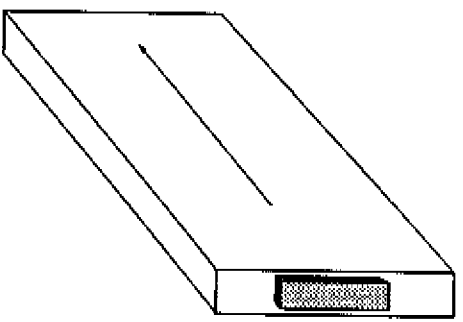

Figure 4.4: Direction of the slices investigated by TEM, given by the filled pattern in the film. The arrow denotes the machine direction.

Results. Because the TEM results were approximately similar for all three materials (L1o, L1 and L8) and the clearest pictures were obtained for material L8, only the results for this grade are shown. In figure 4.5 the result for film nr. 26, being the most uniaxally oriented film, is depicted, while in figure 4.6 the result for film nr. 30 (the most biaxial) is shown.

From figure 4.5 it is easily concluded that for this uniaxally oriented film (σ_{MD}=7.6 $10^5 Pa$ and σ_{MD}/σ_{TD} = 9.87, see Chapter 3) the visual lamellae are more or less parallel to each other and are mainly oriented so that their normal is in the machine direction. The length of the lamellae is

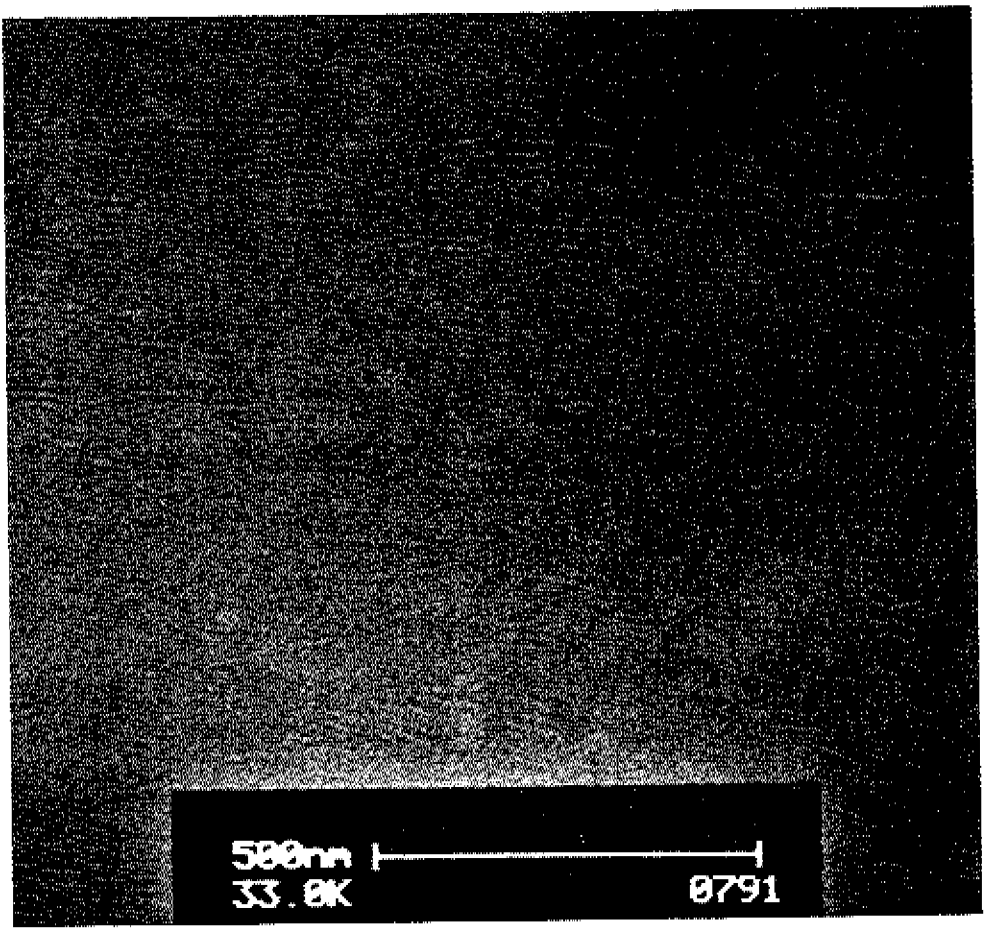

Figure 4.5: TEM micrograph of film nr. 26 (LDPE L8, see Chapter 3)

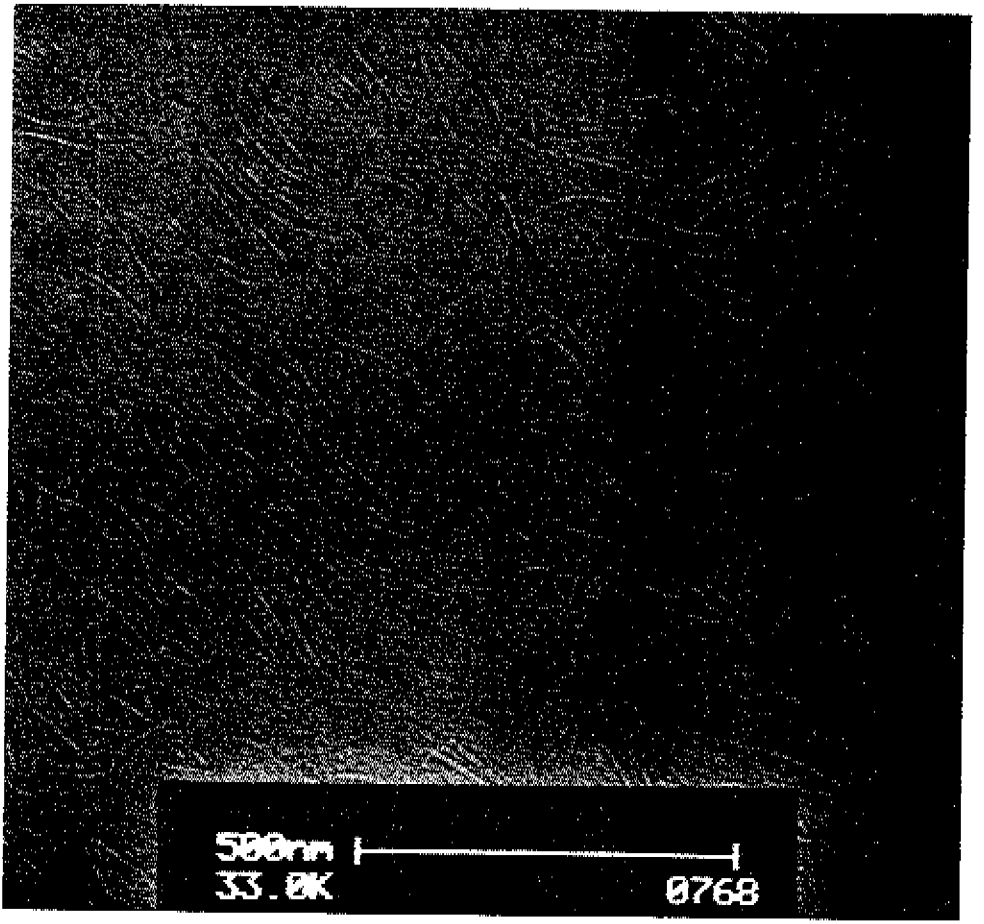

Figure 4.6: TEM micrograph of film nr. 30 (LDPE L8, see Chapter 3)

approximately 100 nm.

For the more biaxially oriented film (figure 4.6, σ_{MD}=2.2 $10^5 Pa$ and $\sigma_{MD}/\sigma_{TD} = 3.67$, see Chapter 3) the length of the lamellae is the same, but they are more or less randomly distributed. Furthermore, it is observed that in this case the lamellae are not as straight as for the uniaxial case. The lamellae tend to turn as their length increase.

Similar features have been observed for the other two grades. Relatively high uniaxial orientation of the macromolecules in the melt results in highly oriented, stacked lamellae which are straight, while a more or less biaxial ori-

entation in the melt (but low stresses in all directions) result in a more or less randomly distribution of stacked lamellae. These results are in agreement with the morphological model proposed by Choi *et al.* [1982] and discussed in the preceding section. As was the case for the melt index 8 material, the length of the lamellae for the melt index 1 materials was approximately 100 nm for both uniaxial and biaxial films.

Apparently, independent on the grade, LDPE blown films exhibit similar film morphologies, depending on the orientation state of the macromolecules at the onset of crystallization, as initiated by the melt flow.

4.4 Conclusions

The fundamentals of the model for crystal morphologies at low stress, set up by Keller and Machin [1967], seem to hold for LDPE blown films. A row nucleated structure with twisted lamellae is obtained in LDPE blown films. The fact that not all normals on these lamellae are pointing in the same direction is taken into account by an extension to this model as proposed by Choi *et al.* [1982]: the crystalline morphology consists of packages of stacked lamellae for which the main orientation distribution depends on the stresses and the stress ratio at the freeze line.

The results of TEM on the most uniaxial and the most biaxial films for the LDPE's investigated in this research are in line with this proposed morphology. For the most uniaxial films, almost a perfect orientation of the lamellae in the machine direction is observed, while for the more biaxially oriented films a more or less random distribution of the lamellae could be discerned. The length of the lamellae is in both cases equal. No differences were observed between the three different grades.

Based on this dependence of the morphologies to the stresses at the freeze line, in Chapter 5 it is tried to correlate the film properties to these stresses.

Chapter 5

Film properties

5.1 Introduction

In Chapter 4, section 3 it was discussed that morphologies of blown films can be correlated with stresses at the freeze line, as was shown by Choi *et al.* [1980,1982], Kwack *et al.* [1988] and White and Cakmak [1988]. Unfortunately, none of these authors investigated the influence of these stresses on the ultimate film properties. Though Kanai [1987] and Kanai *et al.* [1986] did not plot the film properties versus stresses, they pointed out that these stresses have a great impact on the properties, at least for HDPE. With respect to this suggested influence of stresses on properties, it is interesting to note that only very recently Yilmaz and Cakmak [1994] found the mechanical properties to correlate well with the spinline stress for melt spun fibers of an amorphous Poly(Arylene Ether Sulfone), independent of the processing temperatures.

In section 5.2, the stresses at the freeze line will be correlated with the mechanical properties. In section 5.3 the shrinkage of blown films, which is a measure for the frozen-in orientation, is calculated with the PTT model and compared with measured shrinkage values. Section 5.4 deals with the optical properties of films and, finally in section 5.5 the main points of this chapter are summarized and discussed.

5.2 Mechanical properties

Various mechanical properties (the longitudinal and transverse moduli, tensile strength, yield stress, elongation at break, tear resistance, and the im-

pact strength) of the blown films (see Chapter 3) have been measured at DSM. For all properties an average of -at least- five experiments was determined to obtain the final representative values. All mechanical tests were performed at room temperature. Here, they are discussed as a function of the draw ratio DR (except for the impact strength which is related to the ratio DR/BUR) and as a function of the stresses at the freeze line, calculated using the PTT model (see Chapter 3). Analogous to the macroscopic ratio's DR and DR/BUR, all properties are discussed with regard to σ_{MD}, except for the impact strength, which will be related to the stress ratio σ_{MD}/σ_{TD}. Given the great unbalance of the films (for all experiments $\sigma_{MD} \gg \sigma_{TD}$, see Chapter 3), and the resulting dependence of the crystalline morphology on σ_{MD} (see Chapter 4), this seems to be the most logical choice. Apart from that, plotting properties other than impact versus BUR or σ_{TD} and DR/BUR or σ_{MD}/σ_{TD} did not result in any correlation and only obscured the dependence on processing conditions and LDPE grade.

In the analyses of the results, the influence of the density (and,thus, differences in crystallinity of the films) is not incorporated. The crystallinity did not depend to a great extent on the processing conditions and proved to be, as measured via optically measured densities (Gurp [1992]), $\chi = 0.432 \pm 0.002$ for grade L1o, $\chi = 0.427 \pm 0.002$ for grade L1 and $chi = 0.422 \pm 0.004$ for grade L8. This independence of crystallinity on processing conditions was also found by e.g. Simpson [1993], who investigated among other things the influence of draw ratio, blow up ratio and freeze line height on the crystallinities of HDPE and LDPE films by means of DSC.

5.2.1 Longitudinal and transverse moduli

Tensile tests were performed on samples with initial length $l_0 = 100mm$, using a tensile speed 25 mm/min. Moduli in longitudinal and transverse direction were obtained from the mean slope of the stress between 1 % and 2 % elongation (according to DSM internal standards). (Measuring this $E_{(1-2\%)}$ modulus has the advantage that irregularities occurring in the beginning of the stress strain curve are excluded; after all, at low strains the measuring error is relatively high). Results are shown in figure 5.1, where the moduli are depicted as functions of the draw ratio DR.

For all three grades, it is seen that an increasing DR results in increasing moduli. However, the effect of the DR on the moduli for the melt index 1 materials L1 and L1o, which proved to behave very alike, is more pronounced than for the melt index 8 material L8. Consequently, the curves for the

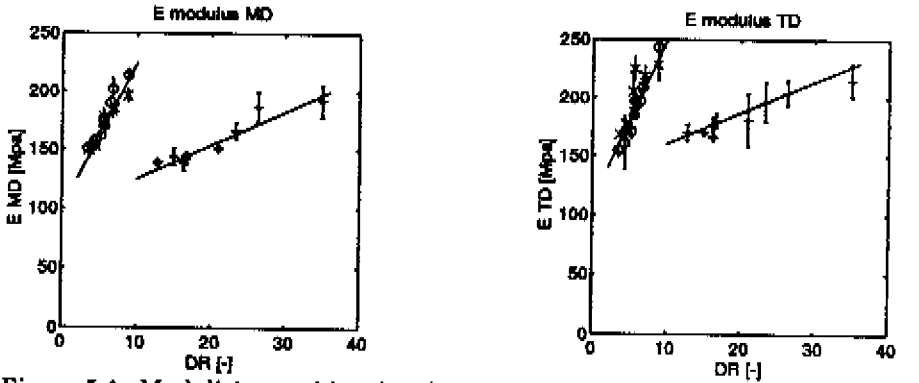

Figure 5.1: Moduli in machine (MD) and transverse direction (TD) versus Draw Ratio for grades L1o (o), L1 (x), L8 (+).

different grades do not match one with another. It is also seen that the moduli in transverse direction exceed the moduli in longitudinal direction, which is commonly found for LDPE blown films.

Since the morphology depends on the stress exerted to the film at the freeze line and since the modulus is a linear elastic property, it might be expected that equal stresses at the freeze line should result in equal moduli. From figure 5.2, where the moduli are plotted versus σ_{MD}, it indeed is seen that the data obtained for the various grades collapse onto one master curve. As already mentioned in the preface of this chapter similar results, albeit for a much simpler system, were recently reported by Yilmaz and Cakmak [1994]. For melt spun Poly(Arylene Ether Sulfone) filaments they found that

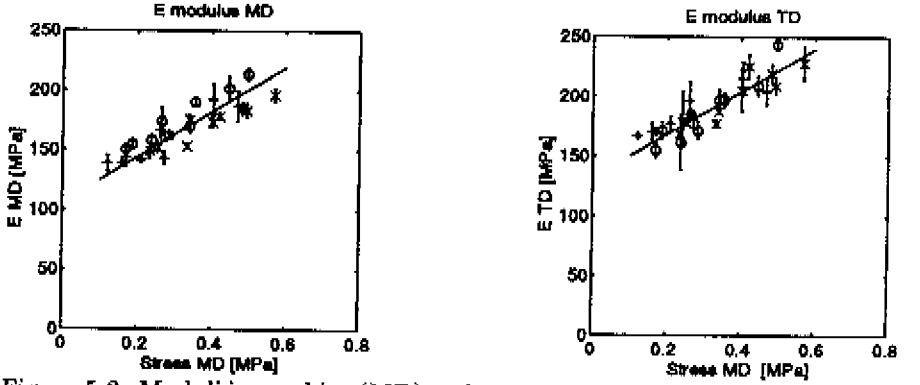

Figure 5.2: Moduli in machine (MD) and transverse direction (TD) versus the stress at the freeze line σ_{MD} for grades L1o (o), L1 (x), L8 (+).

different processing temperatures resulted in different lines, when the moduli were plotted versus the draw down ratio, while plotting these moduli versus the birefringence measured resulted in one master curve.

Correlation coefficients found for the relations $\sigma_{MD} \leftrightarrow E_{MD}$ and $\sigma_{MD} \leftrightarrow E_{TD}$ were 0.92 and 0.91, respectively. Apparently, independent of the type of LDPE, die geometry and the precise processing conditions during blowing, to a great extent equal stresses at the freeze line result in equal longitudinal and transverse moduli.

5.2.2 Tensile strength, yield and elongation at break

Tensile tests were performed according to ISO R527. From the stress strain curves the tensile strength (stress at break) and elongation at break were obtained in both machine and transverse direction, while in the latter case also a yield stress was observed.

Tensile strength and elongation at break in the machine direction. In figure 5.3 the tensile strength and the elongation at break, both in the machine direction, are shown as functions of the draw ratio DR. Increasing the draw ratio results in an increasing tensile strength and a decreasing elongation at break for all grades. As was also the case for the moduli, the effect of the draw ratio on these properties depends on the type of LDPE.

In figure 5.4 the tensile strength (MD) and elongation at break (MD) are plotted versus the stresses at the freeze line. Also here results for the melt index 1 materials and the melt index 8 material collapse onto one single

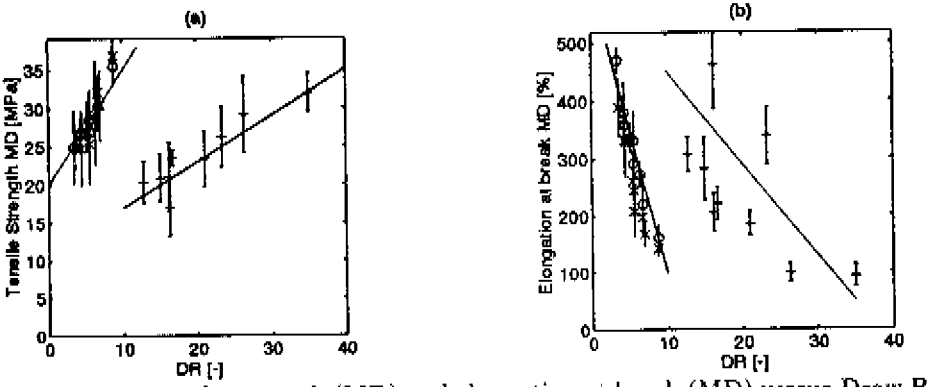

Figure 5.3: Tensile strength (MD) and elongation at break (MD) versus Draw Ratio for grades L1o (o), L1 (x), L8 (+).

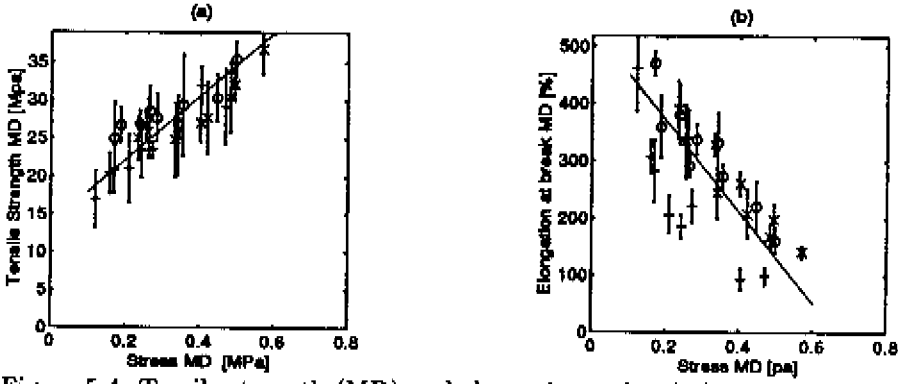

Figure 5.4: Tensile strength (MD) and elongation at break (MD) versus the stress at the freeze line σ_{MD} for grades L1o (o), L1 (x), L8 (+).

master curve. Correlation coefficients obtained for the relations $\sigma_{MD} \leftrightarrow$ tensile strength (MD) and $\sigma_{MD} \leftrightarrow$ elongation at break (MD) were 0.89 and -0.73, respectively. The values of these coefficients are not very satisfying but, given the results of figure 5.3, support the fact that, independent of the type of LDPE, die geometry and the processing conditions, equal stresses at the freeze line result in equal tensile strength (MD) and elongation at break (MD).

This is a surprising result, since the failure point in the stress strain curve, which determines the tensile strength, occurs after significant plastic deformation which is essentially a cold drawing process and, consequently, it might be expected to see some distinction between the different materials.

Yield stress. Before reaching the elongation at break in the transverse direction, the samples first showed yielding behaviour, which was, as expected because of the fact that the main orientation is in the machine direction, not the case in the machine direction.
Because the yield stress borders the linear part of the stress strain curve, similar results as found for the moduli are expected for this property. Although the yield stress proved to be weakly dependent on the processing conditions, it indeed is seen that the two master curves in figure 5.5a (yield stress vs. DR) collapse more or less onto one unifying master curve if the yield stress is plotted versus the stress at the freeze line (figure 5.5b).

Closer examination of this figure shows that the yield stresses for grade L1o exceed those of the other two grades. Apparently, the relatively small differences in crystallinities show their influence in the yield stress. Because

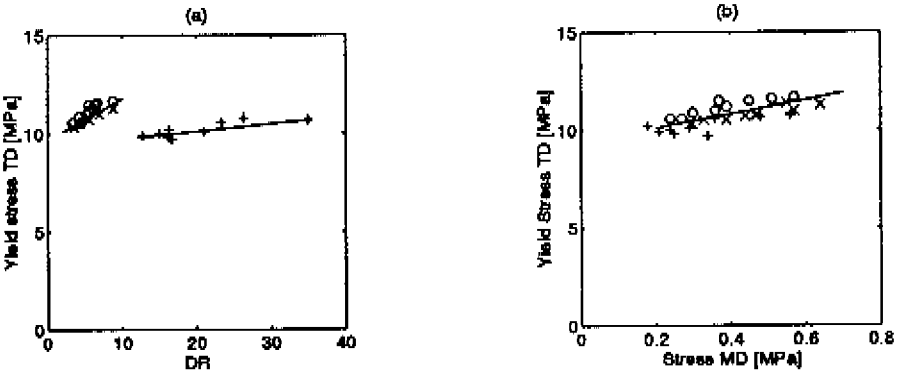

Figure 5.5: Yield stress (TD) versus Draw Ratio (a) and stress at the freeze line σ_{MD} (b) for grades L1o (o), L1 (x), L8 (+).

of this effect, the correlation coefficient for the relation $\sigma_{MD} \leftrightarrow$ yield stress is only 0.71.

Since, generally, the yield stress is positively correlated with the moduli (see e.g Brown [1986]), the effect of crystallinity should also be seen in figures 5.1 and 5.2. Indeed, the longitudinal moduli for grade L1o exceed those for the other two grades. The transverse moduli, however, do not show a clear distinction between the three grades.

Tensile strength and elongation at break in the transverse direction. The effect of draw ratio on the tensile strength and elongation at break in the transverse direction is shown in figure 5.6. In contradiction with the effect of draw ratio on the tensile strength in the machine direction, it is observed that increasing the draw ratio results in a decreasing tensile strength in the transverse direction. It is even seen that a correlation between the draw ratio and the tensile strength (TD) exists (correlation coefficient $log(DR) \leftrightarrow$ tensile strength (TD) = -0.90).

From figure 5.6b it is concluded that for the elongation at break (TD) an increasing DR results in a decreasing elongation at break, where the effect for the melt index 1 materials is more pronounced than for the melt index 8 material.

Plotting the tensile strength (TD) and the elongation at break (TD) versus the stress at the freeze line (figure 5.7) does not result in any improvement towards more unifying relations. Figure 5.7b does even obscure the relation between processing conditions, LDPE grade and the elongation at break (TD).

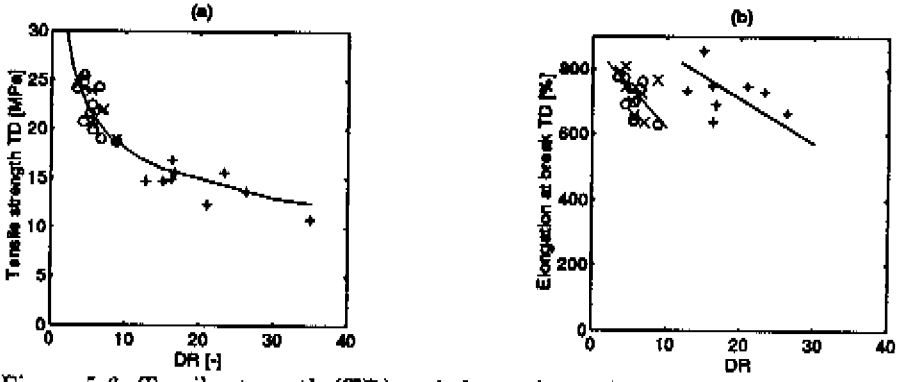

Figure 5.6: Tensile strength (TD) and elongation at break (TD) versus Draw Ratio for grades L1o (o), L1 (x), L8 (+).

From the comparison of figures 5.7a and 5.6a, it is, however, concluded that for the melt index 8 material, the dependence of the tensile strength on DR is only marginally and that it does not depend uniquely on the stress anymore. Apparently, there exists a limiting value for the tensile strength (TD) for this (relatively low molecular weight) material. Thus, care must be taken in the use of the apparently useful correlation $log(DR) \leftrightarrow$ tensile strength (TD), since both extrapolation and even interpolation could lead to highly misleading expectations of tensile strength (TD). So, caution should be taken into account in generalizing the experimental results, since an apparent molecular weight influence can overrule the general applicability. Checking all other relations found hitherto reveals that only the elongation

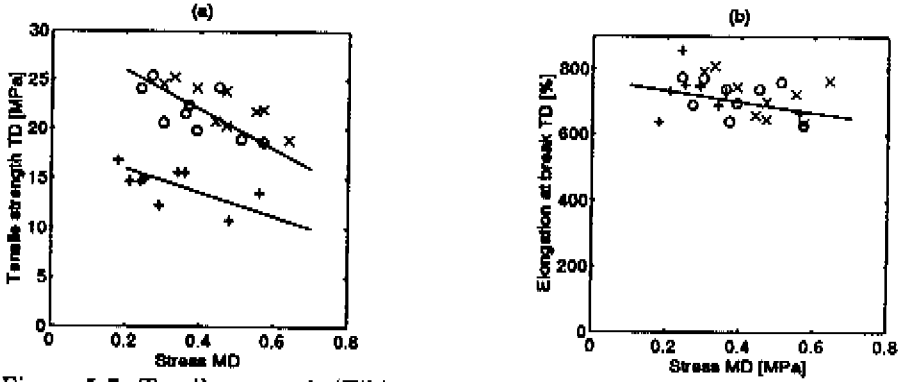

Figure 5.7: Tensile strength (TD) and elongation at break (TD) versus stress at the freeze line σ_{MD} for grades L1o (o), L1 (x), L8 (+).

at break in the machine direction shows a somewhat similar, but much less serious, dependence on the molecular weight (see figure 5.4b).

5.2.3 Tear resistance

In figure 5.8, the influence of the draw ratio DR and the stress σ_{MD} at the freeze line on the Trouser tear resistance in the machine direction, measured according to ISO 6383/1, is demonstrated. For this property, the same surprisingly unifying result as observed for the longitudinal and transverse moduli, the tensile strength (MD), the elongation at break (MD) and the yield stress (TD) is obtained. This is probably due to the specific morphology.

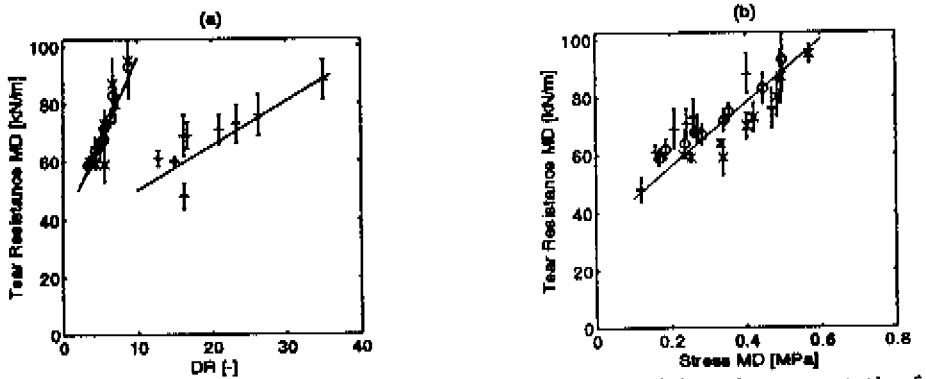

Figure 5.8: Trouser tear resistance versus Draw Ratio (a) and stress at the freeze line σ_{MD} (b) for grades L1o (o), L1 (x), L8 (+).

The correlation coefficient obtained for the relation $\sigma_{MD} \leftrightarrow$ tear resistance is 0.92.

As expected, the tear resistance in the transverse direction did not show any correlation with either processing parameter or stress. After all, tear propagation in PE blown films is generally directed in the machine direction.

5.2.4 Impact strength

The impact strength was determined by measuring the falling dart energy: a weight of 2 kg was dropped from a height of $1m$ on the clamped film. The time-force curve was recorded and, from this curve, the energy absorbed by the film was calculated.

Since the impact strength is a biaxial property, the falling dart energy is plotted versus the ratio $\frac{DR}{BUR}$ and versus the stress ratio $\frac{\sigma_{MD}}{\sigma_{TD}}$ at the freeze line (see figure 5.9).

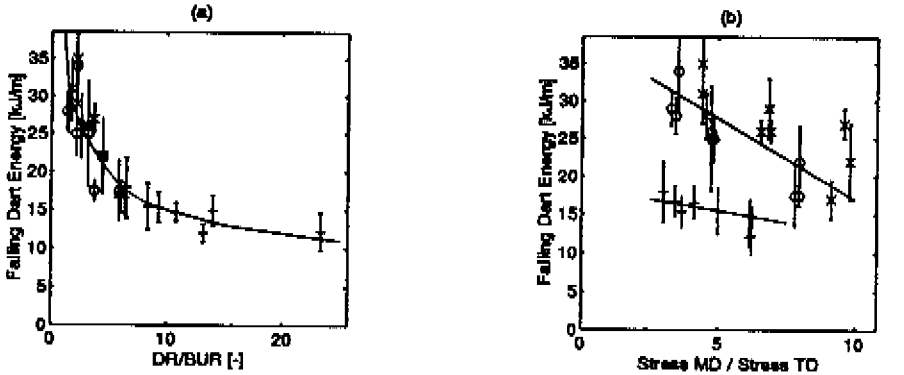

Figure 5.9: Impact strength versus DR/BUR (a) and versus σ_{MD}/σ_{TD} (b) for grades L1o (o), L1 (x), L8 (+).

As was shown in Chapter 3, decreasing the ratio $\frac{DR}{BUR}$ to values closer to unity results in more balanced films and, therefore, it is not surprising to find that this results in a higher falling dart energy. As a matter of fact, the correlation coefficient obtained for the relation $log(\frac{DR}{BUR}) \leftrightarrow$ impact strength equals -0.92.

Plotting the falling dart energy versus the stress ratio (figure 5.9b) destroys this relation. From this plot, and from figure 5.9a, it is concluded that the impact strength exhibits a similar molecular weight dependence as was found for the tensile strength (TD). Apparently, the maximum attainable falling dart energy for the melt index 8 material is lower than for the melt index 1 materials L1 and L1o. An identical argumentation as in the case of the relation $log(DR) \leftrightarrow$ tensile strength (TD) leads to the conclusion that the apparent relation $log(DR/BUR) \leftrightarrow$ impact strength can be overruled by molecular weight effects and, therefore, this relation may not be taken as representative for all LDPE's and processing conditions.

5.3 Shrink properties

Shrinkage of the films in the machine and the transverse direction has been measured at DSM. Specimens with known sizes were placed in a heated oil bath until their final shrinkage was reached. Afterwards, the sizes of the shrunk films were measured and the shrinkage was determined.

In the preceding section it was shown that various mechanical properties are unique functions of the stresses at the freeze line. For the shrinkage it is expected, however, that not only these stresses determine the shrink values, because also the rheological behaviour of the polymer affects the recovery. Therefore, the shrinkage has been calculated from the recovery using the stresses at the freeze line as initial condition and the Phan Thien Tanner constitutive model to describe the rheological behaviour. After all, this model has proved to be the most successful in predicting the stresses at the freeze line (see Chapter 3).

In the calculations several assumptions have been made. The first is that structural changes in the blown films after the onset of crystallization (read: where the temperature in the film reaches a plateau, see Chapter 3) do not affect the later shrinkage of the films. Consequently, solidification of the film and subsequent reheating are negligible for the final shrinkage (see also Fisher [1983]). This means that the shrinkage directly can be calculated from the stresses at the freeze line at the temperature of the shrinkage experiments.

The second assumption is that recovery only takes place in the three main directions. This implies that the deformation rate tensor describing the recovery can be written as

$$D_r = \begin{pmatrix} \dot{\epsilon}_{11} & & \\ 0 & \dot{\epsilon}_{22} & 0 \\ 0 & 0 & \dot{\epsilon}_{33} \end{pmatrix} \tag{5.1}$$

where 11 is in the machine direction, 22 in the thickness direction and 33 in the transverse direction. Because of the incompressibility constraint $\dot{\epsilon}_{22} = -\dot{\epsilon}_{11} - \dot{\epsilon}_{33}$.

Finally, it is assumed that the influences of gravity and surface tension are negligible and that recovery sets in at time $t = 0$.

Since in recovery all external stresses are equal to zero (see e.g. Larson [1983]) the problem to be solved is now reduced to find the recovery rates (equation (5.1)), so that

$$\begin{aligned} \tau_{11}(t, D_r) - \tau_{22}(t, D_r) &= 0, \quad t > 0 \\ \tau_{33}(t, D_r) - \tau_{22}(t, D_r) &= 0, \quad t > 0 \end{aligned} \tag{5.2}$$

The stresses τ_{11}, τ_{22} and τ_{33} are calculated with the Phan Thien and Tanner model (equations (2.9) and (2.10a)). The times at which the stresses and

recovery rates are evaluated are logarithmically spaced between $t = 10^{-6}s$ and $t = 10^{4}s$. The time step was chosen such that no influence on the ultimately reached recovery was observed.

With increasing time the calculation of the stresses becomes unstable for the short relaxation times. Before the onset of instability, however, the stresses contributed by these modes approach (Larson [1983])

$$\begin{aligned} \tau_{11,i} &\approx 2\eta_i\, \dot{\epsilon}_{11} \\ \tau_{22,i} &\approx 2\eta_i\, \dot{\epsilon}_{22} \\ \tau_{33,i} &\approx 2\eta_i\, \dot{\epsilon}_{33} \end{aligned} \tag{5.3}$$

Therefore, stresses contributed by modes for which $t/\lambda_i > 10$ are approximated by equation (5.3).

At time $t = 0$ the stresses are equal to the stresses at the freeze line (see Chapter 3). Equation (5.2) yields a system of nonlinear equations which is solved by the NAG routine C05NBF (see NAG Fortran Library Manual-Mark 13, 1988 1st Edition). This routine chooses corrections at each step as a convex combination of the Newton and scaled gradient directions.

According to Mündstedt and Laun [1980], the temperature at which the recovery is calculated does not affect the ultimately reached recovery. The influence of temperature is only seen in the time the recovery requires. This is also illustrated in figure 5.10, where the calculated shrinkage for experiment 9 is depicted as a function of time. Therefore, the calculations were performed using the relaxation time spectrum at the crystallization temperature.

The shrinkage profile shown in figure 5.10 is very characteristic. In viscoelastic models of differential form with only one mode all recovery is instantly. For multi modes, only a small portion recovers instantly, the major part recovers gradually (Larson [1983]). Furthermore, it is observed that the shrinkage in the transverse direction initially tends to become positive, but because of the incompressibility of the material and the dominating shrinkage in the machine direction ultimately becomes negative.

In figure 5.11 the calculated values of the final shrinkage are plotted versus the experimentally determined values. Clearly, the absolute value of the shrinkage in the machine direction and its weak dependence on the processing parameters and the material is predicted correctly by the model. Although the values for shrinkage in the transverse direction are predicted qualitatively correct, they are all underpredicted. Probably, this is because

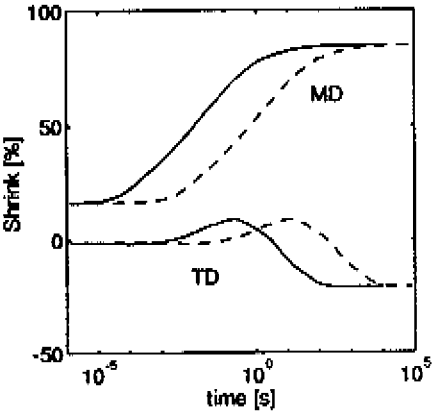

Figure 5.10: Calculated shrinkage for experiment 9 vs. time at 190 ^{o}C (—) and at 100 ^{o}C (- -).

the initial stress τ_{22} at time $t = 0$ (=at the freeze line) is of the same order, but opposite in sign, as the initial value for τ_{33}.

Despite this artifact, the model is capable of predicting the shrink behaviour of LDPE blown films reasonably. Apparently, the structure formation after the onset of crystallization does not affect the shrink behaviour seriously and shrinkage is mainly determined by the stresses at the freeze line and the rheological behaviour of the material.

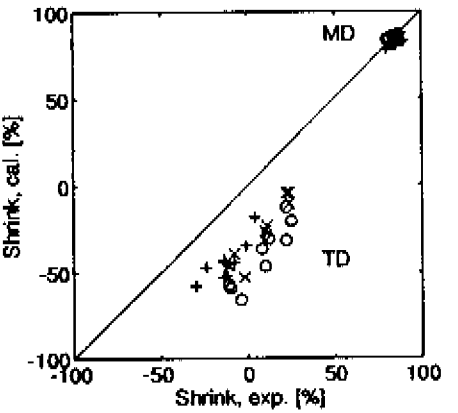

Figure 5.11: Calculated shrinkage vs. experimentally determined shrinkage for grades L1o (o), L1 (x) and L8 (+).

5.4 Optical properties

To understand the influence of the raw material and processing conditions on the optical performance of blown films, it is useful to go back to the classical work of Huck and Clegg [1961] who suggested that the surface quality mainly determines the optical properties and that the bulk of the film only plays a minor role. As was pointed out by Kurtz [1993], the surface quality is influenced to a great extent by extrusion defects, originating from the flow inside and at the exit of the die. This implies that producing blown films using polymer melts exhibiting highly elastic behaviour, due to a broad molecular weight distribution and especially the presence of a high molecular weight tail or long chain branches, results in moderate optical performance of these films, as was shown by e.g. Starck and Lindberg [1979] and Stehling *et al.* [1981].

To match the LDPE grades used in this study with respect to their elastic behaviour, the normal stresses in shear are plotted versus the shear stresses in figure 5.12.

From this figure it is concluded that the elastic behaviour matches according to L1 > L1o > L8. Following the results obtained by Starck and Lindberg [1979] and Stehling *et al.* [1981], this implies that the optical performance of the various grades should follow the opposite sequence.

In figure 5.13 the gloss (the amount of light reflected by the polymer film

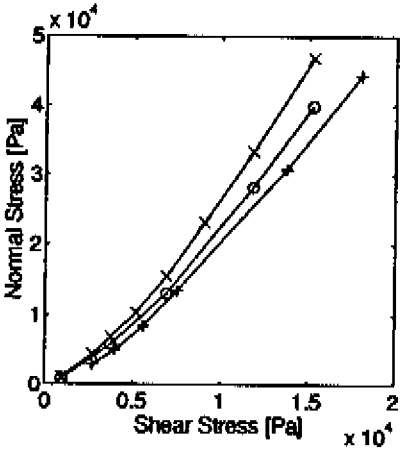

Figure 5.12: Normal stress measured in shear flow versus shear stress for grades L1o (o), L1 (x) and L8(+).

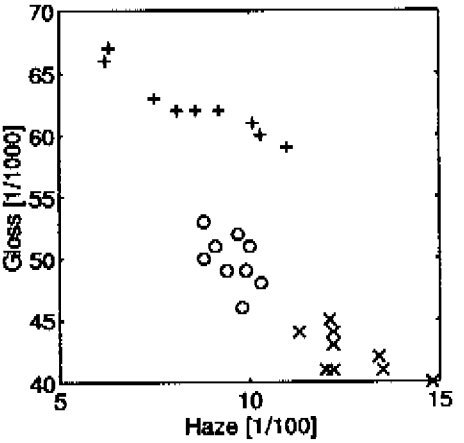

Figure 5.13: Gloss versus haze for grades L1o (o), L1 (x) and L8 (+).

under an angle of 45°) is shown as a function of the haze (the intensity of light scattered by the film under an angle > 2°). Because a higher value of the gloss and a lower value of the haze indicate a better optical performance, it indeed is seen that the optical performance matches the sequence L8 > L1o > L1.

Because from experimental evidence it is known that the optical properties of blown films tend to improve with increasing blow up ratio, they are depicted as a function of the BUR (figure 5.14). Given the impact of the stresses at the freeze line on the mechanical properties (see section 5.2), it is also interesting to plot the gloss and haze versus σ_{MD} (see figure 5.15).

From these figures it indeed could be concluded that generally the optical performance increases somewhat with increasing blow up ratio. Since an increasing blow up ratio results in a decreasing draw ratio (in an attempt to keep the same film thickness) and for all experiments DR > BUR, this result is in accordance with the experimental findings of Kurtz [1993], who found that extrusion defects induced by the flow inside the die are enhanced by stretching in the bubble forming region.

The plots of the optical properties as a function of σ_{MD} show some interesting features. First, no uniform relation between optical properties and stresses at the freeze line is found (as was the case for a number of mechanical properties). Thus, the optical properties seem to depend more on the flow inside the die than in the bubble forming region. Secondly, an increas-

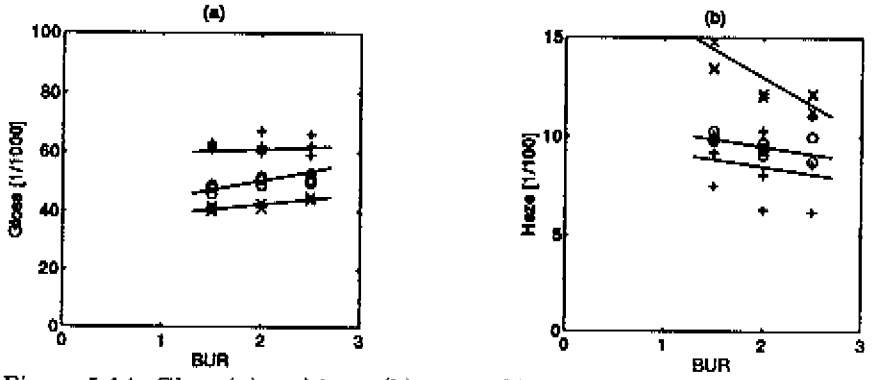

Figure 5.14: Gloss (a) and haze (b) versus blow up ratio for grades L1o (o), L1 (x) and L8 (+).

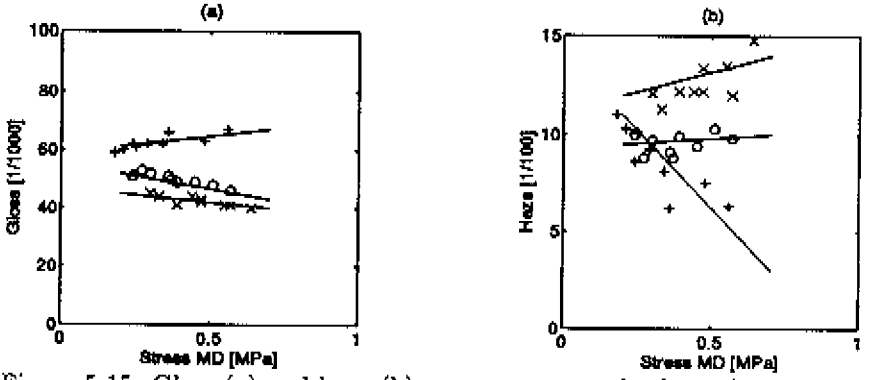

Figure 5.15: Gloss (a) and haze (b) versus stress at the freeze line σ_{MD} for grades L1o (o), L1 (x) and L8 (+).

ing σ_{MD} results in either an increasing or a decreasing optical performance, depending on the type of polymer (MI1 versus MI8 respectively).

It can be concluded that the optical performance of LDPE blown films is mainly determined by intrinsic material characteristics (MWD, high molecular weight tail, long chain branching) as primarily reflected in the differences in the first normal stress difference at equal shear stress. Accordingly, higher stresses at the freeze line increase the disturbances induced in the die (especially for the melt index 1 materials) or decrease them (for the low molecular weight melt index 8 material). This last difference is not yet fully understood.

5.5 Conclusions and Discussion

The main conclusions of this chapter are listed below.

- For the longitudinal and transverse moduli, the tensile strength in MD, the elongation at break in MD, the yield stress and the Trouser tear resistance it is found that equal stresses at the freeze line height result in equal properties, regardless the type of LDPE, die geometry, film thickness and processing conditions applied.

- The correlations $DR \leftrightarrow$ tensile strength in TD and $DR/BUR \leftrightarrow$ impact strength prove to be erroneous. Taking these correlations to be representative for all LDPE's may lead to highly over- or underpredicted values for the tensile strength in TD and impact strength, because of limiting intrinsic material characteristics, such as the molecular weight.

- The shrinkage of LDPE blown films does not depend on the crystalline morphologies. Shrinkage is mainly determined by the stresses at the freeze line, which are a result of the deformation of the melt, and the rheological behaviour of the material. Calculations with the Phan Thien and Tanner model show good agreement with experiments.

- A pronounced elastic behaviour of polymer melts yields moderate optical properties due to surface irregularities on the film, originating from the flow inside and at the exit of the die. A quantitative measure for the elasticity of polymer melts is given by the ratio of the first normal stress difference in shear flow to the shear stress.

The results obtained in this research are more or less in line with the results of Choi *et al.* [1980,1982], Kwack *et al.* [1988], and White and Cakmak [1988], who showed that the stresses measured at the freeze line could be correlated with the morphologies. Since in some cases (longitudinal and transverse modulus, yield stress) similar morphologies are expected to result in similar properties, it indeed might be expected that the stresses also are correlative to the properties, as was shown here. For other properties (tensile strength (MD), elongation at break (MD), tear resistance), correlations obtained with the stresses at the freeze line are, however, surprisingly.

Chapter 6

Conclusions and recommendations

6.1 Conclusions

The objective of the research discussed in this thesis was to understand the influence of the type of polymer **and** the processing conditions on the ultimate properties of blown films.

From a literature research it was learned that the stresses in the film at the freeze line may play an important role in the prediction of the film properties. Therefore, the procedure adapted to reach the objectives followed two main lines:

1. Modelling aspects: the attention was focused on viscoelastic constitutive equations and their capability to predict the experimentally observed stresses in the film during processing.

2. The impact of these stresses at the freeze line height on the film properties.

Three different types of LDPE, exhibiting different rheological behaviour and film performance, were investigated. Rheological experiments in various types of flow were performed to determine the parameters of four viscoelastic constitutive models (Wagner's integral model and Leonov's, Giesekus' and Phan Thien and Tanner's models). Using these models and the film kinematics measured during film blowing, stresses were calculated. Substituting the measured forces like the haul-off force and the pressure difference

across the film, and the kinematics in the balance equations, yielded the experimental stresses which were compared with the predictions. A brief (experimental and theoretical) study was performed towards the resulting film morphology, and, finally, the mechanical and optical properties of the films were measured and related to the stresses at the freeze line.

The main conclusions of the work presented in this thesis are listed below.

Rheology

Measurement of all flow characteristics in shear and uniaxial elongation characteristics using standard equipment is not enough to make a clear distinction between the quality of viscoelastic constitutive equations in describing polymer melt flow. All models could describe the measured quantities satisfactory.

In shear flow, the major differences between the various models are seen in the prediction of the first normal stress difference at high shear rates, while in uniaxial elongation the major differences are seen in the prediction of the elongational viscosity at high strain rates. Measurement of these quantities is, therefore, highly desirable.

Measurement of flow induced birefringence in complex geometries is a promising technique to be able to distinguish between various constitutive models, provided that the stress optical coefficient is known and proper numerical techniques are available. Experiments on the flow of a LDPE melt through a tapered duct have shown that Wagner's equation is not capable of describing the resulting stresses at the centerline. Leonov's, Giesekus' and Phan Thien and Tanner's models predict the stresses qualitatively correct, while the latter two also predict the stresses quantitatively satisfactory.

Film blowing

Though the macroscopic ratio DR/BUR can be almost equal to unity, the ratio of the stress in the machine direction (at the freeze line) to the stress in the transverse direction is still considerably deviating from unity, which indicates that the films are far from biaxially oriented.

Increasing the blow up ratio while keeping the film thickness and freeze line height constant results in a decreasing stress ratio. This is more a result of the decreasing stress in machine direction than the increase of the stress in transverse direction.

In calculating the stresses in the film, the various constitutive equations give different results. The Wagner model exhibits a far too pronounced

strain thinning behaviour, resulting in an underprediction of the experimentally observed stresses. The Leonov model also exhibits a somewhat too strain thinning behaviour to predict the stresses satisfactory. The Giesekus model exhibits too much strain hardening behaviour and, consequently, overpredicts the stresses. Comparison of the stresses calculated using the Phan Thien and Tanner model with the experimentally determined stresses yields satisfactory results.

In modelling the film blowing process the incorporation of the flow in the die is essential. Stresses in the machine direction, calculated without this flow, are slightly too low. Moreover, the stress ratio obtained tends to go to unity, which was experimentally found to be not true. Stresses calculated with incorporation of the flow in the die are similar to those determined experimentally and, consequently, also the stress ratio is calculated satisfactory.

Film morphology

The crystalline morphology of blown films investigated consists of packages of twisted lamellae, originating from row nucleation favored by the flow, with their normals depending on the stress ratio at the freeze line. Because the stress in the machine direction exceeds the stress in the transverse direction most of the packages are directed in the machine direction.

Properties

For the longitudinal and transverse moduli, the tensile strength and the elongation at break in the machine direction, the yield stress and the Trouser tear resistance it is found that equal stresses at the freeze line result in equal properties, regardless the type of LDPE, die geometry, film thickness and processing conditions applied.

The apparent correlations DR $\leftrightarrow$ tensile strength in the transverse direction and DR/BUR $\leftrightarrow$ impact strength, often found for various LDPE's, are the result of special combinations of processing conditions and intrinsic material characteristics. Use of these relations for other combinations may lead to highly under- or overpredicted values of these film properties.

Shrinkage of LDPE blown films does not depend on the crystalline morphologies, but is a function of the stresses at the freeze line and the rheological behaviour of the material.

The optical properties of blown films are mainly dependent on surface irregularities induced by the flow in the die. Surface irregularities increase

with increasing elasticity of the melt and a quantitative measure for the elasticity proves to be the ratio of the first normal stress difference in shear flow to the shear stress.

6.2 Recommendations

The recommendations for further research are summarized below.

Rheology

Measurement of the first normal stress difference at high shear rates is known to be extremely complicated. The slit rheometer that uses the pressure hole error, as proposed by Lodge [1989] still seems to suffer from many experimental and constructional problems. Despite of the many attempts, also the measurement of the pressure difference in a curved slit, as developed in IKT Stuttgart, seems not to give quantitative results. Apparently, we have to be less critical and in order to get some data on the first normal stress difference at high shear rates, the following methodology could be adapted (see also Leblans [1986]). Determine from start-up flow experiments in a cone plate rheometer the parameter k for the third Gleissle mirror relation (Gleissle [1980]), which relates the viscosity to the first normal stress (in a rather complicated way). Using the thus obtained parameter k, a measure for the first normal stress at high shear rates can be deduced from capillary experiments.

After many years of development, Meissner [1994] succeeded in constructing a rheometer for uniaxial elongational flow of polymer melts at high strains. The strain rate range is 0.001 s^{-1} - 1 s^{-1} and the maximum Hencky strain is 7. The equipment is now marketed by Rheometrics Scientific. A few prototypes have been sold and, consequently, only little experience is available.

Meissner also developed an apparatus to measure the rheological behaviour in multiaxial flow (see e.g. Demarmels and Meissner [1985]). Measurement of the uniaxial, planar, ellipsoidal and biaxial viscosities at different strain rates of a PIB were used by Wagner to modify his integral equation (Wagner and Demarmels [1990], Wagner and Schaeffer [1992], Wagner [1993]). Unfortunately, this apparatus is not suited for polymer melts.

Only very recently, promising measurements of elongational viscosities at high strain rates (up to 1000 s^{-1}) have been reported by Dajan and Mackay [1994]. From the entry pressures in an opposed jets rheometer, they were able

to approximate the extensional stresses and the elongation rates (see Mackay *et al.* [1994]). Still uncertainties exist with respect to the measurement accuracy and the non-isothermal effects, while the disadvantage of measuring the global integrated force only, is that no information about the transient effects is obtained.

The iterative method of finding parameters in constitutive equations by measuring pointwise or field information in complex flows, as being developed in the laboratory at the Eindhoven University of Technology (Baaijens [1994]), seems to be able to get around with all these problems but still needs a lot of verification.

Film blowing

The experiments discussed in this thesis were performed on a lab-scale extruder (D=30 *mm*). A straightforward extension is to check whether the results obtained (especially the relation between stresses and properties) also hold for films produced on commercial lines, thus enforcing also the range of machine parameters and processing conditions. Besides the BUR and DR, a.o. the freeze line height, the extrusion temperature, the die land length and the flow rate could be varied.

In this thesis the stresses in the film were calculated using the experimentally determined kinematics and temperatures. Because measurement of these quantities is not common, it is preferable to calculate the kinematics and temperatures. Although the numerical solutions of non-isothermal viscoelastic flows are possible today (see e.g. Baaijens [1991], Dijksman and Kuiken [1994]), a practical method for a fast evaluation of the predictive capability of different constitutive equations could consist of a decoupled method (see e.g. Douven [1991]): calculate the kinematics and temperatures of the film with a relatively simple constitutive model, using the take-up force, bubble pressure and heat transfer coefficient as fit parameters to obtain the desired draw ratio, blow up ratio and freeze line height. The thus obtained kinematics can be used to calculate the stresses with different, more complex, viscoelastic constitutive equations.

Film Morphology

Although it has been shown that the stresses at the freeze line determine the typical morphologies of LDPE blown films, it is not clear whether this also holds for other, more linear, materials. After all, Kwack *et al.* [1988] have found that LLDPE films, crystallized under relatively low stresses, exhibited

a more or less spherulitic structure. So, possibly, the correlations between stresses and morphologies (e.g. Choi *et al.* [1982]) and, consequently, the correlations between stresses and properties found for LDPE films (this thesis) is absent for LLDPE films. Therefore, the effect of stresses on morphologies (and properties) of these materials should be investigated.

Generally, a better understanding of the influence of orientation on the crystallization kinetics **and** the resulting crystalline structures should be pursued. For this purpose, a promising technique seems to be the simultaneous SAXS/WAXS measurements reported by e.g. Ryan [1994]. Using this technique, on-line measurement of the structural changes of the crystallizing melt under deformation can be detected. Combination of such measurements with theories as set up by Eder *et al.* [1990] could lead to new insights in orientation induced crystallization.

Properties

As was mentioned above, the effects of stresses on properties of blown films for materials other than LDPE should be investigated.

For LDPE, the relations found between stresses and properties can be used as reference curves, at least if they are in the same class as the materials investigated in this thesis. For LDPE's with e.g. deviating densities it is likely that the reference curves have to be shifted. In order to check this, films should be produced from such materials under various processing conditions and the film properties could be related to the stresses at the freeze line, calculated with the decoupled method as described above.

A more elegant way to predict the properties for all LDPE blown films is to capture the correlations found in suitable models in which, amongst others, the stresses at the freeze line are encapsulated. For a model of the stiffness, composite theories could be adapted for instance, with the crystals acting as oriented, anisotropic fillers connected through oriented taught-tie molecules in an amorphous matrix (see e.g. Boyd [1979] and Kardos and Raisoni [1975]). Prerequisite for a useful application of such models is, however, that a large number of properties of the constituents (for instance the crystal moduli (see e.g. Tashiro and Tadakoro [1978]) should be measured independently.

References

[1] Ashok B.K., Campbell G.A., *Intern. Polym. Proc.*, **7**: 240, 1992

[2] Ast W., *Extrusion von Schlauchfolien. Theoretische und experimentele Untersuchungen des Abkühlvorganges*, Ph.D. thesis, IKT Stuttgart, 1976

[3] Attané P., Turrel G., Pierrard J.M., *J. Rheol.*, **32**:23, 1988

[4] Baaijens F.P.T., *Rheol. Acta*, **30**:284, 1991

[5] Baaijens J.P.W., Ph.D. thesis, Eindhoven University of Technology, in preparation, 1994

[6] Babel A.K., Campbell G.A., *J. Plastic Film & Sheeting*, **9**:246, 1993

[7] Baumgaertel M., Winter H.H., *Rheol. Acta*, **28**:511, 1989

[8] Bernstein B., Kearsley E.A., Zapas L.J., *Trans. Soc. Rheol.*, **7**:391, 1963

[9] Bie F.O. de, *Viscoelastische Stromingen in een Convergerend Kanaal: Reooptische Experimenten en Numerieke Simulatie*, Master's thesis, Eindhoven University of Technology, 1994 (in Dutch)

[10] Booij H.C., Palmen J.H.M., *Rheol. Acta*, **21**:376, 1982

[11] Booij H.C., Leblans P., Palmen J., Tiemersma-Thoone G., *J. Polym. Sci.*, Polym. Phys. Ed., **21**:1703, 1983

[12] Boyd R.H., *Polym. Eng. Sci.*, **19**:1010, 1979

[13] Brown N., in *Failure of Plastics*, edited by Brostow W. and Corneliussen R.D., Hanser Publishers, New York, 1986

[14] Cain J.J., Denn M.M., *Polym. Eng. & Sci.*, **28**:1527, 1988

[15] Campbell G.A., Cao B., in *Polymer Rheology and Processing*, edited by Utracki L.A. and Collyer A.A., Elsevier Science Publishers Ltd., Amsterdam, 1990

[16] Cao B., Campbell G.A., *AIChE Journal*, **36**:420, 1990

[17] Cao B., Sweeney P., Campbell G.A., *J. Plastic Film & Sheeting*, **6**: 117, 1990

[18] Choi K.J., White J.L., Spruiell J.E., *J. Appl. Polym. Sci.*, **25**:2777, 1980

[19] Choi K.J., White J.L., Spruiell J.E., *J. Polym. Sci.*, **20**:27, 1982

[20] Collyer A.A., Clegg D.W., editors, *Rheological Measurement*, Elsevier Applied Science Publishers Ltd., Amsterdam, 1988

[21] Cox W.P., Merz E.H., *J. Polym. Sci.*, **28**:619, 1958

[22] Dajan A.M., Mackay M.E., in *Proc. 7th Nat. Conf. Rheol. (Australian Soc. Rheol.)*, edited by Hallcy P.J., Makcay M.E., Brisbane, Australia, 1994

[23] Demarmels A., Meissner J., *Rheol. Acta*, **24**: 253, 1985

[24] Demarmels A., Meissner J., *Colloid Polym. Sci.*, **264**:829, 1986

[25] Dijksman J.F., Kuiken G., editors *Proc. IUTAM Symp. on numerical simulation of non-isothermal flows of vicsoelastic liquids*, Kerkrade, The Netherlands, in preparation, 1994

[26] Douven, L.F.A *Towards the Computation of Properties of Injection Moulded Products*, Ph.D. thesis, Eindhoven University of Technology, 1991

[27] Eder G., Janeschitz-Kriegl H., Liedauer S., *Progr. Polym. Sci.*, **15**:629, 1990

[28] Farber R., Dealy J., *Polym. Eng. Sci.*, **14**:435, 1974

[29] Ferry J.D., *Viscoelastic Properties of Polymers*, John Wiley and Sons, New York, 1980

[30] Fisher E., *Ein Rheologisches Modell zur Beschreibung der Produktqualität bei der Verarbeitung von Hochdruckpolyethylen*, Ph.D. thesis, IKT Stuttgart, 1983

[31] Fleissner M., *Intern. Polym. Proc.*, **2**:229, 1988

[32] Frank F.P., Tosi M., *Proc. Roy. Soc. (London)*, **263**:323, 1961

[33] Ghijsels A., Ente J.J.S.M., *Intern. Polym. Proc.*, **4**:284, 1990

[34] Giesekus H., *Rheol. Acta*, **5**:29, 1966

[35] Giesekus H., *J. Non-Newtonian Fluid Mech.*, **11**:69, 1982

[36] Gleissle W., in *Rheology 2, Proc. VIII Intern. Congr. Rheol.*, edited by Astarita G., Marrucci G., Nicolais L., Plenum Press, New York, 1980

[37] Gotsis A.D., Baird D.G., Reddy J.N., *Intern. J. Numer. Methods. Fluids*, **10**:373, 1990

[38] Gupta R.K., *A new Non-isothermal Rheological Constitutive Equation and its Application to Industrial Film Blowing Processes*, Ph.D. thesis, University of Delaware 1980

[39] Gurp M. van, *Optische Dichtheidsbepaling van Polymeerfolies met behulp van een Abbe-Refractometer*, DSM Research NC 92 7827, 1992

[40] Gurp, M. van, Breukink C.J., Sniekers R.J.W.M., Tas P.P., *Proc. Fifth Int. Conf. Laser Anemometry - Advances and Applications*, Veldhoven, The Netherlands, 1993

[41] Han C.D., Park J.Y., *J. Appl. Polym. Sci.*, **19**:3257, 1975a

[42] Han C.D., Park J.Y., *J. Appl. Polym. Sci.*, **19**:3277, 1975b

[43] Han C.D., Kwack T.H., *J. Appl. Polym. Sci.*, **28**:3399, 1983

[44] Hellwege K.H., Knappe W., Lehmann P., *Kolloid-Z.*, **183**:110, 1962

[45] Honerkamp J., *Rheol. Acta*, **28**:363, 1989

[46] Honerkamp J., Weese J., *Continuum Mech. Thermodyn.*, **2**:17, 1990

[47] Huck N.D., Clegg P.L., *SPE Trans.*, **1**: 121, 1961

[48] Hulsen M., *Analysis and Numerical Simulation of the Flow of Viscoelastic Fluids*, Ph.D. thesis, Delft University of Technology, 1988

[49] Hulsen M., Zanden J. van de, *J. Non-Newtonian Fluid Mech.*, **38**:183, 1991

[50] Hsu T.C., Harrison, I.R., *Polym. Eng. Sci.*, **31**:223, 1991

[51] Janeschitz-Kriegl H., *Polymer Melt Rheology and Flow Birefringence*, Springer Verlag, Berlin, 1983

[52] Jarecki L., Ph.D. thesis, Inst. Fund. Tech. Res. Rep., No. 29/1974, Warsaw, 1974

[53] Jarecki L., *Colloid Polym. Sci.*, **257**: 711, 1979

[54] Jarecki L., Ziabicki A., *Polymer*, **18**:1015, 1977

[55] Johnson M.W., Segalman D., *J. Non-Newtonian Fluid Mech.*, **2**:225, 1977

[56] Kanai T., White J.L., *Polym. Eng. Sci.*, **24**:1185, 1984

[57] Kanai T., White J.L., *J. Polym. Eng.*, **5**:135, 1985

[58] Kanai T., *Intern. Polym. Proc.*, **1**:137, 1987

[59] Kanai T., Kimura M., Asano Y., *J. Plastic Film & Sheeting*, **2**:224, 1986

[60] Kardos J.L., Raisoni J., *Polym. Eng. Sci.*, **15**:183, 1975

[61] Kaye A., Technical Report Note No. 134, College of Aeronautics, Cranfield, U.K., 1962

[62] Keller A., Machin M.J., *J. Macromol. Sci. Phys.*, **B1**:41, 1967

[63] Keller A., Kolnaar J.W.H., *Progr. Colloid Polym. Sci.*, **92**:1, 1993

[64] Kurtz S.J., *ANTEC 93 Proc.*, New Orleans USA, 1993

[65] Kwack T.H., Han C.D., Vickers M.E., *J. Appl. Polym. Sci.*, **35**:363, 1988

[66] Lagasse R.R., Maxwell B., *Polym. Eng. Sci.*, 16:189, 1976

[67] Larson R.G., *Rheol. Acta*, **22**:435, 1983

[68] Larson R.G *Constitutive Equations for Polymer Melts and Solutions*, Butterworths, Boston, 1988

[69] Laun H.M., *Rheol. Acta*, **17**:1, 1978

[70] Laun H.M., *Proc. Ninth Intern. Congress Rheol.*, Acapulco, Mexico, 1984

[71] Laun H.M., *J. Rheol.*, **30**:459, 1986

[72] Leblans P.J.R., *Constitutive Analysis of the nonlinear Viscoelasticity of Polymer Fluids in various Types of Flow*, Ph.D. thesis, University of Antwerp, 1986

[73] Liedauer S., Eder G., Janeschitz-Kriegl H., Jerschow P., Geymayer W., Ingolic E., *Intern. Polym. Proc.*, **8**:236, 1993

[74] Liedauer S., Eder G., Janeschitz-Kriegl H., submitted to *Intern. Polym. Proc.*, 1994

[75] Lodge A.S., Meissner J., *Rheol. Acta*, **11**:351, 1972

[76] Lodge A.S., *Rheol. Acta*, **14**:664, 1975

[77] Lodge A.S., *J. Rheol.*, **33**:821, 1989

[78] Leonov A.I., *Rheol. Acta*, **15**:85, 1976

[79] Leonov A.I., *Rheol. Acta*, **25**:1, 1987

[80] Luo X.L., Tanner R.I., *Polym. Eng. Sci.*, **25**:620, 1985

[81] Mackay M.E., Dajan A.M., Wippel H., Janeschitz-Kriegl H., Lipp M., *J. Rheol*, in press, 1994

[82] Meissner J., Hostettler J., *Rheol. Acta*, **33**:1, 1994

[83] Meissner J., Garbella R.W., Hostelttler J., *J. Rheol.*, **33**:843, 1989

[84] Minoshima W., White J.L., *J. Non-Newtonian Fluid Mech.*, **19**:251, 1986a

[85] Minoshima W., White J.L., *J. Non-Newtonian Fluid Mech.*, **19**:275, 1986b

[86] Münstedt H., Laun H.M., *Rheol. Acta*, **19**:492, 1980

[87] Nagasawa T., Matsumura T., Hoshino S., *Appl. Polym. Symp.*, **20**:275, 1973 and *Appl. Polym. Symp.*, **20**:295, 1973

[88] Oonk J., *Kunststof magazine*, **6/7**:18, June/July 1994

[89] Orbey N., Dealy J.M., *J. Rheol.*, **35**:1035, 1991

[90] Papanastasiou A.C., Scriven L.E., Macosko C.W., *J. Rheol.*, **27**:387, 1983

[91] Pearson J.R.A., Petrie C.J.S., *Plastics & Polymers*: 85,April 1970a

[92] Pearson J.R.A., Petrie C.J.S., *J. Fluid Mech.*, **40**: 1, 1970b

[93] Pearson J.R.A., Petrie C.J.S., *J. Fluid Mech.*, **42**: 609, 1970c

[94] Pennings A.J., Kiel A.M., *J. Polym. Sci.*, **C16**:1799, 1967

[95] Peterlin A., *Polym. Eng. Sci.*, **16**: 126, 1976

[96] Petrie C.J.S., *Rheol. Acta*, **12**:92, 1973

[97] Petrie C.J.S., *AIChE Journal*, **21**:275, 1975

[98] Petrie, C.J.S., *Elongational Flows*, Pitman Publishers Ltd., London, 1979

[99] Phan Thien N., Tanner R.I., *J. Non-Newtonian Fluid Mech.*, **2**:353, 1977

[100] Ryan A.J., *Proc. PPS European Regional Meeting*, Strasbourg, France, 1994

[101] Samurkas T., Larson R.G., Dealy J.M., *J. Rheol.*, **33**:559, 1989

[102] Simpson D.A., Harrison I.R., *J. Plastic Film & Sheeting*, **8**:192, 1992

[103] Simpson D.A., *A Study of the Effects of Processing Parameters on the Morphologies and Mechanical Properties of PolyEthylene blown Films*, Ph.D. thesis, The Pennsylvania State University, 1993

[104] Soskey P.R., Winter H.H., *J. Rheol.*, **28**: 625, 1984

[105] Soskey P.R., Winter H.H., *J. Rheol.*, **29**: 493, 1985

[106] Spencer R.S., Gilmore R.D., *J. Appl. Phys.*, **21**:523, 1950

[107] Starck P., Lindberg J.J., *Angew. Makromol. Chem.*, **75**:1, 1979

[108] Stehling F.C., Speed C.S., Westerman L., *Macromolecules*, **14**:698, 1981

[109] Tanner R.I., *Engineering Rheology*, rev. ed., Oxford University Press, New York, 1988

[110] Tashiro K., Tadakoro H., *Macromolecules*, **11**: 914, 1978

[111] Turnbull D., Fisher C.J., *J. Chem. Phys.*, **17**:71, 1949

[112] Wagner M.H., *Rheol. Acta*, **15**:40, 1976a

[113] Wagner M.H., *Ein Rheologisch-thermodynamisches Prozessmodell des Folienblasverfahrens*, Ph.D. thesis, IKT Stuttgart, 1976b

[114] Wagner M.H., *Rheol. Acta*, **16**:43, 1977

[115] Wagner M.H., Raible T., Meissner J., *Rheol. Acta*, **18**:427, 1979

[116] Wagner M.H., Demarmels A., *J. Rheol.*, **34**:943, 1990

[117] Wagner M.H., Schaeffer J., *J. Rheol.*, **36**: 1, 1992

[118] Wagner M.H., *Makromol. Chem., Macromol. Symp.*, **68**:95, 1993

[119] Wales J.L.S., *The Application of Flow Birefringence to Rheological Studies of Polymer Melts*, Ph.D. thesis, University of Technology Delft, 1976

[120] Ward I.M., *Mechanical Properties of Solid Polymers*, John Wiley & Sons, Chicester, 1985

[121] White J.L., Yamane H., *Pure Appl. Chem.*, **59**:193, 1987

[122] White J.L., Cakmak M., *Adv. Polym. Technol.*, **6**:295, 1986

[123] White J.L., Cakmak M., *Adv. Polym. Technol.*, **8**:27, 1988

[124] Winter H.H., *Pure Appl. Chem.*, **55**:943, 1983

[125] Yamane H., White J.L., *Intern. Polym. Proc.*, **2**, 107, 1987

[126] Yilmaz F., Cakmak M., *Intern. Polym. Proc.*, **2**:141, 1994

[127] Zanden J. van der, *SEPRAN Numerical Simulation of Viscoelastic Fluid Flow*, User's manual version 1.0, Ingenieursbureau Sepra, 1990

[128] Ziabicki A., *Polimery (Warsaw)*, **18**:617, 1973

[129] Ziabicki A., Jarecki L., *Colloid Polym. Sci.*, **256**:332, 1978

[130] Ziabicki A., Jarecki L., in *High Speed Fibre Spinning*, edited by Ziabicki A., Kawai H., J. Wiley & Sons, New York, 1985

[131] Zoetelief W.F., *On the Numerical Simulation of the Multilayer Injection Moulding Process*, Designer's Course Computational Mechanics (WFW92.100), Eindhoven University of Technology, 1992

Samenvatting

Polyethyleen is een van de oudste en meest voorkomende plastic materialen. Er kunnen drie verschillende soorten polyethyleen worden onderscheiden: het lineaire hoge dichtheid polyethyleen (HDPE), het lineaire (korte keten vertakte) lage dichtheid polyethyleen (LLDPE) en het (lange keten) vertakte lage dichtheid polyethyleen (LDPE). Van deze drie is LDPE (op zich ook weer onder te verdelen is een groot aantal verschillende typen) verreweg de meest voorkomende. Toepassingen worden voornamelijk teruggevonden in films: krimpfolies, voedselverpakkingszakjes, zware industriële en dunne huishoudleijke afvalzakken, landbouwfolies etc.. De meest gebruikte methode om folies te produceren is het reeds in de dertiger jaren gecommercialieerde folieblaasproces. Ondanks de lange historie van LDPE en van het folieblaasproces wordt tot op heden nog steeds niet ten volle begrepen hoe de uiteindelijke mechanische en optische eigenschappen van LPDE blaasfolies afhangen van het gebruikte type LDPE, de machineparameters en de procescondities.

Een literatuurstudie (hoofdstuk 1) leert ons dat in het verleden veel aandacht is besteed aan het beschrijven van de juiste kinematika van de film tussen blaaskop en vrieslijn. In alle onderzoeken moesten echter materiaalen/of procesparameters aangepast worden om een redelijke overeenstemming te krijgen tussen theoretische voorspellingen en experimenten. Experimentele onderzoeken richtten zich veelal op de invloed van het, met name reologische, materiaalgedrag op de stabiliteit van de film tijdens verwerking, en slechts in enkele gevallen werd de invloed van de spanningen bij de vrieslijn op de film morfologie bestudeerd. In deze laatste studies werd echter overtuigend aangetoond dat deze spanningen op een unieke wijze zijn te correleren met de uiteindelijke foliemorfologie. Vreemd genoeg is geen onderzoek terug te vinden dat de invloed van deze spanningen op de uiteindelijke eigenschappen beschrijft. Het doel van dit proefschrift is dan ook deze invloed te onderzoeken en, daarnaast, het vinden van een geschikte

reologische toestandsvergelijking die het mogelijk maakt deze spanningen te berekenen, afhankelijk van procesomstandigheden en type LDPE.

Er zijn drie LDPE's met verschillende reologisch gedrag (twee met melt index 1 MI 1) en een met melt index 8 (MI 8)) en met verschillende eigenschappen (met name de optische) geselecteerd.

In hoofdstuk 2 wordt hun experimenteel bepaalde reologische gedrag in afschuiving en uniaxiale rek besproken. Er worden duidelijke verschillen gevonden tussen het MI 8 materiaal enerzijds en de MI 1 materialen. De meetresultaten zijn gefit met vier constitutieve modellen:Wagner's integraalmodel en Giesekus', Leonov's en Phan Thien en Tanner's differentiaalmodellen. Alle vier de modellen geven een goede overeenkomst met de experimentele resultaten. Aan een van de MI 1 materialen zijn dubbelbrekingsmetingen uitgevoerd tijdens stroming door een convergerend kanaal. Hierin treedt een gemengde afschuif- en planaire rekstroming op. Middels toepassing van de spannings-optische wet zijn de spanningen in het stromende materiaal bepaald. Aangetoond werd dat op de symmetrie lijn, waar enkel planaire rekstroming heerst, het Wagner model niet in staat is de experimenteel bepaalde spanningen te voorspellen: de niet-lineariteitsfunctie die bepaald is voor afschuif en uniaxiale rekstroming vertoont een te deformatiegevoelig gedrag. Eindige elementen berekeningen voor de constitutieve modellen van het differentiaaltype laten zien dat voor alle drie de modellen het kwalitatieve gedrag correct wordt beschreven. Het Leonov model voorspelt echter normaalspanningen die beduidend onder de experimentele waarden liggen, waar het Giesekus en het Phan Thien en Tanner model ook kwantitatief juiste voorspellingen geven. Voor het checken van constitutieve modellen in verschillende typen stroming kan dan ook geconcludeerd worden dat standaardmetingen (afschuiving en uniaxiale rek) niet voldoende discrimerend zijn. Dubbelbrekingsmetingen aan een stromende smelt in een complexe geometrie, daarentegen, blijken wel informatie te bevatten die nodig is voor deze discriminatie. Daar staat dan wel tegenover dat ingewikkelder (eindige elementen) berekeningen uitgevoerd dienen te worden voordat resultaten worden verkregen. Dit impliceert dat enig vertrouwen in bijvoorbeeld de nauwkeurigheid van de gebruikte numerieke methoden aanwezig moet zijn.

Om na te gaan of één van de voornoemde modellen geschikt is om de spanningen tijdens het folieblazen te berekenen zijn experimenten uitgevoerd (hoofdstuk 3). Procesparameters zijn systematisch gevarieerd. Spanningen zijn berekend met de modellen door als input de gemeten kinematika en temperatuur te nemen. Deze spanningen zijn ook experimenteel bepaald middels speciaal daarvoor geconstrueerde krachtopnemers. Vergelijking van

berekende en gemeten spanningen laat zien dat met name het Phan Thien en Tanner model geschikt is. Zowel het Wagner als het Leonov model voorspellen te lage spanningen, terwijl het Giesekus model juist te hoge spanningen voorspelt.

Verder is aangetoond dat bij het berekenen van de spanningen het van wezenlijk belang is dat de afschuifstroming in de kop wordt meegenomen. Zonder deze stroming wordt met name de verhouding van de twee hoofdspánningen in de film verkeerd voorspeld. Daar waar experimenteel gevonden is dat de spanningen in de folies in grote onbalans zijn (de spanning in extrusie richting is vele malen groter dan die in de opblaasrichting, ongeacht de procesparameters), worden in dit geval juist goed gebalanceerde folies uitgerekend. Inbegrip van de stroming in de kop bij de berekeningen voorspelt de experimenteel gevonden resultaten correct.

In hoofstuk 4 wordt de invloed van de spanningen op de uiteindelijke morfologie in de folie besproken. Hiertoe worden eerst de basisprincipes van stromingsgeinduceerde kristallisatie behandeld. Vervolgens wordt de werkelijk gevonden morfologie voorgesteld die bestaat uit gestapelde lamellen, waarvan de orientatie wordt bepaald door initiatie via zogenaamde rij nucleatie, die een gevolg is van stroming. De orientatie van de lamellen blijkt grotendeels afhankelijk te zijn van de spanningen tijdens het invriezen. Door de grote onbalans van de twee hoofdspanningen is voornamelijk de spanning in de extrusierichting bepalend. Een aantal TEM resultaten worden getoond en deze bevestigen het hierboven geschetste beeld.

Tenslotte zijn de mechanische en optische eigenschappen, alsmede de krimpeigenschappen van de folies onderzocht (hoofdstuk 5). Een aantal eigenschappen (longitudinale en transverse modulus, treksterkte en rek-bijbreuk in de extrusierichting, vloeispanning en scheursterkte) blijken goed te correleren met de spanning in de extrusierichting ter hoogte van de vrieslijn, onafhankelijk van kopgeometrie, procescondities en type LDPE. De krimpeigenschappen blijken voornamelijk bepaald te worden door de orientatie ten gevolge van de verstrekking in de smelt. Berekening van de "recoverable strain" voor het Phan Thien en Tanner model vertonen goede gelijkenis met de experimenteel bepaalde krimpwaarden. De optische eigenschappen lijken met name bepaald te worden door extrusiedefecten in de kop en zijn te relateren aan de (elasticiteits) verhouding van het eerste normaalspanningsverschil in afschuiving en de afschuifspanning. Een hoge elasticiteit van de smelt levert een ruwer oppervlak en daardoor ook een matige optiek.

Acknowledgements

A thesis is rarely the result of one person's efforts. Therefore, I would like to thank those people who have contributed to the realization of the research presented in this thesis. First I would like to thank my promoters Prof. Han Meijer and Prof. Frank Baaijens for their support and their guidance during the four years I have worked on this research. Special thanks go to Dr. Henk Booij who taught me the principles of rheology and with whom I had many stimulating discussions.

Furthermore, I want to thank the management of DSM Research for the permission to publish this thesis. I am also grateful to my colleagues in the team at DSM research, who worked on the project 'Basisresearch folieblaasverwerking'. Without their help, finishing this thesis would not have been possible. Specially, I would like to thank Dr. Marnix van Gurp for the many discussions we had during the development of this work.

For helping me with the experimental part of this thesis my gratitude goes to the following people: Jo Palmen (shear experiments on the RMS800), Hans Steuten (uniaxial elongation), Jo Michel (film blowing) and Ruud Sniekers (film blowing, LDA). For performing experiments, I thank: Jo Palmen (stress build-up and relaxation on the RMS 800), Hans Steuten (biaxial elongation), Wilbert Jansen (capillary), Francois de Bie and Christien Breukink (rheo-optics), Dr. Steven de Boer (TEM) and the people from the Processing and Testing laboratory of RTD-PE (mechanical and optical film properties). Peter Engelen and Ronald Tabaksblat I thank for the pleasant collaboration.

Also thanks to Wim Zoetelief for helping me with fitting the discrete relaxation time spectrum and making the lay-out of this thesis, and all the other colleagues at the university for their companionship.

Finally, I want to thank my friends and family, in particular Annette, for supporting me during the time I worked on this thesis.

Curriculum Vitae

Paul Tas

- 20-5-1966: Born in Aardenburg, The Netherlands.
- 1978–1984: St. Eloy Scholengemeenschap, Oostburg.
- 1984–1990: Eindhoven University of Technology: Masters degree at the Department of Mathematics and Computing Science.
- 1990–1994: Eindhoven University of Technology: Research assistant at the Department of Mechanical Engineering.

Stellingen

behorende bij het proefschrift

Film Blowing: from Polymer to Product

1. Het reologische gedrag van modelvloeistoffen voor polymeersmelten kan wezenlijk afwijken van het reologische gedrag van de smelten zelf. Dit komt met name tot uiting in de normaalspanningsverschillen tijdens de stroming van deze materialen in complexe stromingsgeometrieën.

   - Bie F.O. de, Tas P.P., Kikstra W.P., Gurp M. van, in *Proceedings of the Fourth European Rheology Conference*, edited by Callegos C., Sevilla 1994

2. Tot op heden is bij de modelvorming van het folieblaasproces de stroming in de blaaskop vaak ten onrechte verwaarloosd.

   - Dit proefschrift, hoofdstuk 3.

3. Kristallisatie van de folie tijdens verwerking heeft effect op de uiteindelijke eigenschappen van de folie. Bij de modellering van het proces en de uiteindelijke eigenschappen hoeft deze stap echter niet meegenomen te worden daar de spanning in de folie op het moment dat kristallisatie start bepalend is voor de uiteindelijke morfologie en daarmee ook voor de uiteindelijke eigenschappen.

   - Dit proefschrift, hoofdstuk 4 en 5.

4. Bij het onderzoek naar de invloed van het type polymeer en de verwerkingsomstandigheden (tijdens folieblazen) op de eigenschappen van de folie is tot op heden nooit de juiste relatie gelegd tussen de verschillende onderzoeksdisciplines. Daarom is de geboekte progressie nooit volledig tot zijn recht gekomen.

5. In modellen die de oriëntatie-geïnduceerde kristallisatie beschrijven dient het aantal kiemen niet alleen af te hangen van de totale deformatie en de totale deformatietijd maar ook van de spanning ten gevolge van de stroming.

- Eder G., Janeschitz-Kriegl H., Liedauer S., it Progr. Polym. Sci., **15**:1990

- Ziabicki A., Jarecki L., in *High Speed Fibre Spinning*, edited by Ziabicki A., Kawai H., J. Wiley & Sons, New York, 1985

6. Bij het modelleren van polymeerverwerkingsprocessen kan het deformatieveld uitgerekend worden met gegeneraliseerd Newtonse materiaalmodellen. De uiteindelijke eigenschappen van het verkregen produkt zullen echter ook afhangen van het visco-elastische karakter van het polymeer en de restspanningen in dit produkt ten gevolge van stroming zullen dan ook berekend moeten worden met een visco-elastisch materiaalmodel. Daarom zou de industrie ook meer aandacht moeten besteden aan het vinden van geschikte constitutieve modellen voor de stroming van polymeersmelten.

   - Douven L.F.A., *Towards the Computation of Properties of Injection Moulded Products*, PhD thesis, Eindhoven University of Technology, 1991.

7. In wetenschappelijke publicaties worden materiaalgegevens te weinig vermeld. Hierdoor is het vaak onmogelijk om eigen werk te vergelijken met andermans werk en is het niet altijd even duidelijk of er echt vooruitgang is geboekt in onderzoek.

8. Het belang van (wiskundige) modellering ter verbetering van produktieprocessen wordt door de industrie helaas nog te vaak onderschat.

9. De populariteit van een profvoetballer wordt slechts ten dele bepaald door zijn prestaties op het veld. Van groter belang is immers de wijze waarop de media over deze persoon berichten.

10. Paars is in.

Eindhoven, oktober 1994 Paul Tas